copy #1

SAND84-0410/4
R5

UNCERTAINTY IN RADIONUCLIDE RELEASE UNDER SPECIFIC LWR ACCIDENT CONDITIONS

VOLUME IV: TC ANALYSES

P. K. MAST,* D. R. BRADLEY, J. E. BROCKMANN,
R. J. LIPINSKI, ~~and D. A. POWERS~~

December 1984

DRAFT

SANDIA NATIONAL LABORATORIES
ALBUQUERQUE, NM 87185

Operated by

SANDIA CORPORATION

for the

U.S. DEPARTMENT OF ENERGY

Prepared for
U.S. Nuclear Regulatory Commission
Washington, DC 20555

Under Memorandum of Understanding DOE 40-550-75

NRC FIN No. A1227

---

*Science Applications International Corporation

ABSTRACT

An estimation of the sources of uncertainty in the calculated radiological source term for an assumed TC accident in the Grand Gulf plant has been completed. The major conclusions of this study are:

- The uncertainties associated with in-vessel fission product release and in-vessel retention that had been identified in the previous Surry TMLB' and S_2D studies are also relevant for the Grand Gulf TC sequence.

- Uncertainties associated with ex-vessel aerosol production via core concrete interaction are much less important than for the Surry reactor. The reason for this lies in the much lower concrete ablation temperature for the Grand Gulf limestone concrete than the basaltic Surry concrete.

- The suppression pool in the Grand Gulf BWR design is an extremely important means of reducing radioactivity release to the environment. It is shown that associated with suppression pool scrubbing, there is a factor of ten uncertainty in the upward and downward direction in the decontamination factor. This has a significant impact on radioactivity release to the containment building.

- The uncertainty range in the radioactivity release through the suppression pool into the containment building and then into the environment is a factor of 1000 when in-vessel release, in-vessel retention, and suppression pool scrubbing uncertainties are taken into

account. However, even for the extreme "high" release case, suppression pool scrubbing is very effective so that total release fractions are much lower than the "high" estimates for the Surry TMLB' and S_2D sequences.

The largest single uncertainty associated with the Grand Gulf TC sequence concerns suppression pool disruption. It has been shown that high pressure melt ejection and the subsequent vessel blowdown could overpressurize the drywell to such an extent that gas flow rates through the suppression pool exceed the fluidization velocity. The suppression pool would then be dispersed into a droplet flow regime. It is likely that if this were to occur, most of the fission products released in-vessel and during the HPME would enter the containment building atmosphere. A much more detailed analysis of this phenomenon, including accounting for the tortuous flow path for ejected core melt from vessel to drywell, would be required to eliminate this concern.

1. INTRODUCTION

The radiological consequences of a reactor accident are determined, in large part, by the magnitude and characteristics of the radioactivity release, or radiological "source term," from the plant. Important characteristics of the source term, other than magnitude of release of the many radionuclides involved, include physical and chemical nature of the released species, release timing and duration, and thermal-hydraulic features of the accompanying gas discharge (sensible heat, velocity and direction of ejection, etc.). One aim of studies of severe-accident phenomena is to provide an improved understanding of accident progression and hence, ultimately of this radiological source term.

In 1975, the Reactor Safety Study (RSS) published by the U.S. Nuclear Regulatory Commission (NRC) provided estimates of the radioactive source terms that might result from a severe core-damage accident in a nuclear power plant.[1] In those areas where detailed knowledge of the phenomena that might take place in the accident was not available, the estimates given in the RSS were intended to be conservative (i.e., the intent was to overestimate the radiological source term resulting from the hypothetical accident).

Since publication of the RSS, there have been substantial advances in the state of knowledge concerning the nature of severe accidents in nuclear power plants and of the fission-product release that might be associated with such accidents. These developments have indicated that the source-term estimates in the RSS might be overly conservative. In response to this concern, the NRC in 1980 requested a reevaluation of the assumptions and methods used to derive the radiological source-

term estimates of the RSS. This reexamination resulted in the publication in 1981 of a report, "Technical Bases for Estimating Fission Product Behavior During LWR Accidents (NUREG-0772)."[2]

The computational tools (mathematical models coded into computer language) for performing the massive, complex calculations needed to model the phenomena of a severe accident in a nuclear power plant have likewise undergone improvements since the publication of the RSS, and particularly since the events at TMI-2. As part of the continuing source-term reassessment, the NRC is sponsoring a demonstration (headed by Battelle Columbus Laboratories [BCL]) of a calculational procedure for the mechanistic determination of source terms. The approach adopted in the BCL determination of source terms represents a departure from that used in the RSS. It is recognized in the new effort that the release of fission products from the reactor fuel, and the subsequent behavior of the fission products, depend continuously on the nature and the timing of accident phenomena as well as on the details of nuclear plant construction. Models for the estimation of fission-product release and behavior are embedded in accident-analysis codes that incorporate the effects of the various phenomena characteristic of specific sequences of events within the plant. In this sense, the estimation of the radioactive source terms is being placed on a technical, mechanistic foundation similar to those long used in severe-accident analyses to calculate source terms for hydrogen and steam. Preliminary results of the BCL study are available in draft form in the volumes of a report series designated BMI-2104.[3]

Extensive peer review of interim results from the reevaluation has suggested that considerable uncertainty still exists in the estimation of severe-reactor-accident source terms.

To appreciate more fully the quality of the current state of the art in estimating severe-accident source terms, an estimate of the uncertainty in model predictions is essential. Comparison of the reassessed source-term estimates with the estimates from the RSS, and application of the new radioactive-release estimates, would be more meaningful if there were information available concerning the magnitude of the uncertainty associated with the estimates and whether that uncertainty was preferentially up or down with respect to the base case.

Sandia National Laboratories, Albuquerque (SNLA), has been estimating the uncertainty in the results of Battelle's recalculations. The SNLA effort is referred to here as the Quantitative Uncertainty Estimation for the Source Term (QUEST). The results of the QUEST study are described in general terms in Volume I of this report; detailed descriptions, supporting data, and analyses are contained in Volumes II, III, and IV.

References

1. U.S. Nuclear Regulatory Commission, "Reactor Safety Study - An Assessment of Accident Risks in U.S. Commercial Nuclear Power Plants", WASH-1400 (NUREG-75/014) (Washington, DC: U.S. Nuclear Regulatory Commission, 1975).

2. U.S. Nuclear Regulatory Commission, "Technical Bases for Estimating Fission Product Behavior During LWR Accidents," NUREG-0772 (Washington, DC: U.S. Nuclear Regulatory Commission, 1981).

3. J. A. Gieseke, P. Cybulskis, R. S. Denning, M. R. Kuhlman, and K. W. Lee, Radionuclide Release under Specific LWR Accident Conditions -- Volumes I - VII (Drafts), BMI-2104 (Columbus, OH: Battelle Columbus Laboratories, July, 1984)

2. OBJECTIVES

2.1 Objectives

The objective of the QUEST study is to investigate the uncertainty in selected specific radiological source terms as calculated in the BCL study. These determinations are meant to be examples of uncertainty in specific source terms, just as the BMI-2104 results are examples of source terms for specific LWR accident conditions.

The scope of the study was limited. Only three combinations of plant and accident sequences are considered:

- the TMLB' and S_2D accident sequences in the Surry plant (a large, dry, pressurized-water reactor [PWR])
- the TC accident sequence in the Grand Gulf plant (a boiling-water reactor [BWR] with a Mark III containment)

Operator intervention is not considered in these accidents. This volume deals only with the third of these three plant-sequence combinations, the Grand Gulf plant with the TC accident sequence. Volume II deals with the TMLB' analysis and QUEST methodology in detail. Volume III deals with the S_2D analysis. Descriptions of the above plants and sequences may be found in BMI-2104; paraphrases of these descriptions for the Grand Gulf plant are provided in Appendix A of this volume for convenience.

2.2 Source-Term Characterization

The radiological source term in this study is divided into the following species groups: Cesium iodide (CsI), cesium hydroxide (CsOH), tellurium (Te), refractory fission products (RFP), and inert aerosols. Refractory fission products include barium (Ba), lanthanum (La), cerium (Cr), strontium (Sr), neodymium (Nd), praseodymium (Pr), and samarium (Sm), as well as the actinides neptunium (Np) and plutonium (Pu). Inert aerosols include structural materials, control-rod materials, and concrete components.

The source term will be characterized for each of the aerosol groups described as the suspended mass and total aerosol radioactivity within containment as a function of time, assuming no containment failure. This characterization allows separation of the question of containment failure likelihood or mode from the question of potential source-term magnitude.

3. METHODS

3.1 Overview of Accident Source-Term Determination

A severe nuclear-reactor accident progresses through many phases, all of which contribute to the nature of the radiological source term. As the water in the reactor vessel is removed, the core heats up due to the decay heat of fission products and oxidation of the clad on the fuel. The heatup causes the vaporization of fission products and structural materials, which may condense and form aerosols.

The vapors and aerosols produced in-vessel may plate out or settle out on surfaces within the reactor coolant system (e.g., in the upper plenum, piping, or steam generator). Later heating of these surfaces may cause revaporization of the deposited materials. As the accident progresses, hot materials drop to the bottom of the reactor vessel and eventually melt a hole in the bottom. Core materials are released fr the vessel, and the associated steam and gas flow may resuspend some of the aerosols deposited inside the vessel. The combination of all the above processes is a net retention of vapors and aerosols within the reactor coolant system.

If the molten core materials are ejected from the reactor vessel at high pressure (as they may be in the TC sequence), aerosols may be formed during the ejection process. In the cavity, if the core materials are not permanently cooled by water, the molten debris will attack the concrete. The resulting melt-concrete interactions provide an additional major source of aerosols.

The aerosols released from the reactor vessel and the aerosols produced ex-vessel flow from the drywell through the suppression pool into the outer containment building. Scrubbing of aerosol-laden gases by the suppression pool results in a substantial decrease in the amount of fission products that can escape to the environment. In the TC sequence, containment failure precedes vessel failure such that once fission products enter the containment building they can be released to the environment. There is, however, additional settling of radioactive material in the containment building even beyond what is trapped in the suppression pool. That which is not retained constitutes the radiological source term.

The suite of codes used in BMI-2104 models many of the features of the accident progression described above. Figure 3-1 displays the relationships among the various codes used in determining the radiological source term. A description and assessment of each of these codes may be found in Reference 1.

The ORIGEN code determines the fission-product inventory in the core. (The uncertainty in ORIGEN is negligible and so is not addressed in this study.) The MARCH 2.0 code calculates the overall accident thermal hydraulics, including the rate of water removal from the reactor coolant system (RCS), core temperature and clad-oxidation rates during the meltdown process, the time of vessel breach, and the temperatures of the molten materials released from the vessel. The fuel temperatures calculated by MARCH are given to the CORSOR code, which calculates fission-product release rates from fuel within the RCS. The gas-flow rates and temperatures calculated by MARCH are given to the MERGE code, which calculates gas and surface temperatures along the flow path out of the RCS. The temperatures calculated by

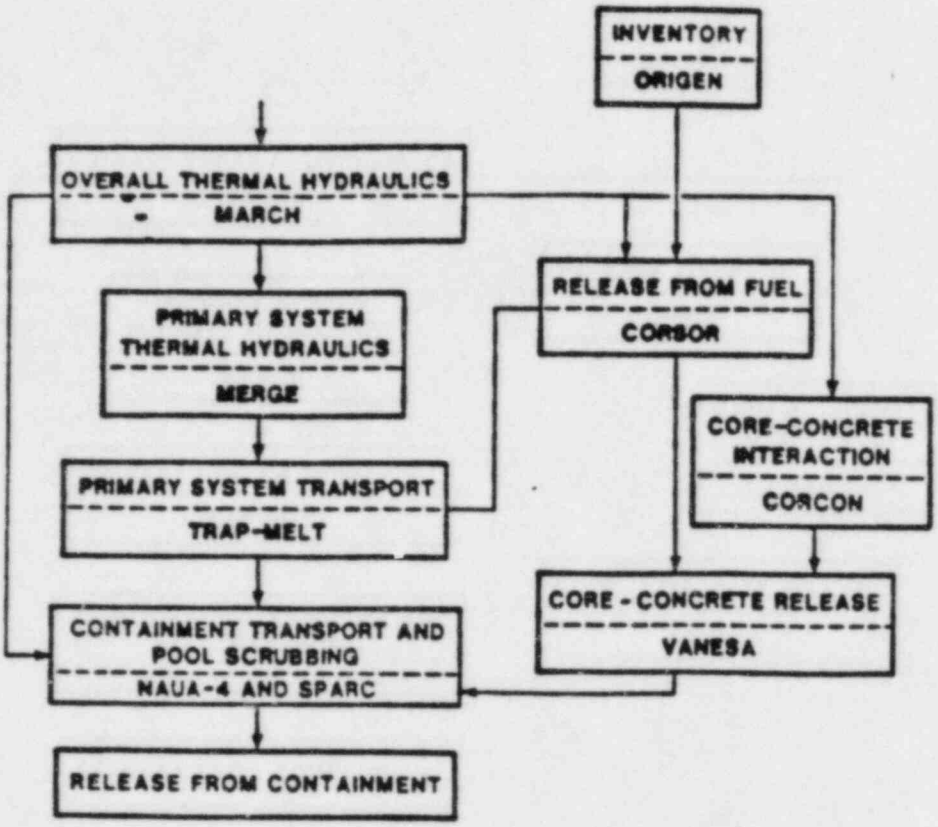

Figure 3-1 Relationships among codes used in determination of source-term code-input uncertainty.

MERGE are used by the TRAP-MELT code, along with the fission product release rates obtained from CORSOR, to determine the amount of fission-product retention in the RCS.

The CORCON code calculates temperature and gas-flow rates through the melt during core-concrete interactions, using initial melt mass, composition, and temperatures determined by MARCH. The VANESA code calculates the aerosol-release rate during core-concrete interactions using time-dependent melt temperatures and gas-flow rates from CORCON. NAUA-4 calculates the agglomeration and settling of aerosols within the containment building and removal of aerosols by containment spray. NAUA uses aerosol sources from CORSOR (after attenuation by TRAP-MELT) and VANESA, and steam-condensation rates from MARCH. SPARC calculates the retention of fission products in the suppression pool in a BWR.

As the modeling of a severe accident progresses, uncertainty develops in two ways. First, uncertainty can be introduced at a particular stage of the calculation because the knowledge or models of that particular stage of the accident are not accurate. For example, the release-rate coefficients for CORSOR are uncertain. Sometimes certain phenomena are omitted from the models for simplicity. For example, NAUA does not treat turbulent agglomeration of aerosols. These are all sources of uncertainty. The second way uncertainty develops is by propagation. Uncertainty introduced into the analysis in a previous stage will be propagated through the present stage and amplified or attenuated by the physical processes considered. For example, uncertainties in fuel-temperature history produced by MARCH can yield very large uncertainties in fission-product release in CORSOR.

3.2 Components of the Source-Term Uncertainty

The TMLB' analysis reported in volume II provided the most detailed analysis of source term uncertainty. In that assessment, source term uncertainty was divided into two components:

- Code-input uncertainty (δ_c), which is the variation in the calculated source term due to justifiable variations in the input to th computer codes used in BMI-2104 (MARCH 2.0, MERGE, CORSOR, TRAP-MELT, CORCON, VANESA, NAUA, and SPARC)

- Phenomena uncertainty (δ_p), which is the uncertainty in the calculated source term due to uncertainties in known phenomena that are important to the source term.

The code-input uncertainty indicates the range in source terms that might be calculated by different users of the code suite used in BMI-2104. The phenomena uncertainty includes not only some uncertainties that are addressed in δ_c but also some that are not addressed in δ_c either because the models of the uncertain phenomena are not affected by changes in code-input parameters, or because the phenomena are not included in the codes. Thus δ_p is a more complete estimate of the present state of uncertainty than is δ_c and encompasses δ_c. It was found in the TMLB' analysis that δ_p was greater than δ_c, although it was not too much greater, and that δ_c did not offer any significant insights not found in δ_p. Thus for the S_2D analysis, reported in Volume III, and the TC analysis reported herein, only δ_p is considered.

The actual determination of source term uncertainty, δ_p, involves a two-stage process. First, the important sources of

uncertainty along with the range over which they might vary must be determined. Second, the sources of uncertainty must be combined and propagated to determine their effects on the final source term.

3.3 Determination of Sources of Uncertainty and their Ranges

The uncertainty in suspended radionuclides comes from many sources. Every stage of the severe-accident sequence can contribute to the final uncertainty. Only those sources that strongly influence the magnitude and nature of suspended radionuclide release from containment are considered for this study.

Compiling a list of potential sources of phenomena uncertainty involves reviewing literature on accident progression, investigating experimental results for unexpected effects, and considering alternate models for accident behavior. Fortunately, a research program at Sandia National Laboratories has recently completed a review of phenomena uncertainties in severe accidents.[2] Although the uncertainties listed are not quantified, the extensive list provides a basis for consideration in this study.

The first step in identifying which phenomena uncertainties are important to the source term is to determine how those uncertainties can be handled quantitatively. For those instances where the phenomena can be addressed directly through code-input parameters in the BMI-2104 codes, simply varying those code-input parameters will solve the problem. For those cases where the phenomena exist in the codes but are not addressable by code-input parameters, simple code modifications can be made to add new input parameters. In the event the phenomenon is missing, the choice is threefold: The phenomena can be added to the code, a more advanced code that already includes the phenomenon can be used, or extensive scoping calculations can be done.

Once the methods for handling the phenomena uncertainties are developed, identification of the important ones can be made by a backward progression. That is, the phenomena and parameters that strongly affect the suspended aerosol concentration in the containment building are determined first. These are input parameters to and models in the CONTAIN code. Next, the phenomena and parameters that strongly affect the input parameters to CONTAIN are identified. These are input parameters to and models in the VANESA code. This backward progression is continued until a chain of parameters and models that strongly affect the suspended aerosol concentrations in containment is identified.

In addition to identifying the individual sources of uncertainty, it is necessary to estimate over what ranges they might vary. Only after such an estimation is made can the sources be combined and propagated to yield the net uncertainty in the radiological source term. The ranges for the sources of uncertainty are determined in two ways. First, when data are available for a parameter, the uncertainty range is determined from the scatter in the data. Second, when data are not available, the uncertainty range is determined from predictions of alternate models.

3.4 Combining and Propagating Uncertainties

Three methods of combining and propagating code and phenomena uncertainties are considered. First, it is possible to vary a single input parameter about a given base case (specifically, a BMI-2104 case) and examine the effect of such variation on the estimated radiological source term. This

approach yields a measure of the relative size and importance of each parameter. At the end of this process, however, it is difficult to combine the individual parameter uncertainties into an overall uncertainty estimate. The QUEST study makes limited use of this approach.

Second, it is feasible to perform sensitivity studies on the component codes of the suite under consideration. This approach gives an indication as to which parameters are important to a given code. In addition, the relative influence of these parameters on the source term can be estimated by linking the sensitivity studies of the various codes. Again, the resultant uncertainties are not readily combined into an overall uncertainty statement. This approach is used for the purpose of obtaining background data for application to the major methodology adopted for combining and propagating individual uncertainties, described below.

In the third approach, a specific value is chosen for each input parameter or uncertain phenomenon from within the uncertainty range for that parameter of phenomenon. This set of input values is then used in calculating a specific radiological source term. This process is repeated until the range in possible radiological source terms becomes apparent. This approach allows the combination of uncertain parameters in a manner that avoids inconsistencies (such as assuming 100% oxidation of zirconium metal both in-vessel and ex-vessel in order to maximize both in-vessel and ex-vessel aerosol generation).

In order to minimize the number of full source-term calculations that need to be performed, the input parameters may

be consciously chosen with regard for those that would lead to high or low calculated source terms. Sensitivity studies on component codes, and scoping calculations, can aid the selection process. The source terms produced by the first few calculations cannot be guaranteed to span the full space that is possible, but they should give a quick estimate of the full span.

The tools used for the spanning calculations are the suite of codes used in BMI-2104. They are modified for the δ_p calculations to determine the effect of uncertain phenomena. In addition, some individual codes are replaced with other codes or with extensive scoping calculations that have a greater flexibility to span the ranges of phenomena uncertainties of interest.

This third approach was used to get a total uncertainty bound on the source term for both the TMLB' analysis (Volume II) and the S_2D analysis (Volume III), accounting for uncertainties at all points in the accident sequence. While many of the phenomenological uncertainties did impact the final source term uncertainty, it was clear that there were several key phenomenological uncertainties that dominated. Clear examples of this are the amount of in-vessel fission product retention for the early source term, and the effectiveness of sprays and the debris coolability for the late source term in S_2D. Because of time and manpower constraints and because of considerably more difficulty in using some of the BMI-2104 codes (principally TRAPMELT and MARCH) to perform sensitivity studies for this BWR sequence, it was decided for the TC analysis to concentrate on those phenomenological uncertainties that were thought to have the largest influence on source term uncertainty. Emphasis is also placed on those uncertainties not previously addressed in the previous two volumes of this report.

3.5 References

1. T. S. Kress, Review of the Status of Validation of the Computer Codes Used in the NRC Accident Source Term Reassessment Study (BMI-2104), Draft, ORNL/TM-8842 (Oak Ridge, TN: Oak Ridge National Laboratories, 1984).

2. J. B. Rivard, V. L. Behr, R. G. Easterling, J. M. Griesmeyer, F. E. Haskin, S. W. Hatch, A. M. Kolaczkowski, R. J. Lipinski, M. P. Sherman, A. R. Taig, and A. J. Wickett, Identification of Severe Accident Uncertainties, SAND83-1689, NUREG/CR-3440 (Albuquerque, NM: Sandia National Laboratories, 1985).

4. SENSITIVITY STUDY RESULTS

Limited sensitivity studies were performed with MARCH, CORSOR, CORCON, VANESA, NAUA, and CONTAIN for the TMLB' accident in Surry and with MARCH and CONTAIN for the S_2D accident in Surry. Many of the results from those previous studies are at least qualitatively applicable to the Grand Gulf TC sequence. Thus, only limited additional sensitivity studies were performed for this analysis; one for CORCON and one for SPARC. Sensitivities and uncertainties related to the suppression pool effectiveness (as modeled by SPARC) represent the major new uncertainty relative to the previous Surry analyses.

4.1 CORCON-VANESA Sensitivity Study Results

VANESA determines the aerosol-generation rate stemming from melt-concrete interactions. VANESA currently has no user-variable input parameters. All of its input parameters are propagated from CORCON (which calculates gas generation from melt-concrete interactions) and from CORSOR (which determines the radionuclide inventory for VANESA). So a combined CORCON-VANESA sensitivity study was performed. Input parameters to CORCON were varied, and the CORCON output was immediately propagated to VANESA. The details of this study may be found in Appendix B.

The CORCON input parameters that were varied are listed in Table 4-1, along with the high and low values used.

The VANESA output parameters considered were aerosol-generation rate (for various elements), mean particle diameter, and particle-material density, because the NAUA sensitivity study (in the TMLB' analysis) identified these as important (or moderately so) to the source term.

Table 4-1 Input parameters and ranges for CORCON-VANESA sensitivity study

Parameter	Base Value	Low Value	High Value
Melt temperature (K)	1898	2200	2600
Fraction of Zr unoxidized (%)	60	10	90
Mass of steel in melt (kg)	81270	8217	162540
Interaction start time (min)	197.6	100	1800
Fraction of core in melt (%)	100	50	100
Evaporable water (%)	3.94	3.94	7.88
Concrete type	Limestone	Limestone-Common Sand	Limestone
Emissivity of surroundings and melt phases	1.0	0.001	0.5
Ablation temperature (K)	1875	1690	1780

The particle mean diameter and the particle-material density were found to be relatively insensitive to all input variations to CORCON. Those parameters that most strongly influence the aerosol-generation rates were found to be the

- Fraction of the core involved in ex-vessel interactions
- Amount of zirconium metal in the debris
- Amount of steel in the debris.

All of these parameters are propagated from the MARCH code. It should be emphasized, however, that in all cases the sensitivity was much less than was found for the sensitivity study done for Surry (reported in TMLB' volume). The reason for this is the much lower ablation temperature in the limestone concrete.

VANESA is also sensitive to the initial radionuclide inventory in the melt, which is obtained from CORSOR. Because this sensitivity to inventory is apparent, the initial radionuclide inventory in the melt was not varied in this sensitivity study.

4.2 SPARC Sensitivity Study Results

The presence of a suppression pool in the Grand Gulf BWR is the most significant difference between this analysis and the previous Surry analyses. In the TC sequence, radionuclides must normally pass through the suppression pool prior to release to the containment building, the auxiliary building, and eventually the environment. Thus, barring suppression pool bypass or disruption (see Appendix C), significant mitigation of fission product release is achieved because of the removal by the suppression pool of radionuclides from the gases passing through it. Uncertainties in this scrubbing efficiency as treated by the SPARC code are discussed in Appendix D.

The SPARC input parameters that were varied include:

- Particle size and material density
- Percent soluble material in gas
- Bubble diameter
- Bubble aspect ratio
- Bubble swarm rise velocity

The results of the sensitivity study shows that the decontamination factor is very sensitive to the particle size distribution, a parameter that is propagated from previous codes (VANESA). However, this sensitivity is reduced somewhat if a fairly broad size distribution is assumed. Uncertainties due to such user supplied parameter values as bubble size and shape also exist. However, these uncertainties are largely dominated by uncertainties in the physical mechanisms of decontamination (i.e., phenomenological uncertainties).

5. SOURCES OF UNCERTAINTY AND THEIR RANGES

The uncertainty in the potential radionuclide release during an LWR accident comes from many sources. Every stage of the severe-accident sequence can contribute to the final uncertainty. However, only those sources of uncertainty that strongly influence the magnitude and nature of the potential radionuclide release are considered in this study.

The identification of the influential sources of uncertainty is based on sensitivity studies (primarily those performed for the TMLB' analysis reported in Volume II, plus that described in Section 4), on the experiences of persons familiar with the codes, and on reviews of severe-accident phenomena. Some important phenomena uncertainties were identified in the TMLB' and S_2D analyses. Additional phenomena uncertainties will be discussed in this section.

In addition to identifying the individual sources of uncertainty, it is necessary to determine over what range they might vary. Only after such a determination is made can the sources be combined and propagated to yield the net uncertainty in the radiological source term. The ranges for the sources of uncertainty will be determined from scatter in available data and from alternate models describing the phenomena of interest. That is, every range must be technically justified. These ranges and their justifications are presented in this section.

5.1 Phenomena Uncertainties and Their Ranges

The suite of codes used in the Battelle study contains various phenomenological uncertainties.[1,2] These uncertainties arise from modeling that does not accurately describe the processes under consideration, either because of approximations

used or because the processes themselves are not currently well understood. In addition, some uncertainties arise because some processes are not included in the codes, sometimes because the processes have only recently been discovered or recognized as important. An extensive list of phenomena uncertainties in LWR severe accidents has been developed recently at Sandia National Laboratories.[3] The uncertain phenomena that are considered to be important to the radiological source term will be described in this subsection.

The accident sequences are divided into five sequential regimes within which the uncertain phenomena will be discussed. The five regimes are:

1. In-vessel production of fission-product, control- rod, and structural vapors and aerosols

2. Net retention within the reactor coolant systems (RCS) (including the opposing influences of retention and resuspension or revaporization)

3. Ex-vessel production of radiological and inert aerosols

4. Net removal of fission products by the suppression pool.

5. Net retention within the reactor containment building (RCB)

The in-vessel production regime is addressed by the MARCH and CORSOR codes. The net in-vessel retention regime is addressed by the MERGE and TRAP-MELT codes. The ex-vessel production regime is addressed by the CORCON and VANESA codes. The suppression pool behavior regime is treated by the SPARC code. The net ex-vessel regime is addressed by the NAUA code and CONTAIN codes.

5.2 Phenomena Uncertainties Found in the TMLB' and S_2D Analysis

Most of the uncertain phenomena associated with in-vessel production, retention in RCS, ex-vessel production, and retention in RCB that have previously been identified as being important in the TMLB' (and S_2D) sequence are also important in the TC accident. These include uncertainties in fuel temperature, fuel configuration, fission-product release rate coefficients, retention in the reactor coolant system (RCS), aerosol production during high-pressure melt ejection, and molten pool behavior. An additional important uncertainty involves the suppression pool behavior, which is discussed in the next section as well as in Appendix B. A summary of these important uncertain phenomena and uncertainty ranges is given in Table 5-1. A summary of additional phenomena not explicitly included in the TMLB' analysis is given in Table 5-2. More detailed explanation of the tables may be found in Volume II.

Some additional discussion is warranted concerning the uncertainty in retention of fission products in the RCS. In the TMLB' analysis, it was found that natural circulation in the reactor vessel and RCS could lead to large velocities ($\sim$ 1 m/s). Current codes only consider net velocities produced by boiloff of the vessel water. Since net boiloff velocities in the TMLB' accident are typically 0.001 to 0.01 m/s, natural circulation could easily dominate the thermal-hydraulics and introduce large uncertainty into the fission-product retention calculations.

In the TC accident, the time from the start of core melt to core collapse is about the same time as in the TMLB' accident, so the net steam velocities are not that much different. Thus the uncertainty in retention of fission-products in the RCS is about the same for the TC accident as it is for a TMLB' accident.

Table 5-1 Sources and ranges of phenomena uncertainty considered in δ_p calculations

Regime	Source	Range
In-vessel production of vapors and aerosol	Meltdown progression and clad oxidation	Modeled by MARCH
	Release rates of volatile fission products, control-rod materials, and structural materials	0.1x to 10x nominal
	System boundary conditions	
In-vessel net retention of vapors and aerosols	Natural circulation between core, plenum and other volumes	
	Revaporization from heating of surfaces	10% to 99% net retention
	Aerosol depletion factors	
	Aerosol resuspension from gas flow during breach	
Ex-vessel production of aerosols	Aerosol generation during high-pressure melt ejection	8 to 800 kg
	Interlayer molten pool heat transfer	1x to 20x CORCON nominal
	Surroundings heatup	ES = 0.001 - 1.0
Ex-vessel net retention of aerosols	Multicompartmentalization	1,5
	Number of aerosol components	7
	Turbulent-energy-dissipation	10^{-5}-0.02 m^2/s^3
	Coupling between aerosol behavior and containment-atmosphere thermodynamics	included

Table 5-2 Phenomena not explicitly considered in δ_p calculations

Phenomenon	Reason for Neglect
Boron chemistry	Difficult to quantify effect; partially included in the 10% to 90% RCS retention range.
Steam explosions	Effect on source term similar to that of high-pressure melt ejection. (Effect on containment not within scope of this study.)
Vessel depressurization before failure	Modeled by means of small melt-ejection aerosol source
Delayed melting of outer rows of fuel elements and delay in fission-product release	Effect of quantities involved is included in net RCS retention range, but effect of delay is not. Some questions on how material escapes vessel.
Revaporization of deposited fission products in RCS	Effect of quantities involved is included in net RCS retention range, but effect of delay is not. Some question of how material escapes vessel.
Hydrogen burns	Model development needed; could alter aerosol form
Diffusiophoresis	Included in CONTAIN calculations; effect of uncertainty in diffusiophoresis is small
Re-evolution of iodine gas from evaporating pools	Effect partly engulfed by effects of resuspension at containment failure
Radioactive decay chains	$^{132}Te \rightarrow {}^{132}I$ is included in calculations and seems to be chain with strongest effect on late suspended radioactivity

5.3 Uncertainty in Suppression Pool Behavior

The key difference between the Grand Gulf TC sequence and the Surry TMLB' and S_2D sequences discussed in previous volumes of this report is the effect of the suppression pool in the BWR Mark III design. Unlike the Surry plant where fission products escaping from a breach in the vessel directly enter the containment building atmosphere, fission products escaping from a breach in the Grand Gulf vessel must pass through the drywell and the suppression pool prior to entering the containment building atmosphere. Thus, barring suppression pool bypass or failure there is a very significant reduction in the amount of fission products that could escape to the environment relative to the previous Surry results.

There are two major uncertainties relative to the suppression pool behavior; the possibility of suppression pool bypass or disruption and the uncertainty in the decontamination factor for radionuclide-containing gases passing through the pool.

5.3.1 Suppression Pool Bypass

The question of suppression pool bypass and/or disruption is addressed in detail in Appendix B. The mechanism by which it is postulated that suppression pool failure might occur is a high pressure melt ejection (HPME) that leads to drywell pressurization and either direct drywell failure or suppression pool disruption by the high pressure/high velocity gas from the drywell. It is shown in the appendix that a HPMF can occur in the Grand Gulf TC sequence, if a "hands-off" sequence is assumed.

This is due principally to the fact that the early containment failure in the TC sequence and the resultant low (atmospheric) containment building and drywell pressure inhibit activation of the Automatic Depressurization System. Thus, the primary system pressure remains high to the time of vessel failure.

A HPME is of consequence in the Grand Gulf TC sequence primarily if it leads to significant overpressurization of the drywell atmosphere. As discussed in Appendix B, the requirement for rapid heating of the drywell volume is the existence of a fairly simple flowpath from the vessel failure location to the drywell volume. This criterion is only marginally met in Grand Gulf, and one would not expect most of the ejected melt to be dispersed in the drywell. Thus, the analyses described in Appendix B assumed that only ~ 10% of the molten core mass participated in the direct heating of the drywell atmosphere.

Drywell overpressurization has two potential consequences, drywell structural failure and disruption of the water in the suppression pool. It is shown in Appendix B that direct failure of the drywell is unlikely because the venting of the drywell is sufficient to mitigate the potential pressure rise rate resulting from the HPME and vessel blowdown. However, it was shown that the pressure developed during a HPME and the subsequent vessel blowdown could produce steam flow rates through the pool that could greatly reduce its efficiency in retaining fission products for a short period of time.

A simple analysis of drywell pressurization indicates that for a period of about 16 seconds after vessel failure the steam flow rates through the suppression pool exceed the minimum flow velocity for fluidizing water by a factor of about 2. If the

suppression pool is dispersed into a 10-m long droplet flow regime, the fission product aerosols are exposed to the water spray for about 4 seconds. This is not much time for fission-product retention in the dispersed spray as compared to the normal fission product retention resulting from bubbly flow through the pool. Thus it is likely that most of the fission products released in-vessel and during the HPME would enter the containment building atmosphere.

5.3.2 Decontamination Factor Uncertainty

The uncertainty in suppression pool effectiveness because of phenomenological uncertainties in pool scrubbing behavior are discussed in detail in Appendix D and have been previously summarized in Section 4.2. These uncertainties are much smaller than the uncertainty due to possible suppression pool disruption (discussed in previous section). Thus, even in the worst case the suppression pool is an effective remover of radionuclides as long as high steam velocities do not occur that fluidize the pool.

5.4 References

1. J. A. Gieseke, "Summary of Source Term Analyses for Five LWR Plants," Trans Eleventh Water Reactor Safety Research Info Mtg, Gaithersburg, MD, October 24-28, 1983.

2. J. A. Gieseke, P. Cybulskis, R. S. Denning, M. R. Kuhlman, and K. W. Lee, Radionuclide Release under Specific LWR Accident Conditions -- Volumes I-VII (Drafts), BMI-2104 (Columbus, OH: Batelle Columbus Laboratories, 1983).

3. J. B. Rivard, V. L. Behr, R. G. Easterling, J. M. Criesmeyer, F. E. Haskin, S. W. Hatch, A. M. Kolaczkowski, R. J. Lipinski, M. P. Sherman, A. R. Taig, and A. J. Wickett, Identification of Severe Accident Uncertainties, SAND83-1689, NUREG/CR-3440 (Albuquerque, NM: Sandia National Laboratories, forthcoming).

4. Surry Power Station Units 1 and 2, Final Safety Analysis Report, Virginia Electric and Power Company, Richmond, Va. (1970).

6. SOURCE-TERM UNCERTAINTY FROM UNCERTAIN PHENOMENA (δ_p)

The suite of codes used in the Battelle study contains various phenomenological uncertainties. These uncertainties arise from modeling that does not accurately describe the processes under consideration, either because of approximations used or because the processes themselves are not currently understood. In addition, some uncertainties arise because some processes have only recently been discovered or recognized as important. The phenomena uncertainties that are considered to be important to the radiological source term are discussed in Section 5, along with the range of uncertainty associated with them. In this section, some of these uncertainties will be combined and propagated to determine their effect on the radiological source term.

To determine δ_p, self-consistent sets of values for uncertain phenomena were chosen, with each set yielding a specific radiological source term. The phenomena values were chosen from within uncertainty ranges based on technical assessments and described in Section 5. Values were chosen that might result in high source terms or low source terms. The resulting high and low calculated source terms then became an estimate of the current range of source-term uncertainty.

In the previous uncertainty analyses performed for the Surry TMLB' and S_2D sequences, the codes from the BMI-2104 study and selected additional codes (CONTAIN) were used to combine and propagate the phenomenological uncertainties to arrive at a final source term uncertainty. For this Grand Gulf TC analysis, an estimate of the final source term uncertainty will be made without actually applying these codes. The results of the

sensitivity studies described in Chapters 4 and 5 as well as the insights gained from the previous Surry analyses will be used instead.

As in the previous QUEST analyses, selected self-consistent source terms will be defined that represent the spread in uncertainty in the final source term. Because containment failure precedes vessel failure in the TC sequence, separate early and late high and low source terms will not be considered. Thus, we will only consider a low, base-case, and high source term. However, because of the extreme effect that possible suppression pool disruption due to high pressure melt ejection could have on the radiological release, this high release case is considered separately and is designated early-high (since suppression pool disruption would occur shortly after vessel failure). The base case being considered herein is identical to the base case described in BMI-2104.

Table 6-1 gives the general conditions for the various stages of an accident that would be expected to result in the low, high, and early-high source terms. As has been the case in previous analyses, these combinations of uncertainties are not unique in defining high or low source terms. Thus, other combinations of parameter uncertainties could also result in high or low source terms, possibly even outside the ranges we have defined. However, the cases chosen are thought to be representative of the high and low values for the source term uncertainty.

There are several ways to achieve a final low release to the environment. The "low" case chosen herein has high in-vessel production coupled with high in-vessel retention so that the bulk

of the fission products remain within the RCS. Drywell production is also assumed to be low with retention in the drywell, suppression pool, and containment all high.

The nominal "high" case defined herein has high production both in-vessel as well as in the drywell. Low retention is assumed in-vessel, in the drywell, in the suppression pool, and in containment.

The case designated "early-high" is identical to the "high" case except that suppression pool disruption due to high pressure melt ejection is also assumed.

While all of the phenomena uncertainties described above affect the final source term uncertainty, previous sensitivity studies have shown that the in-vessel production/RCS retention and suppression pool behavior dominate. Thus, the following discussion will deal primarily with the effect on source-term of these uncertainties. CsI, CsOH, and Tc will be considered since these are the fission products discussed in detail in BMI-2104.

Table 6-1 Conditions expected to result in high or low source terms for Grand Gulf TC sequence

	Low	High	Early-High
In-vessel production	Hi	Hi	Hi
Net retention in RCS	Hi	Lo	Lo
Drywell production of aerosols by core-concrete interaction	Lo	Hi	Hi
Retention in Drywell	Hi	Lo	Lo
Suppression Pool Retention	Hi	Lo	Lo
Suppression Pool Disruption	No	No	Yes
Retention in Containment	Hi	Lo	Lo

6.1 In-Vessel Production of Vapors and Aerosols

The range of in-vessel production of vapors and aerosols is determined by uncertainties in core thermal hydraulics and fission product release phenomena. Uncertainties in core thermal hydraulics had been previously investigated in the Surry analyses by varying such MARCH parameters as the core melt temperature, the core heat of fusion, the fraction of the core molten prior to slumping, and others. The uncertainty in fission product release phenomena was accounted for with a plus or minus factor of ten in the release-rate coefficients in CORSOR.

The Grand Gulf TC sequence "base case" as reported in Volume III of BMI-2104 shows that 100% of the Cs and I and 25% of Te are released in-vessel. Because of similarities in the meltdown sequence, the Surry TMLB' analyses can provide some guidance as to the uncertainty in these release values. The "base case" release values for Surry TMLB' as reported in Volume II of this report are 98.6% for Cs and I and 33.2% for Te. Thus, the base case values are very close to the Grand Gulf TC sequence base case values. It seems reasonable therefore to assume that the high and low release values for Surry TMLB' should at least qualitatively represent the uncertainty range for the Grand Gulf TC. These values are summarized in Table 6.2. As can be seen, for the high-release case, 100% of the Cs, I, and Te are calculated to be released. For the low release-case, only about 12% of the Cs and I and 2.2% of the Te are released.

6.2 Net Retention in the RCS

Previous analyses of net retention in the RCS had shown a

tremendous uncertainty in this important potential mitigating effect because of uncertainties in such phenomena as natural circulation. Net retention was shown to vary between 10% and 90% (see Appendix B of Volume II of this report) when uncertainties in natural circulation and possible revaporization were considered.

The Grand Gulf TC sequence base case results reported in Volume III of BMI-2104 showed that of the material released in-vessel, 18.6% of the I, 48.0% of the Cs, and 90% of the Te were retained within the reactor coolant system. This compares with the limits of 10% and 90% for low and high retention discussed above.

Table 6.2 Estimates of in-vessel fission product release for Grand Gulf TC sequence

	Initial Inventory (kg)	Fractional Release		
		Base Case*	High**	Low**
Cs	245	1.00	1.00	0.13
I	17.7	1.00	1.00	0.11
Te	37.0	0.25	1.00	0.02

* From Table 6.7c BMI-2104, Vol III
** Based on Surry TMLB' results.

If we now go back to the definitions of our "low" and "high" cases as summarized in Table 6.1, we can use the above retention information along with the release information in Section 6.1 to define the fission product distribution shortly after vessel failure. This information is summarized in Table 6.3. The distribution for the "early-high" case would be the same as for the "high" case given above.

6.3 Ex-Vessel Aerosol Generation

The uncertainties in ex-vessel aerosol generation due to core-concrete interaction are not addressed because of larger uncertainties in both in-vessel retention and suppression pool scrubbing. However, the base-case as reported in Volume III of BMI-2104 shows that of the 0.757 Te fraction still in the melt at vessel failure, about 2/3 of this amount is released ex-vessel during the core concrete interaction. Ex-vessel aerosol generation uncertainties are not that important for the assessment of our "high" and "low" cases because, for both, complete in-vessel release of fission products is assumed.

6.4 Drywell Retention

Uncertainties in retention of fission products within the drywell due to gravitational settling, phoresis mechanisms, etc., are not considered in this analysis because it is felt that uncertainties in in-vessel release and retention and suppression pool scrubbing are much more important. Drywell retention in the BMI-2104 base case does not have a significant impact on final release to the environment. Thus, the assessment of the "high" and "low" cases described in Table 6.1 was performed assuming the same fractional retention of release fission products in the

drywell as was found in the base case described in BMI-2104. The numbers for fraction of fission products released in-vessel (not retained in RCS) fraction of fission products released ex-vessel during core-concrete interaction, and fraction of core inventory retained in the drywell due to settling, etc., for the BMI-2104 base case are summarized in Table 6.4. From these values it is possible to calculate the fraction of released fission products in the drywell that were retained in the drywell. These fractions will be used as estimates for the assessment of the "high" and "low" cases as well.

Table 6.3 Spatial location of fission products in Grand Gulf TC sequence shortly after vessel failure

	Cs	I	Te
Initial Inventory (kg)	245	17.7	37.0
"Base Case" - Fraction			
- Retained in RCS	.486	.186	.219
- Ex-vessel in Melt	-	-	-
- Ex-vessel Released	.51	.814	.024
"Low Case" - Fraction*			
- Retained in RCS	.90	.90	.90
- Ex-vessel in Melt	-	-	-
- Ex-vessel Released	.10	.10	.10
"High-Case" - Fraction**			
- Retained in RCS	.10	.10	.10
- Ex-vessel in Melt	-	-	-
- Ex-vessel Released	.90	.90	.90

* Low Case - High Release, High Retention

** High Case - High Release, Low Retention

Table 6.4 Drywell retention summary for Grand Gulf TC sequence base case

	Fraction			
	Released in-vessel and not retained in RCS	Released ex-vessel during core-concrete interaction	Retained in Drywell	Drywell Retention Factor
Cs	.51	-	.0014	.0027
I	.814	-	.036	.0442
Te	.024	.497	.06	.1152

6.5 Suppression Pool Scrubbing

Uncertainties in suppression pool scrubbing will be considered in this section separately from effects due to possible suppression pool disruption (section 6.8). Table 7.10 in Volume III of BMI-2104 presents the final distribution of fission products in the Grant Gulf TC sequence. With those fission products in containment plus those released to the environment representing the total of what passed through the suppression pool, it is possible to use the data in the table to define a time-averaged decontamination factor. This is shown in Table 6.5.

Table 6.5 Final Distribution of Fission Products in Grand Gulf TC Sequence with Calculation of Average DF

	Fraction of Core Inventory					
	RCS	Drywell	Pool	Containment	Environment	DF
Species						
CsI	0.19	$3.6x15^{-2}$	0.77	$1.9x10^{-4}$	← $6.8x10^{-3}$	111
CsOH	0.51	$1.4x10^{-3}$	0.49	$9.2x10^{-6}$	$3.5x10^{-4}$	1362
Te	0.22	0.32	0.45	$4.3x10^{-4}$	$8.8x10^{-3}$	50

The assessment of suppression pool scrubbing in Appendix D had concluded that an uncertainty factor of plus or minus 10 existed in the decontamination factor. This uncertainty range along with the base-case average values summarized in Table 6.5 will be used to estimate suppression pool decontamination factors for CsI, CsOH, and Te for the "high" and "low" cases. These values are summarized in Table 6.6. The DF value obtained in this manner for Te for the "high" case is probably overly conservative. In the base-case, much of the Te is released late in time during the core-concrete interaction. At that time, the SPARC analyses reported in BMI-2104 show the decontamination factor to be low because of pool conditions. Much of the CsI and CsOH was released early in time, in-vessel when the pool decontamination factor was much higher. Since the "high" case, as we have defined it herein, assumed extensive in-vessel release of Te, it is only reasonable to assume that a higher suppression pool decontamination factor would be applicable to Te scrubbing as well. Thus the DF value for Te of 5 in Table 6.6 is thought to be very conservative.

6.6 Net Retention in Containment Building

Uncertainties in net retention within the containment building have not been considered in the analysis. The base case results from BMI-2104 showed very little retention in the containment building. Uncertainties that do exist in this phenomenon are likely to lead to downward uncertainties in the source term. For the analysis of the "High" and "Low" cases defined herein, it is simply assumed that the retention in the containment building relative to the fraction released to the environment is the same as in the BMI-2104 base case. This would tend to underestimate the containment building retention for the "High" case because of the higher suspended aerosol concentrations. Thus, this is overly conservative for the "High" case.

Table 6.6 Summary of Decontamination Factors Used in Grand Gulf TC Uncertainty Analyses

	Decontamination Factor		
Species	"Low"	"Base Case"	"High"
CsI	1110	111	11
CsOH	13620	1362	136
Te	500	50	5

Table 6.7 Final Distribution of Fission Products in Grand Gulf TC Sequence - "Low" Case

	Fraction of Core Inventory				
	RCS	Drywell	Pool	Containment	Environment
CsI	.90	.004	.096	3×10^{-6}	9.7×10^{-5}
CsOH	.90	.0003	.099	2×10^{-7}	7.1×10^{-6}
Te	.90	.008	.092	1×10^{-5}	1.9×10^{-4}

Table 6.8 Final Distribution of Fission Products in Grand Gulf TC Sequence - "High" Case

	Fraction of Core Inventory				
	RCS	Drywell	Pool	Containment	Environment
CsI	.1	.04	.78	2×10^{-3}	7.6×10^{-2}
CsOH	.1	.0025	.89	2×10^{-4}	6.4×10^{-3}
Te	.1	.069	.65	1×10^{-2}	1.7×10^{-1}

6.7 Cumulative Release to Containment - "High" and "Low" Cases

The uncertainties in in-vessel release and retention, summarized in Table 6.3, and the uncertainties in suppression pool decontamination factors, summarized in Table 6.6, were used in conjunction with nominal estimates of drywell retention (Table 6.4) and containment retention to estimate upper and lower bound fission product release fractions to the environment. The results for the "Low" case are given in Table 6.7 and the results for the "High" case are given in Table 6.8. The range in release fractions to the to the environment is seen to be almost a factor of 1000. However, even the overly-conservative "High" case shows considerable mitigation of release to the environment.

6.8 Uncertainties Due to Suppression Pool Disruption

It is shown in Appendix B that a high pressure melt ejection could lead to temporary suppression pool fluidization such that the aerosol-laden gases passing through the suppression pool would experience little scrubbing action. This period of scrubbing failure occurs coincident with the release of fission products left suspended in the reactor vessel at the time of failure, coincident with the release of fission products resuspended during vessel blowdown after failure, and coincident with the production of aerosols by gas coming out of solution and sparging through the molten core materials during the high-pressure melt ejection. Thus, the net result is that a potentially large radiological source term could be ushered through the suppression pool without retention.

In the "high" case summarized in Table 6.6, close to 90% of the available CsI, CsOH, and Te are seen to be available for

passing through the suppression pool. Thus, if there were limited suppression pool effectiveness, most of these fission products could escape into the containment building.

It is felt that the level of analysis used to obtain the bounding "high" and "low" case values in tables 6.5 and 6.6 is too crude to be of value in quantifying an estimate for the "early high" case. Simply following the logic of letting most of the available fission products pass through the suppression pool with a fractional release from containment to environment on the same order of magnitude as in the base-case would lead to absurdly high release values to the environment. An accurate quantification of source term for this scenario requires a more detailed assessment of

- HPME path from failed vessel to drywell

- drywell retention given the much higher aerosol concentration than in the base case

- radionuclide removal in a dispersed flow-regime suppression pool

- containment retention given the higher aerosol concentrations

This was not possible within the time and manpower constraints of this study.

6.9 Summary

The amount of radionuclides that escape into the containment and the environment during a TC accident in the Grand Gulf reactor is not accurately known because of uncertainties in the phenomena leading to such release. The range of uncertainty in release through the suppression pool, taking into account uncertainties in in-vessel release and retention through suppression pool scrubbing, is large. The range in estimated release to the environment for Cs, I, and Te is a factor of almost a 1000 between what we have designated our "High" and "Low" cases. The base case as reported in BMI-2104 falls near the middle of this range. However, even in the overly conservative "High" case analyzed herein, significant mitigation in fission product release to the environment is evident.

The potential effects of suppression pool disruption cased by a high pressure melt ejection are large. Temporary suppression pool fluidization, such that aerosol-laden gases passing through the suppression pool would experience little scrubbing action, could result in a large radiological source term. The size of the source term was not quantified, because it was felt that the level of detail of the analysis used herein would significantly overestimate the radiological release. A series of code calculations, accounting for the details of the high pressure melt ejection and the flowpath (and obstruction) from failed vessel to drywell is required. This was beyond the scope of what was possible in this study.

7. SUMMARY AND CONCLUSION

An estimation of the sources of uncertainty in the calculated radiological source term for an assumed TC accident in the Grand Gulf plant has been completed. The major conclusions of this study are:

- The uncertainties associated with in-vessel fission product release and in-vessel retention that had been identified in the previous Surry TMLB' and S_2D studies are also relevant for the Grand Gulf TC sequence.

- Uncertainties associated with ex-vessel aerosol production via core concrete interaction are much less important than for the Surry reactor. The reason for this lies in the much lower concrete ablation temperature for the Grand Gulf limestone concrete than the basaltic Surry concrete.

- The suppression pool in the Grand Gulf BWR design is an extremely important means of reducing radioactivity release to the environment. It is shown that associated with suppression pool scrubbing, there is a factor of ten uncertainty in the upward and downward direction in the decontamination factor. This has a significant impact on radioactivity release to the containment building.

- The uncertainty range in the radioactivity release through the suppression pool into the containment building and then into the environment is a factor of

1000 when in-vessel release, in-vessel retention, and suppression pool scrubbing uncertainties are taken into account. However, even for the extreme "high" release case, suppression pool scrubbing is very effective so that total release fractions are much lower than the "high" estimates for the Surry TMLB' and S_2D sequences.

- The largest single uncertainty associated with the Grand Gulf TC sequence concerns suppression pool disruption. It has been shown that high pressure melt ejection and the subsequent vessel blowdown could overpressurize the drywell to such an extent that gas flow rates through the suppression pool exceed the fluidization velocity. The suppression pool would then be dispersed into a droplet flow regime. It is likely that if this were to occur, most of the fission products released in-vessel and during the HPME would enter the containment building atmosphere. A much more detailed analysis of this phenomenon, including accounting for the tortuous flow path for ejected core melt from vessel to drywell, would be required to eliminate this concern.

It should be noted that these conclusions are the result of a scoping look at the uncertainties for a particular plant and accident. More refinement on the uncertainty bands could be achieved with additional effort. Scoping estimates for other plants and sequences will have to be made before it can be determined how generally applicable these conclusions are.

APPENDIX A

Plants and Sequences Considered

QUEST considers only three combinations of plant and accident sequence:

The Surry plant (a large, dry pressurized-water reactor [PWR]) with the TMLB' and S_2D accident sequences (believed to dominate risk in this plant)

The Grand Gulf plant (a boiling-water reactor [BWR] with a Mark III containment) with the TC accident sequence (believed to be risk-dominant for this plant).

NOTE: Volume IV of this report deals only with the third of these three plant-sequence combinations, i.e., the Grand Gulf plant with the TC accident sequence. The other plant-sequence combinations are dealt with in other volumes of this report.

The Grand Gulf Nuclear Station comprises two twin units in a common facility with some shared systems. Each unit has a BWR/6 boiling water reactor incorporating a pressure vessel 251 inches (6.4 m) in diameter with 800 fuel assemblies, designed and supplied by the General Electric Company. The thermal power output of each unit is approximately 3800 MW, and the net electrical output is approximately 1250 MW.

The Mark III containment design employed in the Grand Gulf plant is illustrated in Figure A-1. In this design, the suppression pool is located at the periphery of the containment. In the event of a loss-of-coolant accident, the water level in the

channel internal to the weir wall would be depressed, uncovering horizontal vent pipes. Steam in the drywell would then be relieved to the suppression pool through the vents. In the Mark III design, the vapor space of the wetwell actually forms an outer containment volume surrounding the drywell. The containment is a steel-lined, reinforced concrete structure.

The internal design gage pressures of the drywell and containment are 30 and 15 psi (0.2 and 0.1 MPa), respectively. BMI-2104 assumes that failure of the containment would occur at an internal absolute pressure of 72 psi (0.5 MPa) (based upon discussions with industry representatives). This absolute failure pressure is considerably higher than the 45 psi (0.3 MPa) nominal value utilized in the RSSMAP analyses of Grand Gulf and is 3.8 times the design value. The expected location of failure is in the upper region of the containment at the junction of the cylindrical wall with the hemispherical dome. Little basis exists for predicting the leakage characteristics of the containment following failure. A large leakage was assumed to result for the purposes of this study. Because the failure location was elevated with respect to the suppression pool, it was assumed that the latter would remain in place following failure.

The standby gas-treatment system at Grand Gulf provides for mixing between the auxiliary and enclosure buildings. The capacity of the system to exhaust to the atmosphere is quite small, however: 4000 cfm (1.9 x 10 L/s). It is expected that the enclosure building would fail shortly following failure of the primary containment. Other plant data used in the analyses are provided in Table A-1.

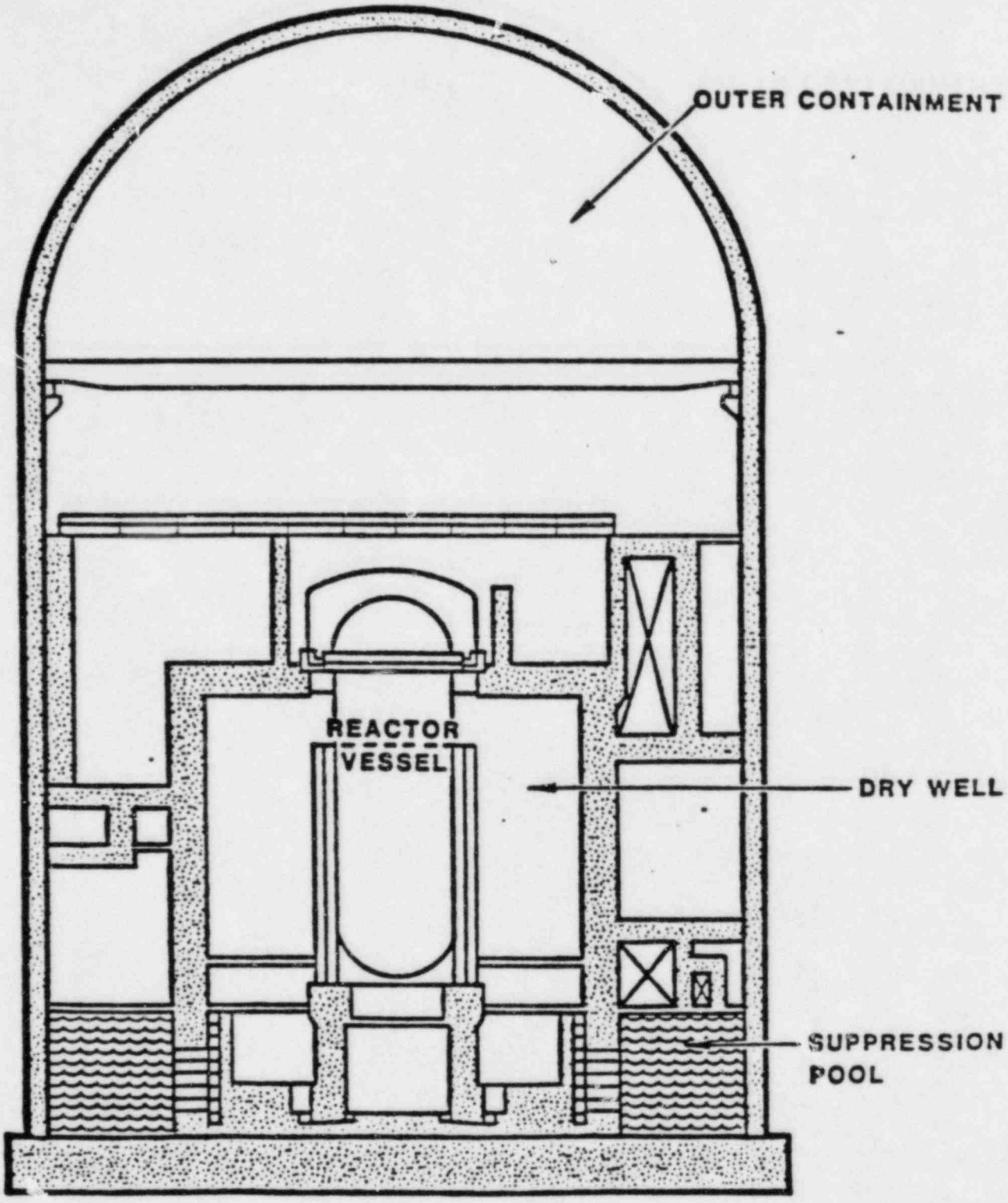

Figure A-1 BWR Mark III containment design (typical of Grand Gulf). [DMI-2104, Vol. III)

Table A-1 Grand Gulf plant data [DMI-2104, Vol. III]

Nominal power	3 800 MW (thermal)
Steam pressure in core (gage)	1 040 psi (7.17 MPa)
Primary system operating temperature	555°F (291°C)
Primary system total coolant inventory	25 940 ft^3 (734.5 m)
Liquid volume in vessel	3 771 ft^3 (106.8 m)
Steam volume in vessel	9 638 ft^3 (272.9 m)
Steam volume in recirculation loop	827 ft^3 (23.4 m)
Reactor coolant system liquid mass	6.815 x 10 lbm (3.091 x 10 kg)
Reactor coolant system steam mass	24 000 lbm (1.1 x 10^4 kg)
Reactor vessel	
Inside diameter	251 inches (6.38 m)
Inside height	73 ft (22 m)
Design pressure (gage)	1250 psi (8.6 MPa)
Design pressure	575°F (302°C)
Thickness (with clad)	6.265 inches (0.1591 m)
Core	
Equivalent diameter	15.96 ft (4.865 m)
Active fuel height	12.5 ft (3.81 m)
Total cross sectional area	169 ft (15.7 m)
Flow area of core	84.3 ft (7.8 m)
Number of fuel assemblies	800
Rods per assembly	62
Pitch	5.3 x 10^{-2} ft (0.016 m)
Assembly dimensions	5.46 inches square (0.139 m square)
Fuel rod diameter	4.025 x 10^{-2} ft (0.012 m)

Table A-1 Grand Gulf plant data [BMI-2104,Vol III] (Continued)

Clad thickness of fuel rods	5.543×10^{-3} ft (1.69 mm)
Total number of fuel rods	49 600
Core Weight	
UO_2	366 400 lbm (166 200 kg)
Zircaloy	174 700 lbm (79 240 kg)
Miscellaneous	30 450 lbm (13 810 kg)
Fuel pellet diameter	3.417×10^{-2} ft (0.0104 m)
Total vessel weight	1.945×10^{6} lb (882 000 kg)
Drywell	
Free volume	270 100 ft^3 (7648 m)
Design temperature	330°F (170°C)
Internal design pressure (gage)	30 psi (0.2 MPa)
Vent pipes	
Number	135
Internal diameter	2.33 ft (0.71 m)
Suppression pool	
Water volume	136 000 ft^3 (3 850 m^3)
Design temperature	185°F (85°C)
Internal design pressure (gage)	15 psi (0.1 MPa)

In sequence TC (a transient event with failure of the reactor protection system), the control rods fail to insert and the reactor stays at elevated power, dumping heat to the suppression pool through the safety/relief valves. The emergency core cooling system supplies makeup water to the primary system, with the resulting equilibrium power level being determined by the makeup-flow rates and the core reactivity coefficients. Since the equilibrium power level of the reactor (16 percent of full power) exceeds the heat-removal capability for cooling the pool, the temperature of the pool rises, and the pressure in the containment increases to the failure pressure. After the containment fails, the containment pressure decreases, the suppression pool boils, and the makeup pumps stop delivering coolant to the vessel. As the core heats up and melts, fission products released from the fuel flow with the gases through the steam separator (see Figure A-2). The flow then divides with a major fraction, estimated at about 85 percent, passing through the steam dryers and the balance bypassing the steam dryers through an outer annular region. These flows merge at the steam line and pass through safety/relief valves and relief lines. The flow exits the relief line into the suppression pool through a sparger. From the top of the suppression pool, gases and entrained aerosols disperse in the outer containment volume before leaking through the breach in containment. Although it is possible that the containment spray system could survive failure of the containment, this would be difficult to demonstrate with confidence. In these analyses, it is assumed that the spray system does not operate.

The enclosure building would be expected to fail at the time of containment failure. The mode of failure of the enclosure building would be sensitive to the mode of failure of the containment building.

Following melt-through of the reactor vessel, the fission products airborne in the vessel would flow to the drywell as the system depressurized. Fission products released with time from RCS surfaces would also enter the drywell. Attack of the concrete by the molten core would also result in a source term to the drywell. The fission products would then be carried via the suppression pool to the outer containment volume, and through the break in containment to the environment.

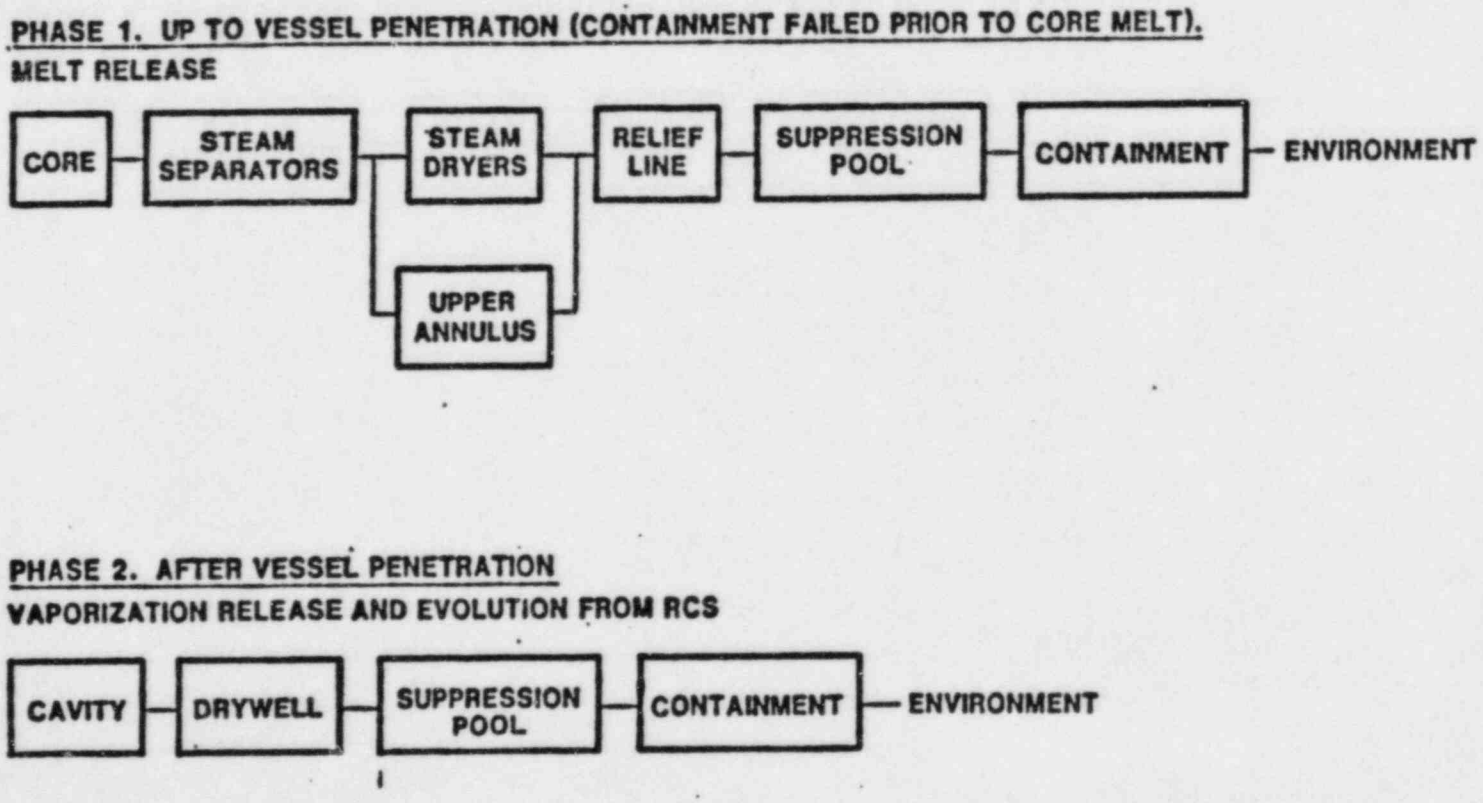

Figure A-2 Flow path for fission-product transport in sequence TC. [BMI-2104, Vol. III]

APPENDIX B

High-Pressure Melt Ejection Effects in Grand Gulf

R. J. Lipinski

This appendix addresses the possible source-term consequences of a high pressure-melt ejection (HPME) at vessel failure during a TC accident at Grand Gulf. The first section introduces the features of a HPME. The second section addresses the question of whether a HPME can occur at Grand Gulf during a TC accident. The third section considers the time scale of a HPME. The fourth and fifth sections consider the effects of a HPME, in particular whether a HPME can fail the drywell integrity or cause a tmeporary failure of suppression pool scrubbing because of excessive gas flow.

HPME Characteristics

The Zion Probabilistic Safety Study (1) noted that molten core debris resting on the bottom of a PRW reactor vessel could fail the vessel locally where instrumentation penetrated the vessel. If this failure occurred while the vessel was at high pressure, the melt could be forcefully ejected, and debris fragmentation and dispersal could occur. Recent experiments at Sandia National Laboratories, Albuquerque (SNLA) (2,3) have shown even more fragmentation and dispersal than suggested in ZPSS. Figure 1 shows the results from this HIPS-2C test in which 80 kg of molten materials from iron-alumina thermite were ejected under 117 bars of pressure through a hole initially 25 mm in diameter into a 1/10 scale model of the Zion reactor cavity and keyway. There was no enclosure building for this test. The 2-m tall apparatus may be seen in the lower right corner of Figure 1a.

The resulting dispersal, fragmentation, and aerosol cloud may be seen in Figures 1b through 1d. The height of the plume in Figure 1d is 34 meters.

An important consequence of fragmentation and ejection of molten materials into a volume of gas is a rapid direct heating of the gas by the stored sensible heat of the fragments and by oxidation of metallic fragments. This heating results in a rapid rise in pressure. Such an effect was observed in the SPIT-19 test (3) in which 10 kg of molten materials were ejected with 128 bars of pressure. The ejected gases were calculated to cause a negligible pressure increase in the building that enclosed the experiment. But the direct transfer of heat to the building atmosphere caused a pressure increase from 1.0 bars to 1.3 bars. This resulted from a rapid transfer of 20% of the available thermal energy, or 10% of the availble thermal and chemical energy, to the building atmosphere.

Another important feature of a HPME is the production of copious amounts of aerosols. (Note the aerosol cloud in Figure 1d.) The aerosols appear to be formed when dissolved gasses rapidly come out of solution during the depressurization. The large volumetric gas flow through the melt sparges the volatile contents of the melt (which then condense into aerosols), and also breaks up the bulk melt materials. The former aerosols are typically smaller (about 1 micron) than the latter (about 10 microns and larger) and could be composed selectively of volatile or semi-volatile fission products. Such aerosols can pose a significant source term.

1.a t = 0.1 sec.
MELT JUST EMERGING FROM CAVITY EXIT.
VELOCITY = 30 m/sec.
VERTICAL SCALE IS 38 METERS.

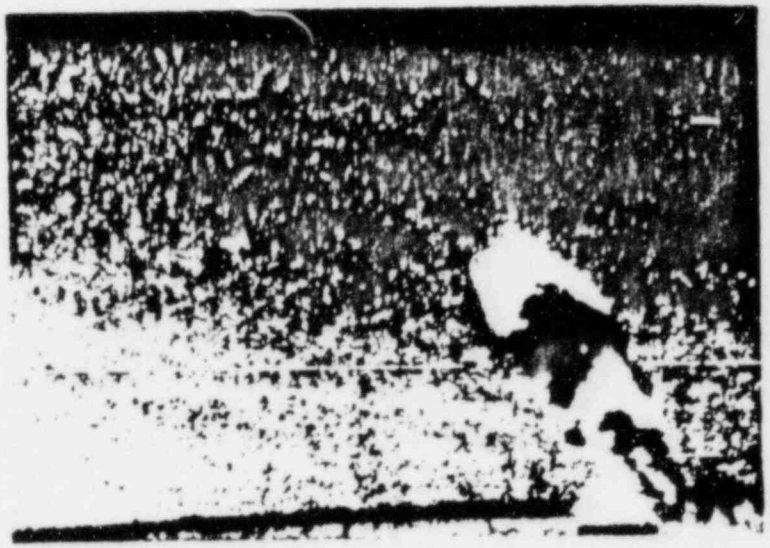

1.b t = 0.5 sec.
MELT EJECTION FROM CAVITY COMPLETE.
AEROSOL CLOUD BEGINS TO FORM.

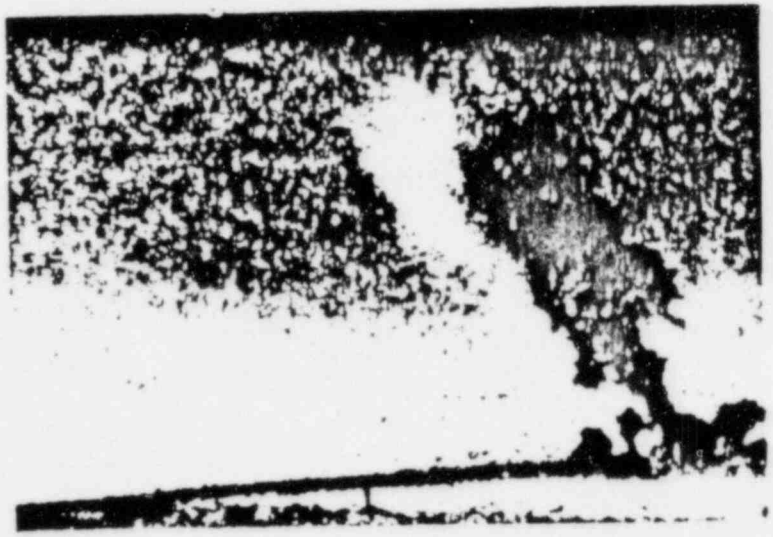

t = 1.0 sec.
1.c EJECTED MELT REACHES MAXIMUM HEIGHT.

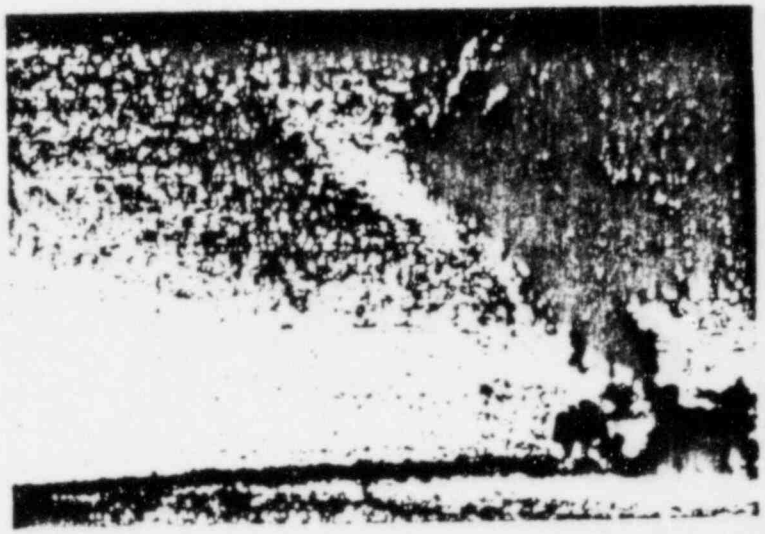

t = 1.5 sec.
1.d SEPARATION COMPLETE

Figure 1 Melt Ejection from 1/10th Scale Concrete Cavity

Can a HPME Occur at Grand Gulf?

A HPME requires (1) high pressure (over 5 to 10 bars) in the reactor vessel at the time of failure, (2) molten materials at the base of the vessel at the time of failure, and (3) a small failure hole in the base of the vessel. For the HPME to rapidly pressurize a containment volume, there is an additional requirement of a fairly simple path from the vessel failure location to the dispersal target volume. These four requirements will be considered one at a time.

A "hands-off" TC sequence in the Grand Gulf BWR is predicted to result in a core meltdown with the reactor vessel remaining at high pressure (4). This prediction depends on the assumption that the vessel is not depressurized by the Automatic Depressurization System (ADS). The ADS is activated when (1) the reactor water level is low (near the top of the core), (2) the drywell pressure is high, and (3) the low pressure injection pumps or residual heat removal pumps are running. All three conditions must be satisfied to activate the ADS (5). In the TC sequence, the containment fails and the drywell pressure is predicted to drop to atmospheric 10 minutes before core uncovery. Thus, the requirement of high drywell pressure is not satisfied and the ADS is not expected to operate during the core degradation phase of the accident. The reactor vessel pressure is expected to remain high.

The existence of a large melt mass in the reactor core region is well within the present state of uncertainty. The details of core meltdown progression are not known, and it is possible that a blockage may form within the core region when melting (or liquefying fuel drips and refreezes. Such a blockage could accumulate a melt mass above it before it was penetrated. Such a

molten mass might fragment and freeze when it fell into the water in the bottom of the rector vessel. In such a case, the debris would have to remelt before vessel failure in order to produce a HPME. Alternatively, the large molten mass could penetrate through the water without fragmenting and begin immediately to attack the vessel bottom. Such a possibility is predicted by Henry and Fauske's model for melt fragmentation (6). Thus the existence of a large mass of molten materials at the bottom of the reactor vessel at the time of failure is within the current state of uncertainty.

The final criterion of a HPME is a local failure of the vessel bottom. Figure 2 shows the penetration of a control rod through the bottom of the Grand Bulf pressure vessel (from Reference 5). The junction with the control rod housing is a J weld on the inside of the vessel. It is certainly plausible that this weld would fail first under attack by molten debris. Since the pressure in the vessel is predicted to be about 80 bars at this time, molten materials would be forced out the failure point and could quickly ablate a larger hole. Such a scenario is also suggested for the Zion PWR in the Zion Probabilistic Safety Study (1).

For a HPME to have significant consequences with respect to pressurization or aerosol dispersal, there must be a fairly simple path from the vessel failure point to the rest of the containment volume of interest. Two likely ejection paths for the Grand Gulf plant are shown in Figure 3. One is through a 0.9-m by 2.1-m hole in the pedestal wall below the reactor vessel for pedestal access and control rod drive removal. The base of the hole is 3.0 meters above the bottom of the cavity. The other path is through an access hole containing the control rod hydraulic lines. The base of that access is 6 meters above the cavity floor.

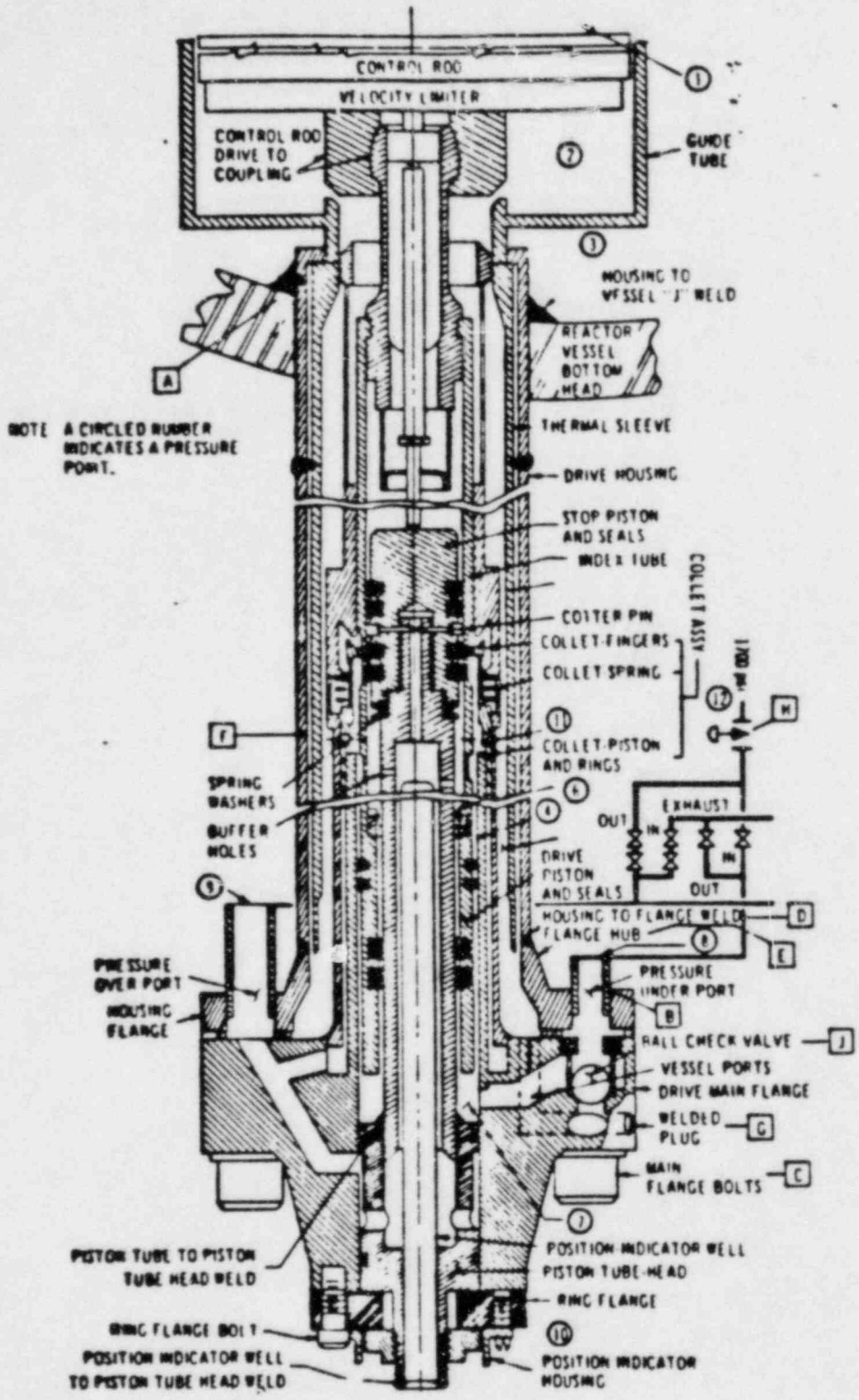

FIGURE 2 Control Rod Drive Schematic

Once outside the pedestal wall, there is a clear path to the rest of the drywell volume. These are direct enough paths so that any aerosols released during the HPME will be easily swept into the drywell volume. However, since the lowest hole in the pedestal is 3 meters above the reactor cavity floor, it is likely that most of the ejected melt will not be swept into the drywell. Nonetheless, considering the vitality of the ejection shown in Figure 1, it is very plausible that a sizeable fraction of the ejected melt will be rapidly distributed throughout the drywell volume.

In summary, the three requirements for a HPME appear to be satisfied for a TC sequence at Grand Gulf. The three requirements are (1) high pressure (over 5 to 10 bars) in the reactor vessel at the time of failure, (2) molten materials at the base of the vessel at the time of failure, and (3) a small failure hole in the base of the vessel. However, the requirement for rapid heating of a containment volume (i.e., the drywell) is the existence of a fairly simple path from the vessel failure location to the containment volume. This criterion is only marginally met, and one would not expect most of the ejected melt to be dispersed throughout the drywell.

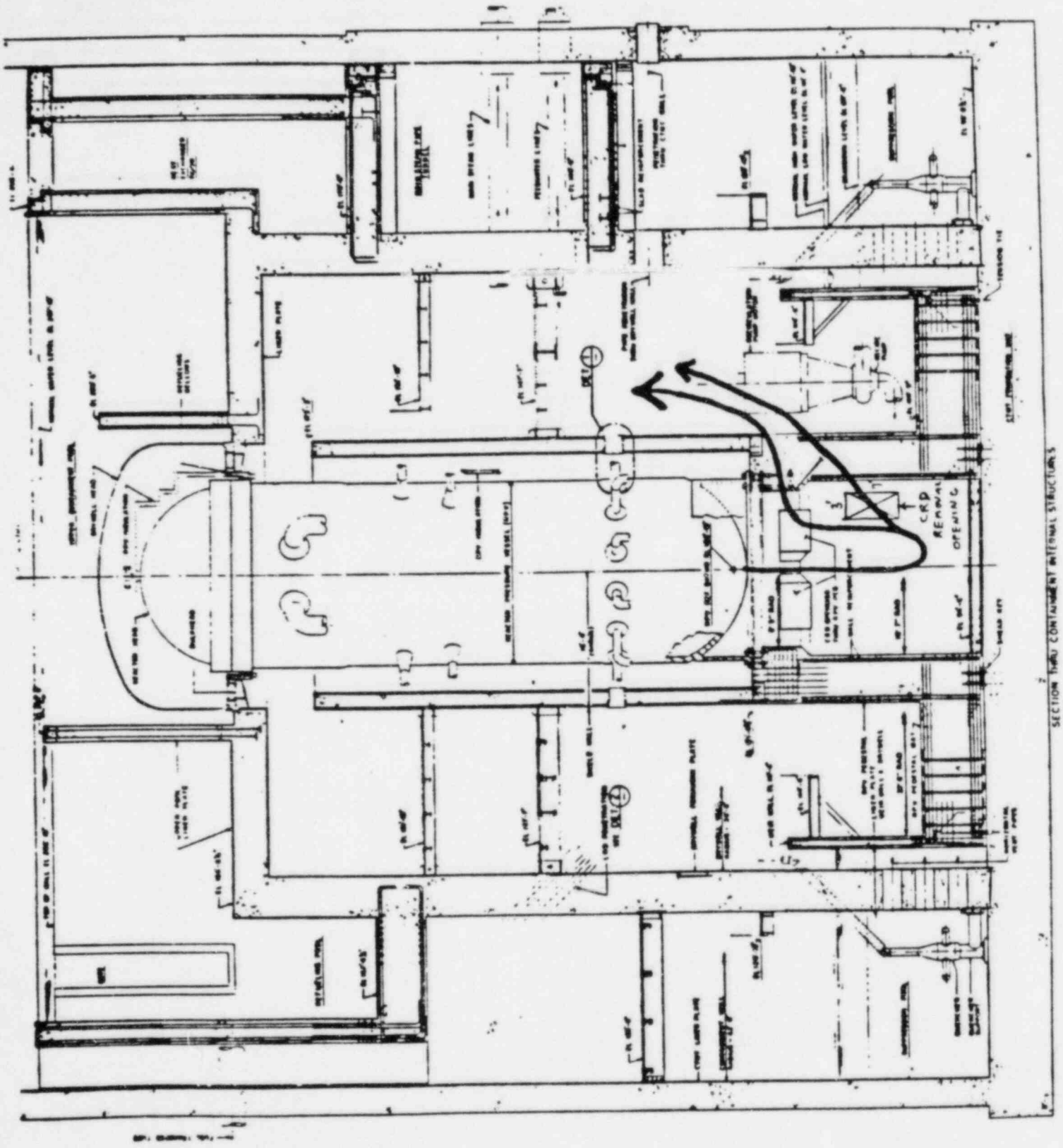

Figure 3 Path for HPME through control rod drive Openings in pedestal

Timing of a HPME at Grand Gulf

A model for the time involved in a HPME was developed in ZPSS. The resulting equations are

$$U = \left[\frac{2(P_o - P_a)}{\rho_f}\right]^{1/2} \tag{1}$$

$$r = r_o + B\,t \tag{2}$$

$$m = \rho U \pi \left[r_o^2 t + r_o B\, t^2 + \frac{B^2 t^3}{3}\right] \tag{3}$$

$$B = \frac{f\,\rho_f\,C_f\,U\,(T_f - T_{f,m})}{2\,\rho_s\,(C_s(T_{s,m} - T_s) + h_{lf,s})} \tag{4}$$

where U is the melt velocity, r is the radius of the hole in the vessel, m is the ejected melt mass, B is the hole growth rate, f is a friction factor (0.005), ρ_f is fuel density, C_f is fuel specific heat, T_f is fuel temperature, $T_{f,m}$ is fuel melting temperature, ρ_s is steel density, C_s is steel specific heat, $T_{s,m}$ is steel melting temperature, T_s is steel temperature, and $h_{lf,s}$ is the latent heat of fusion for steel.

The above equations were applied to the Grand Gulf TC conditions with an assumed molten fuel temperature 400°C above the melting temperature, and an initial hole size of zero. The predicted vessel hole size and ejected melt mass are shown in Figure 4. It takes a few seconds to develop a hole of a few centimeters, during which time very little mass is ejected. After that, the bulk of the available melt mass is ejected in a few seconds. For a base case of 50% of the core material (i.e., about 100,000 kg), 90% of the melt is ejected in about 5 seconds.

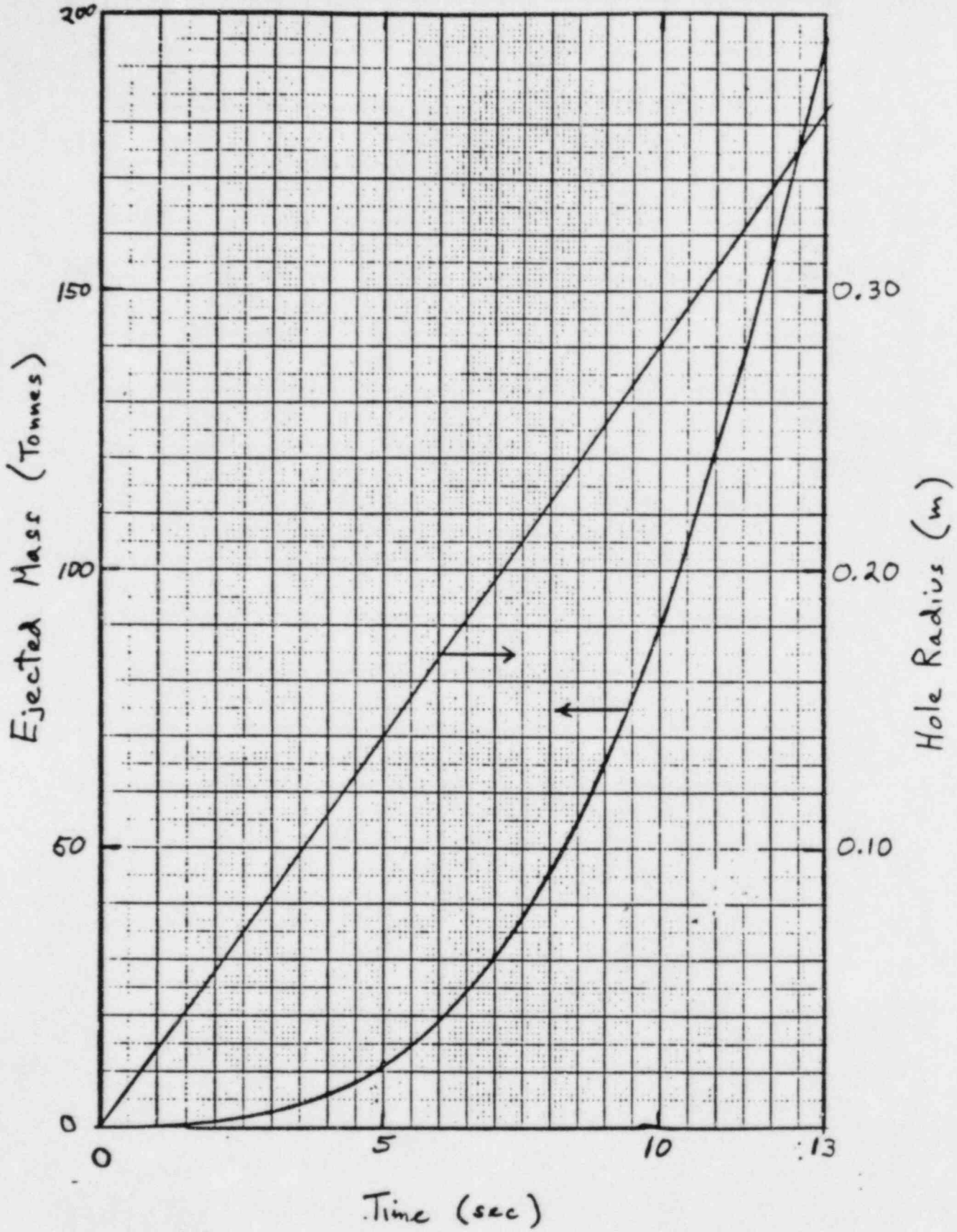

Figure 4 Hole Size and Ejected Mass
for Grand Gulf TC Sequence

The ejected melt can give its heat rapidly to the drywell atmosphere only while the particles are airborne. A particle can fall the 25-m height of the drywell in 2.3 seconds. Thus, the major effects of a HPME will occur over a relatively short period of about 7 seconds.

After the melt is ejected, the high-pressure steam remaining in the reactor vessel must also be ejected. The hole in the vessel after melt ejection is about 0.60 meters in diameter. By coincidence, this is the same diameter as the recirculation pipes. Thus, the blowdown following the melt ejection is similar in steam flow rate to that in a large-break LOCA (but is not as long since there is no liquid water in the vessel to maintain the steam flow). The time required to blow down the steam in the vessel is 11 seconds (assuming critical flow).

In summary, the HPME heating process occurs over about 7 seconds (for a melt mass equal to 50% of the mass in the core region), and the vessel blow down lasts for about 11 seconds after that.

Possible Consequences of a HPME: Failure of Drywell Integrity

In the Grand Gulf plant, a high pressure melt ejection would pressurize the drywell. The possibility of a resulting failure of the drywell must be assessed, but consideration must be taken of the 135 vent tubes (0.71-m I.D.) leading into the surrounding suppression pool with a combined area of 53.2 m^2. In order to assess the possibility of drywell failure, estimates of drywell pressurization assuming no venting were made first, and then the effect of venting was estimated.

Pilch has developed a code that estimates the pressure increase in a containment building caused by a rapid dispersal of molten fragments (7). The code includes heating from both latent and specific heat, as well as an option for heating from oxidation of the hot metals in the melt. This code was used to make a scoping study of the Grand Gulf drywell pressurization

assuming no gas flow through the vent tubes.

The input parameters varied in the study were melt mass ejected into the drywell atmosphere, fragment diameter, initial temperature, and chemical heating. The base case conditions are given in Table 1. They were obtained from the conditions at core slumping using the MARCH code as modified for BWR's by S. Hodge (8). The melt mass at the time of core slump was 75% of the core in this MARCH run, but the mass involved in the HPME base case was reduced to 10% because of the indirect path out of the reactor cavity. In addition, there is an inherent assumption that after slump the melt penetrates the lower plenum without much quenching or oxidation. [Such penetration is predicted by the Henry-Fauske model (6)]. The average fragment diameter is small (2 mm), since large fragments would not make the necessary turns to exit the cavity as easily as small ones would (which is why the dispersed mass is small). The molten material was assumed to be swept to the top of the drywell, and the fragments were allowed to heat the atmosphere only while they were falling.

Table 1: Base case parameters for the sensitivity study for high-pressure melt ejection pressurization of the Grand Gulf drywell (assuming no venting).

Drywell volume (m^3)	7649
Initial pressure (bars)	1.0
Initial steam fraction	1.0
Melt mass (kg)	1500 (50% of core)
UO_2 fraction	0.64
Zr fraction	0.25
ZrO_2 fraction	0.05
Fe fraction	0.06
Initial temperature (K)	2300
Particle diameter (mm)	2.0

The results of the sensitivity study are shown in Figure 5. The curves terminate at 2.3 seconds because heat is transferred efficiently only while the particles are falling, and 2.3 seconds is the time it takes a particle to fall the height of the drywell (25 m). The drywell pressure is sensitive to the melt mass involved, the melt initial temperature, the average particle diameter, and in-flight oxidation of metal.

The final drywell pressure (without venting) ranges from 3 to 6 bars if the effect of oxidation is not included. With oxidation, the pressure increase can be higher. The time required to approach the final pressure level ranges from about 0.3 to 1.5 seconds, assuming all the melt is released instantly. But the melt is predicted to be released over about a 5 second time span (as described previously), so the actual time span involved in pressurizing the drywell is about 6 seconds.

The design differential pressure for the drywell is 2.0 bars. Most of the cases considered lie in the range of differential pressures of 2.0 to 5.0 bars. These pressures are above design, but are probably not enough for failure to be expected, since calculated failure pressures are usually two to six times design pressures. However, with in-flight oxidation included, the drywell pressurization (without venting) approaches values where failure becomes a concern. Therefore, it is necessary to consider the effect of the vent tubes to the suppression pool.

In order to vent the steam in the drywell, the water behind the weir wall and inside the vent tubes must be cleared out. The surface area of the water behind the weir wall and the vertical cross sectional area of all the vent tubes are each about 50 m^2,

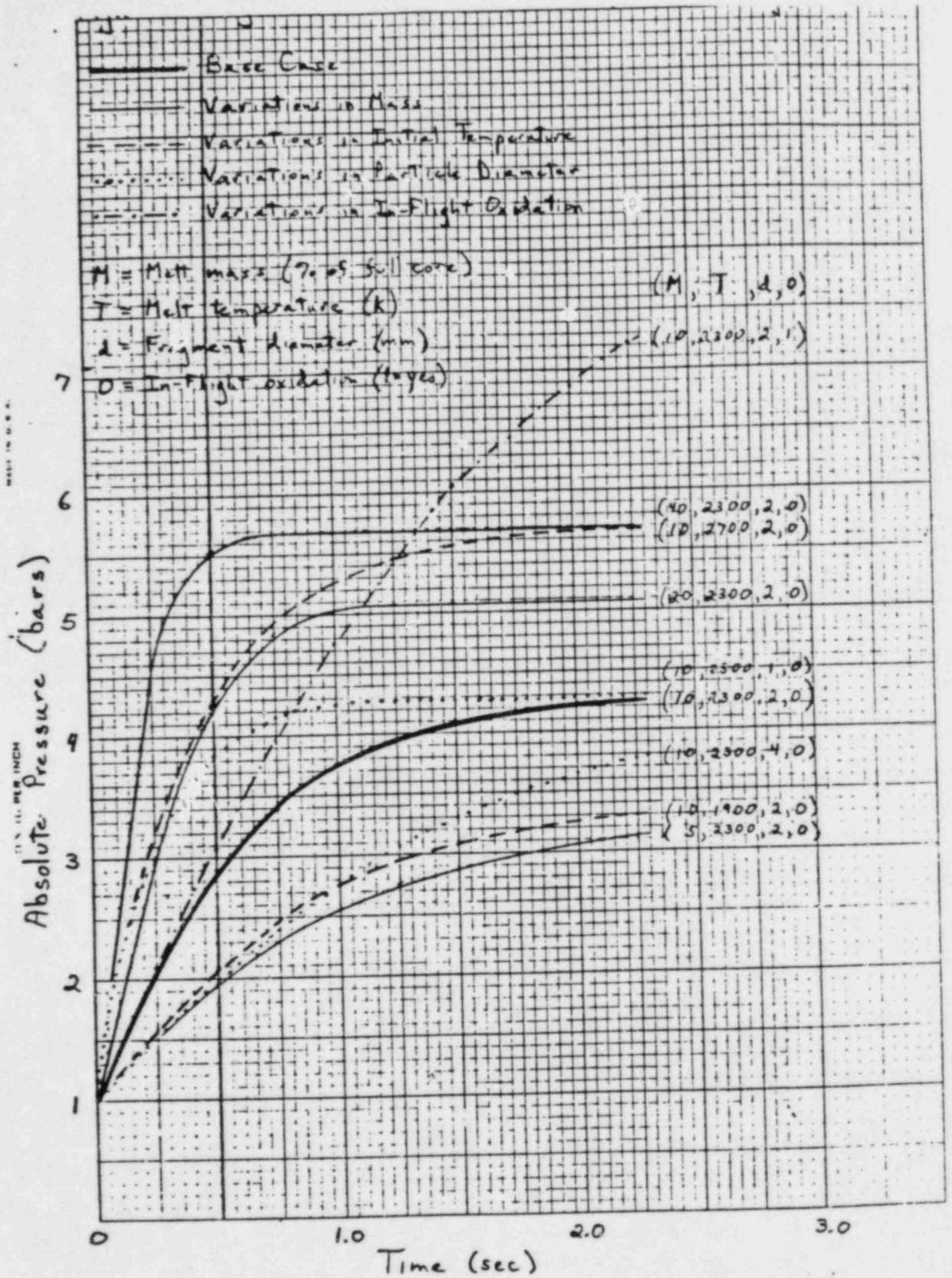

Figure 5 Drywell Pressurization from HPME
(With No Venting)

so the water may be treated as one continuous slug. In order to vent into the suppression pool, the water slug must be pushed a distance of about 5.0 meters. The time required for the slug to be accelerated this distance is

$$t = \left[\frac{2\rho}{\Delta P} L_s L_t\right]^{1/2}$$

where ρ is the water density, ΔP is the ressure difference across the slug, and L_s is the slug length, and L_t is the travel distance. For an average ΔP = 3E5 Pa, the time required is 0.4 seconds. Since, as mentioned previously, the melt ejection and pressurization process takes about 6 seconds, water inertia in the drywell and tubes is not sufficient to allow pressurization of the drywell to damaging pressures.

After the water is cleared from the vent tubes, the rate of pressurization of the drywell depends on how much the suppression pool retards the steam flow. (Since the pool is saturated, and the steam is very much superheated, condensation will not occur.) The pool water is most efficient in retaining the gas when the water mass is in slug form. An appropriate slug thickness (L_s) to use is the thickness of water above the top vent tube (2 m). An appropriate acceleration distance is half the height of the drywell (12 m). With an average ΔP = 3E5 Pa, the time required for the slug traverse is 0.4 seconds. Again, this is smaller than the 6-second duration of the melt ejection and pressurization process, so the full pressurization of the drywell shown in Figure 5 cannot occur. (Note: Flow resistance in the vent tubes is negligible.)

Since the flow path from the reactor cavity is somewhat indirect for large amounts of melt dispersal, and since peak calculated pressures in the drywell without venting are only about three times the design pressure, and since the time scale for venting (about 2 seconds) is less than that for pressurization (about 3 seconds), it is concluded that failure of the drywell integrity by a HPME is not within the current range of reasonable uncertainty.

Possible Consequences of a HPME: Suppression Pool Failure

The suppression pool can remove fission-product gases and aerosols from steam vented from the drywell. However, the pressure developed during a HPME and the subsequent vessel blowdown may produce steam flow rates through the pool which could greatly reduce its efficiency in retaining fission products for a short period of time. A loss of retention capability during the period immediately following vessel failure would be particularly unfortunate for two reasons.

First, a HPME produces large amounts of aerosols from the sparging action of gases through the melt. These aerosols could be composed preferentially of volatile or semi-volatile fission products, and would form a radionuclide source in the reactor cavity coincident with vessel failure. Second, the aerosols remaining suspended in the reactor vessel at vessel failure, as well as those resuspended during the vessel blowdown, would be blown out of the vessel and would also form a strong radionuclide source in the reactor cavity coincident with vessel failure. Both of these aerosol sources would be blown out of the reactor cavity and into the drywell volume easily and rapidly because aeerosols follow gas flows much easier than large melt fragments.

The aerosols then could be ushered through the suppression pool without retention because of the high gas flow rate induced by HPME direct heating of the drywell atmosphere and the subsequent rapid vessel blowdown through a large hole in the bottom of the vessel.

Figure 5 indicates a drywell pressurization to about 4 bars for the base case if venting is artificially prevented. This would occur over a period of about 6 seconds (ejection time plus atmosphere heat time), yielding an average pressurization rate of 0.4 bars/sec. A large-break LOCA with critical steam flow through a 0.6-m diameter pipe break would pressurize the drywell at a rate of about 0.5 bars/sec (again, without venting). Thus, the loading rate in the drywell from a HPME is very similar to that of a large-break LOCA. In addition, the vessel hole left after the melt ejection is about equal to that of a large pipe break (0.6-m diameter). So the vessel blowdown following a HPME is also like a large-break LOCA and would last about 11 seconds. The total duration of the combined LOCA-like load is about 16 seconds.

The response of the suppression pool to a large-break LOCA is difficult to predict with precision, but it is discussed in the General Electric Standard Safety Assessment Report (GESSAR) (9). The predictions of pool behavior are based on test data from an experimental model of a suppression pool and associated containment structures. The pool is predicted to move from slug flow to spray flow within about 3 seconds. This is duplicated in Figure 6, taken from reference 9.

In the LOCA case, the pool behavior is driven by the non-condensible air component of the gas flow. After only 3 to 5 seconds, the air supply is exhausted and only steam follows. Since the pool is subcooled in the LOCA analysis, the steam is then condensed within the pool and the water collapses back into a pool. Howver, in the HPME case during a TC accident, the pool is saturated, the steam is very superheated, and there is some hydrogen in the mixture. Thus steam condensation will not occur and the pool will remain suspended for the full duration of the HPME and blowdown.

The fission-product removal efficiency for a froth or spray as depicted in Figure 6 is difficult to assess. The superficial velocity of the superheated steam through the suspended water may be estimated from the total mass of steam moved and the duration of the HPME and vessel blowdown. A blowdown of 14300 kg of steam into a cross-sectional area of 620 m^2 over 16 seconds requires an average steam velocity of 2.5 m/s. (Wallis' minimum flow velocity for fluidizing water into drops is 1.3 m/s for steam near saturation, which supports the GESSAR description of the pool as being in droplet form.) If the droplets are dispersed over 10 meters (as suggested in Figure 6), the aerosols in the flow will be exposed to the water for only about 4 seconds. This is not much time for fission-product retention in the dispersed spray.

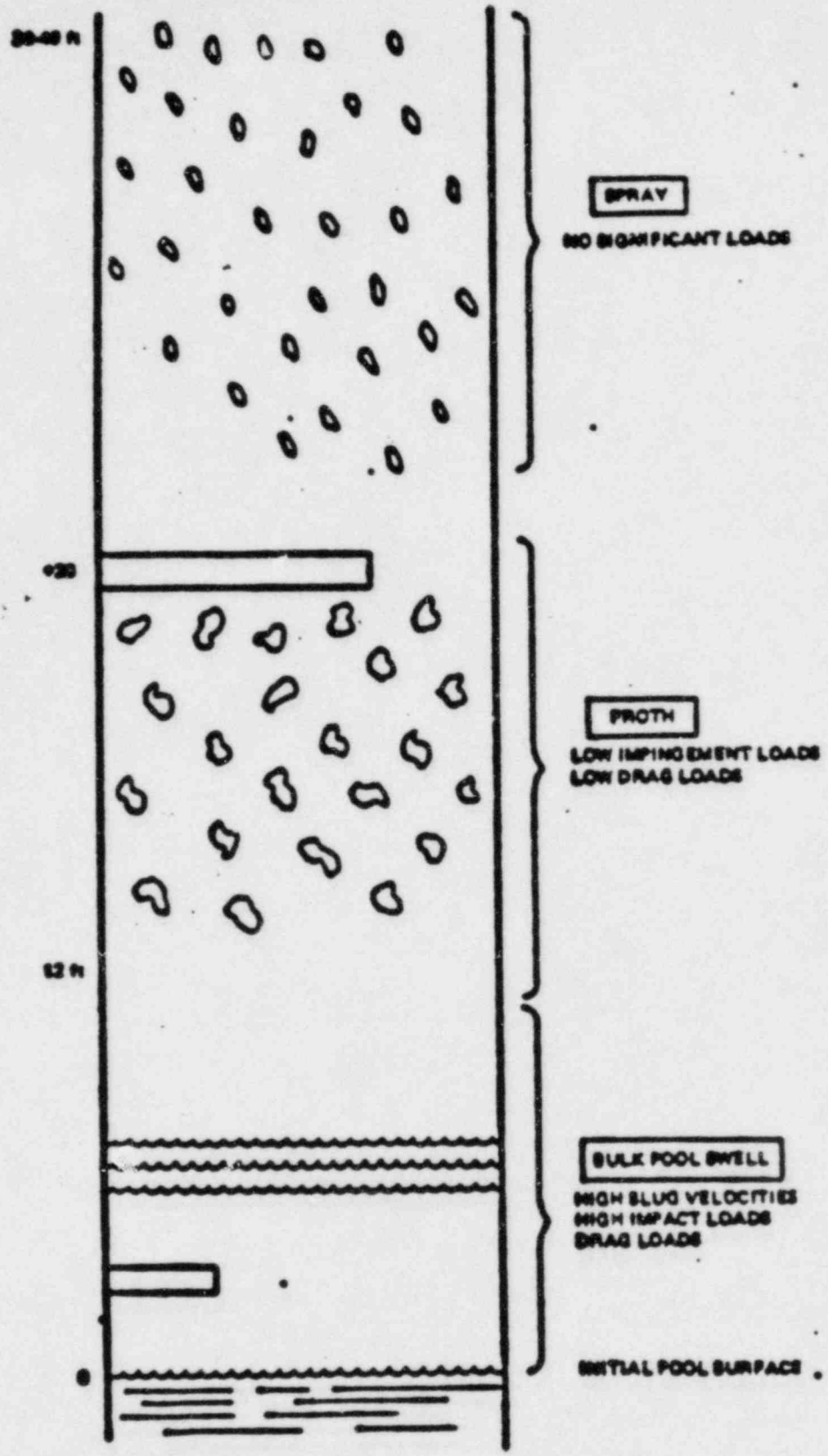

Figure 6 Schematic of the Mark III Pool Swell Phenomenon (from Ref. 9)

Conclusions

A high-pressure melt ejection following vessel failure during a TC accident sequence in Grand Gulf, and the subsequent blowdown of steam from the rector vessel, load the drywell with steam at about the same rate as during a large-break LOCA (0.6-m diameter break). However, the duration is only about 16 seconds. Because of the 135 vent tubes leading into the suppression pool (each tube having a diameter of 0.7 m, this loading on the drywell is not sufficient to fail it structurally. However, the resulting flow of superheated steam through the saturated suppression pool is strong enough to disperse the pool into droplets and essentially eliminate the ability of the pool to retain fission products (but ony temporarily).

This period of scrubbing failure occurs coincident with the release of fission products left suspended in the reactor vessel at the time of failure, coincident with the release of fission products resuspended during vessel blowdown after failure, and coincident with the production of aerosols by gas coming out of solution and sparging through the molten core materials during the high-pressure melt ejection. Thus the net result is that a potentially large radiological source term could be ushered through the suppression pool without retention.

The important uncertain parameters in the events leading to the possible temporary failure of suppression pool scrubbing are (1) the amount of material dispersed high into the drywell, (2) the average fragment diameter of the dispersed mass, (3) the amount of in-flight oxidation of the dispersed metallic fragments, (4) the ablation rate of the hole in the vessel, and (5) the behavior and scrubbing efficiency of the suppression pool with a very high gas flow through it.

References

1. Zion Probabilistic Safety Study, Commonwealth Edison, Chicago, pp. 3.1-66 ff. (1981)

2. W. W. Tarbell, Ktec, Albuquerque, personal communication

3. W. W. Tarbell, in Advanced Reactor Safety Research Quarterly Report, Oct.-Dec., 1983, Sandia National Laboratories, Albuquerque

4. J. A. Gieseke, et al, Radionuclide Release Under Specific LWR Accident Condtions -- Volume IIi BWR, Mark III Design, Batelle's Columbus Labs, Columbus (Draft)

5. Grand Gulf Final Safety Analysis Report, Miss. Power and Light, pp. 5.3-39 and 7.3-9

6. R. E. Henry and H. K. Fauske, Proc. of Thermal Reactor Fuels Mtg. Sun Valley, Idaho (1981)

7. M. Pilch, Sandia National Lboratories, personal communication

8. S. Hodge, ORNL, personal communication

9. General Electric Safety Analysis Report, General Electric, pp. 3B-3 ff.

10. G. B. Wallis, One Dimensional Two-Phase Flow, McGraw-Hill Co., New York, pg. 385 (1969)

APPENDIX C

CORCON Sensitivity Study

D. R. Bradley

C.1 Introduction

The CORCON-MOD1 computer code was developed at Sandia National Laboratories to model the ex-vessel interaction of molten core debris with structural concrete in the reactor cavity.[1] Such a situation may develop in a degraded-core accident when melting of the core occurs followed by failure of the reactor pressure vessel. In the suite of computer codes used in the QUEST study, the MARCH computer code was used for the in-vessel phase of the accident, and thus it provided the initial conditions for the ex-vessel phase that was calculated by CORCON. Output from CORCON was then used in the VANESA code to calculate aerosol generation during the melt-concrete interaction, and finally these results were input into the containment transport codes, NAUA (used in the δ_c study) or CONTAIN (used in the δ_p study). By integrating the code results in this fashion, the impact of ex-vessel core-concrete attack on containment integrity and aerosol/fission-product release can be assessed.

This appendix presents the results of a study that was undertaken to determine the sensitivity of CORCON calculations to uncertainties in input parameters. These results were then input into the VANESA code to determine the sensitivity of aerosol and fission-product release from melt-concrete interactions to the same parameter variations. The VANESA sensitivity study is presented in Appendix D.

The method used in the study and the results presented here are similar to those of an earlier QUEST study[2] of a postulated TMLB' accident at the Surry Nuclear Power Plant. However, there are some important differences between these two studies that will be detailed in the following discussion.

C.2 Description of the CORCON-MOD1 Code

CORCON-MOD1 is a stand-alone computer code that models the interactions of molten core debris with concrete in any one of a number of user-specified axisymmetric cavity geometries. The melt is assumed to be stratified into oxidic and metallic layers according to layer density (denser layers on the bottom). Heat transfer from the molten debris to the concrete ablates (i.e., melts) the concrete surface. When this occurs, evaporable and chemically bound water is released along with chemically bound carbon dioxide. When these gases percolate through the melt, they react chemically with the melt constituents, especially the metallic elements. Hence the gases that exit the melt pool and are released to the containment atmosphere are a mixture of reduced and unreduced species, predominantly H_2, H_2O, CO, and CO_2.

The heat-transfer models in CORCON are based on the assumption that a gas film exists between the melt and the concrete throughout the interaction, and that there is never any direct contact between the molten debris and the cavity surface. At the bottom of the melt, the gas film supports the molten debris in a manner analogous to film boiling, and gases bubble directly into the melt. Along the sidewalls of the cavity, the gases released from the concrete are assumed to enter the film and flow parallel to the concrete surface without entering the melt. Because of these differences in the way gas flow is treated, the heat-transfer mechanisms appropriate to the cavity

sidewalls and bottom are fundamentally different. For this reason, CORCON uses different heat-transfer correlations to evaluate the convective heat-transfer coefficients in these two regions. Muir[1] provides more detailed discussions of the equations used by CORCON.

In addition to convective heat transfer across the gas film, radiative heat transfer is also included. Here it is assumed that the molten debris and concrete surfaces can be treated as optically gray, infinite parallel plates radiating with known emissivities. The surface temperature of the melt is assumed to be the melt-gas interface temperature, which is calculated from a surface-energy balance, while the concrete surface radiates at the user-specified ablation temperature.

Because the surface of the concrete is assumed always to be at the ablation temperature, any heat transferred to the concrete from the melt results in ablation of the cavity surface. At any time, the cavity geometry is defined by the location of a user-specified number of body points, which recede at the local ablation rate. Because the heat flux varies around the periphery of the melt, ablation is also nonuniform. This can be seen in the cavity plot for the base case calculation, which is shown in Figure C-1.

When concrete ablates, it releases both water vapor and carbon dioxide, which CORCON then assumes either percolates through the melt (if it enters from the bottom) or bypasses the melt and flows upward within the gas film (if it enters from the sidewalls). Only the gases that bubble up through the molten debris are allowed to react chemically with it. Here the predominant reactions are oxidation-reduction reactions with the metallic elements in the debris and gas-phase reactions. All

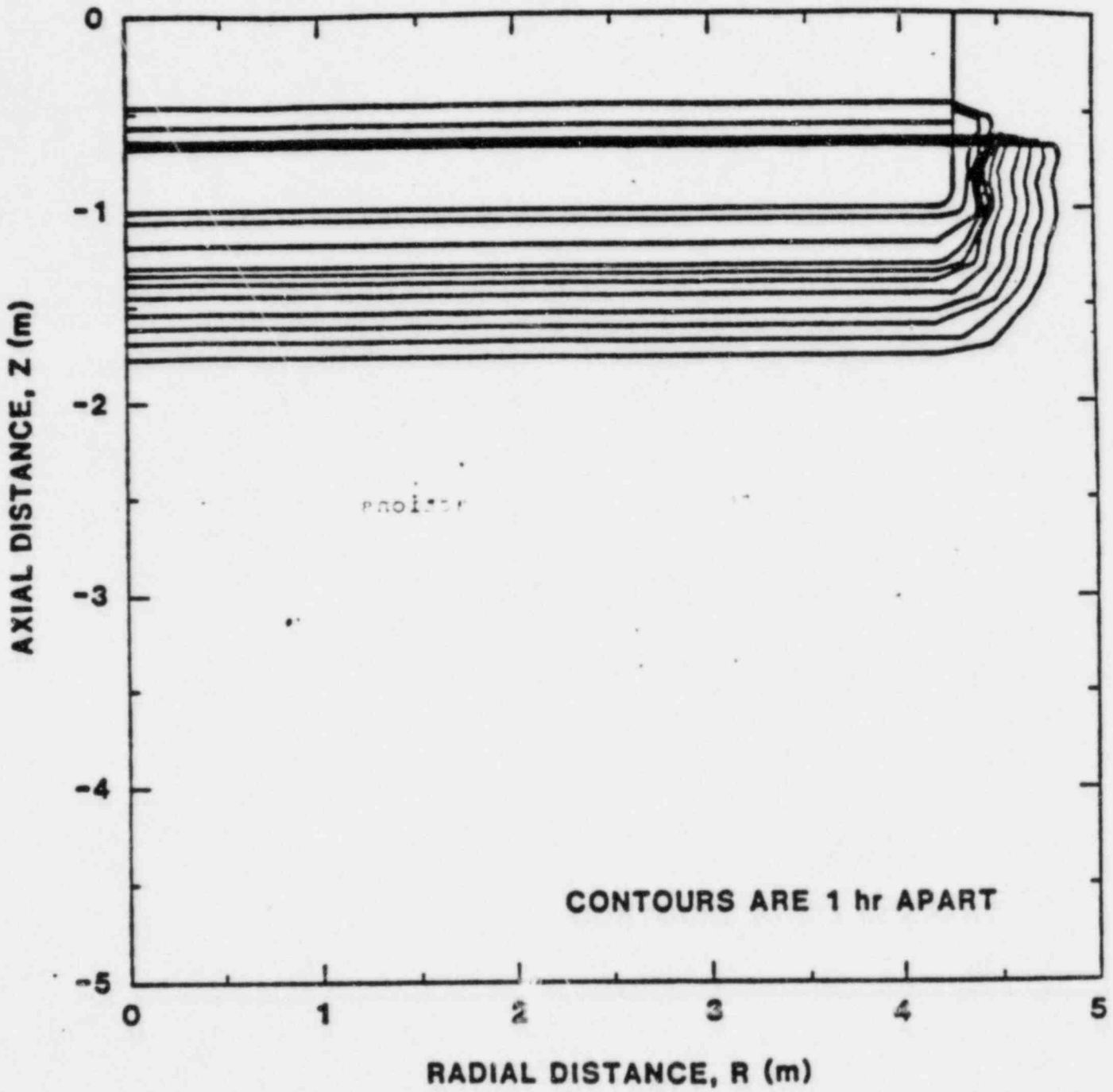

Figure C-1. Cavity plot for base-case calculation.

chemical reactions are assumed to proceed to equilibrium concentrations defined by minimization of the Gibbs free energy. As mentioned earlier, the four most significant gases released to the containment atmosphere are H_2, H_2O, CO, and CO_2.

Initially CORCON assumes that the molten core debris is stratified into a dense heavy oxide layer at the bottom and a less dense metallic layer on the top. As the concrete ablates and the low density concrete oxides (e.g., SiO_2, CaO, MgO) are added to the heavy oxide layer, they reduce its overall density. Eventually the bottom oxidic layer becomes less dense than the metallic layer on top of it. When this occurs, CORCON assumes that the layers reverse position instantaneously. Again, no mixing of the layers is assumed. As might be expected, because of the step change in the local properties of the melt adjacent to the concrete, when layer flip occurs local heat fluxes and thus concrete ablation and gas release change dramatically. This is evident in each of the figures included in this appendix.

One additional note should be made about the version of CORCON used in this study. In the earlier QUEST study of a TMLB' accident at the Surry Nuclear Plant[2], a coding bug was identified that led to unrealistic results. The source of this problem was in the evaluation of the melt viscosity used in the convective heat transfer calculation. An artificially large calculated viscosity led to unreasonably small heat transfer rates and thermal isolation of the melt (predominantly the oxidic phase). As a result, peak melt temperatures of greater than 3000 K were sometimes calculated. Because the aerosol and fission product source terms are so sensitive to melt temperature, this also produced an unusually high aerosol and fission product release. This problem has been corrected in the version of CORCON-MOD1 used in the current study.

There are two categories of input parameters which were examined in the CORCON sensitivity study. Some are propagated from other computer codes (e.g., MARCH) while others are distinctive to CORCON input. The following input variables are included in the first

- Initial melt temperature
- Initial amount of unoxidized zirconium in the melt
- Initial amount of steel in the melt
- Time after scram at which the core-concrete interaction begins.

The second group contains the following variables:

- Fraction of the core that has melted and dropped into the reactor cavity
- Mass fraction of evaporable water in the cavity concrete
- Type of concrete used in the cavity
- Emissivity of the melt layers, and above-pool structures
- Concrete ablation temperature

The parameter ranges chosen for these variables are presented in Table C.1. The upper and lower limits were chosen to represent the range of parameters that might be expected in the event of an accident.

Although nine input parameters were examined, only five were found to significantly influence the CORCON calculation. These variables were:

1. the mass of unoxidized Zr in the melt,
2. the mass of steel in the melt,
3. the fraction of the core in the melt,
4. the concrete type, and
5. the concrete ablation temperature.

The results from these parameter studies are presented in Figures C-2 through C-6.

Table C.1 Parameter Range for the CORCON Sensitivity Study

Parameter	Base Value	Low Value	High Value
Melt temperature (K)	1898	2200	2600
Fraction of Zr unoxidized (%)	60	10	90
Mass of steel in melt (kg)	81270	8127	162540
Interaction start time (min)	197.6	100	1800
Fraction of core in melt (%)	100	50	100
Evaporable water (%)	3.94	3.94	7.88
Concrete type Limestone and Limestone Common S	Limestone	Limestone-	Common S
Emissivity of surroundings and melt phases	1.0	0.001	0.5
Ablation temperature (K)	1875	1690	1780

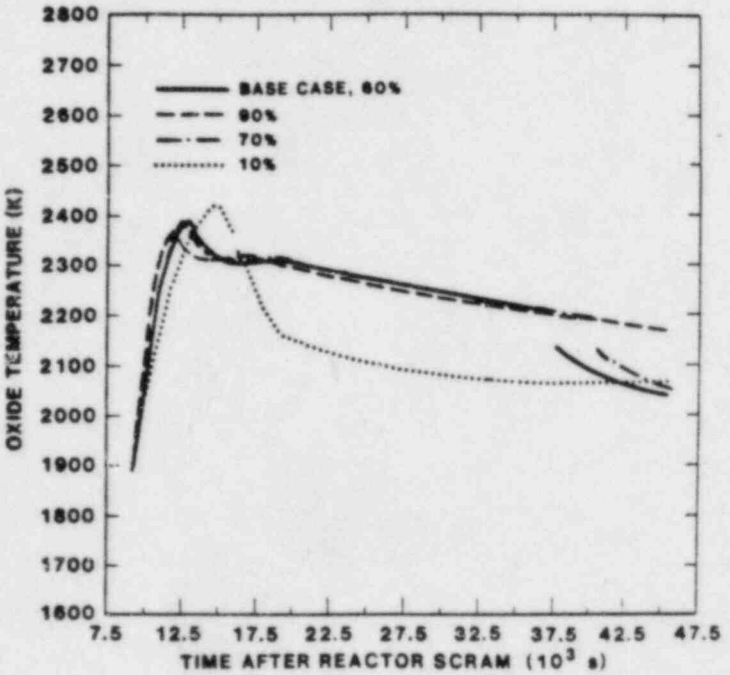

Figure C-2a Effect on oxide temperature.

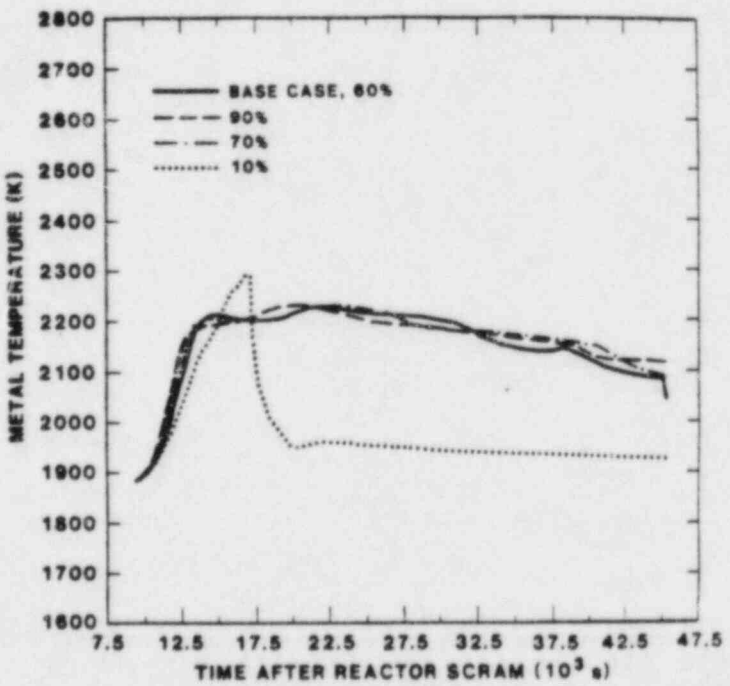

Figure C-2b Effect on metal temperature.

Figure C-2 Effect of variation in zirconium fraction in melt.

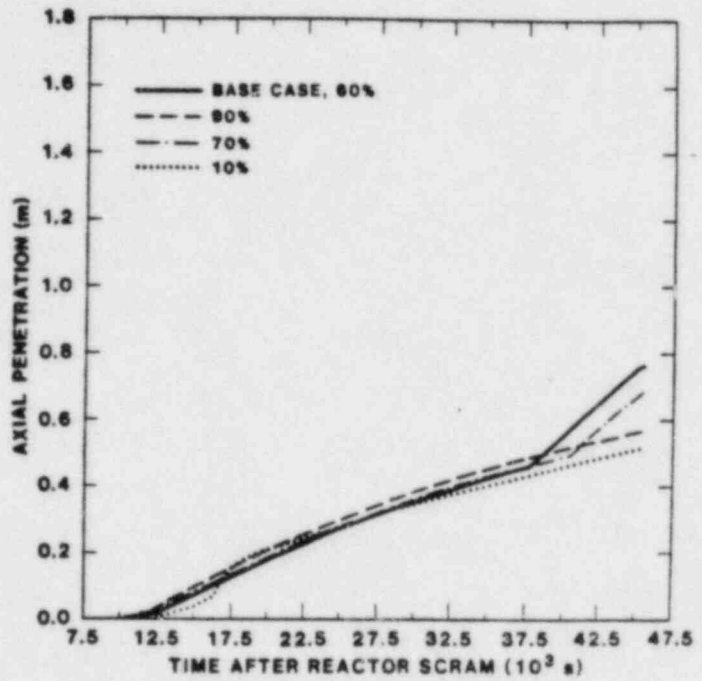

Figure C-2c Effect on axial penetration.

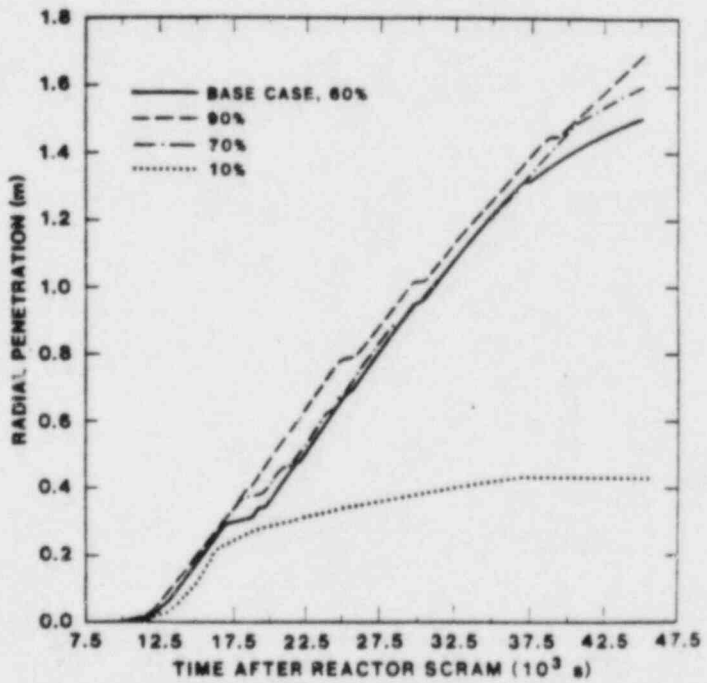

Figure C-2d Effect on radial penetration.

Figure C-2 Effect of variation in zirconium fraction in melt (Continued).

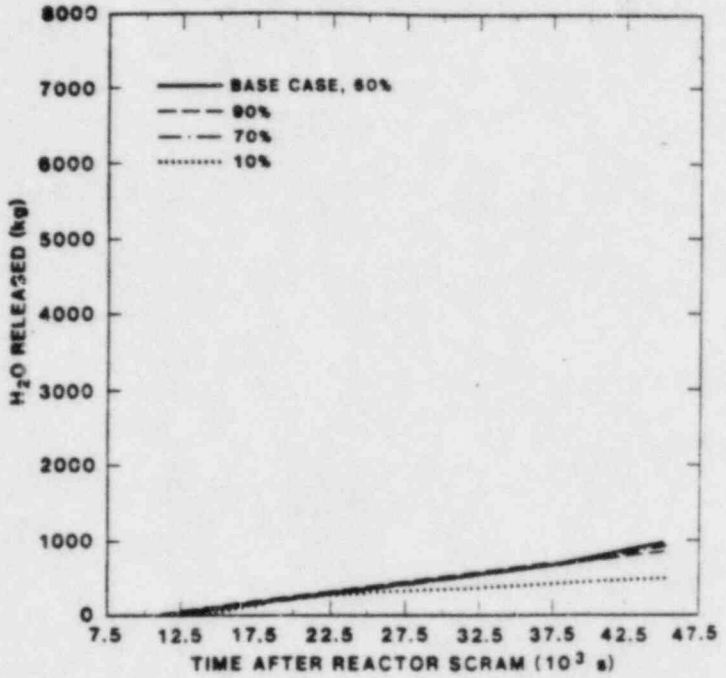

Figure C-2e Effect on H_2O released.

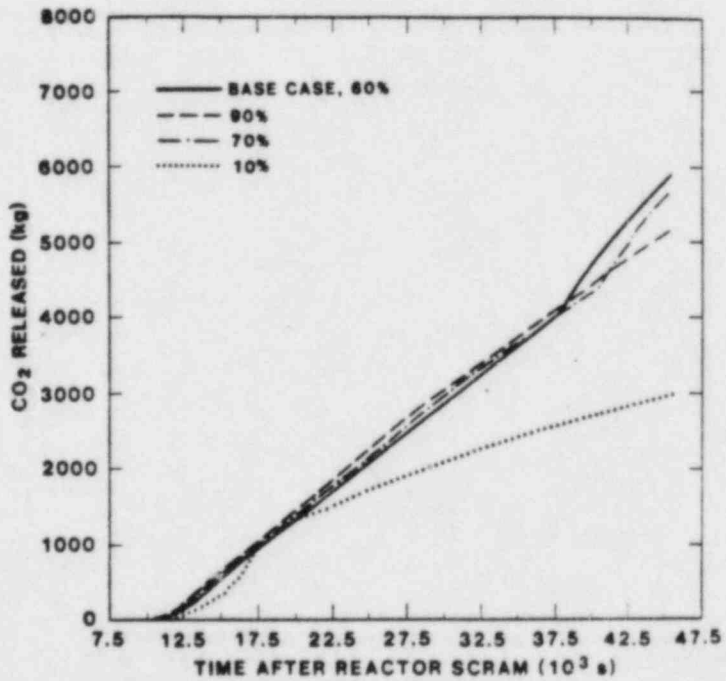

Figure C-2f Effect on CO_2 released.

Figure C-2 Effect of variation in zirconium fraction in melt (Continued).

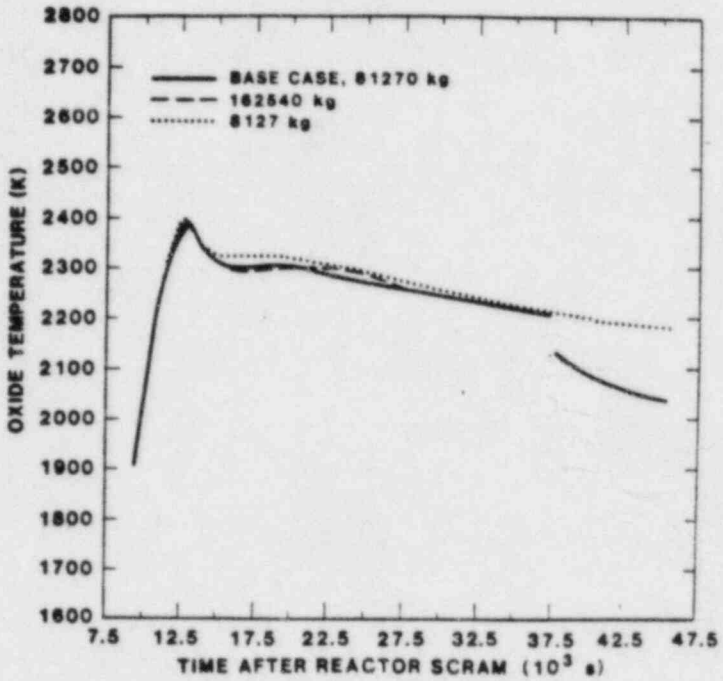

Figure C-3a Effect on oxide temperature.

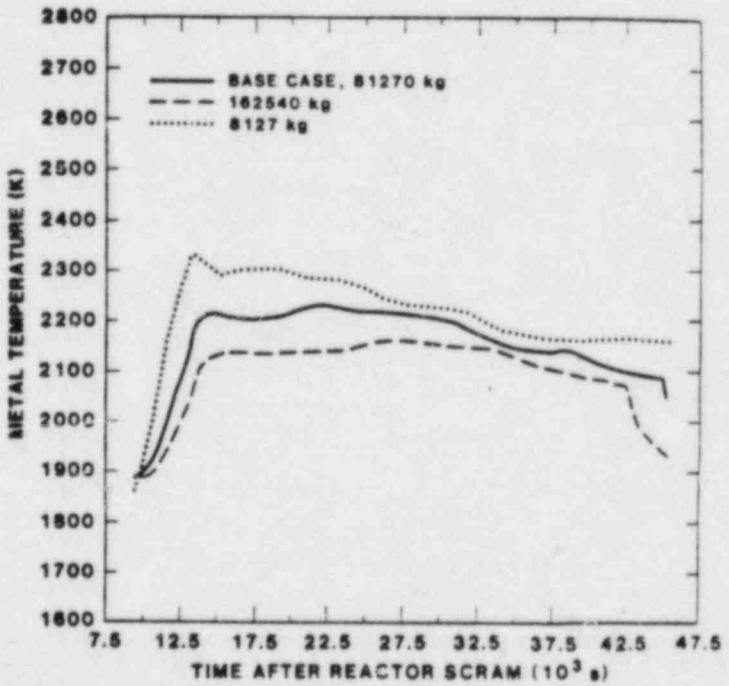

Figure C-3b Effect on metal temperature.

Figure C-3 Effect of variation in mass of steel in melt.

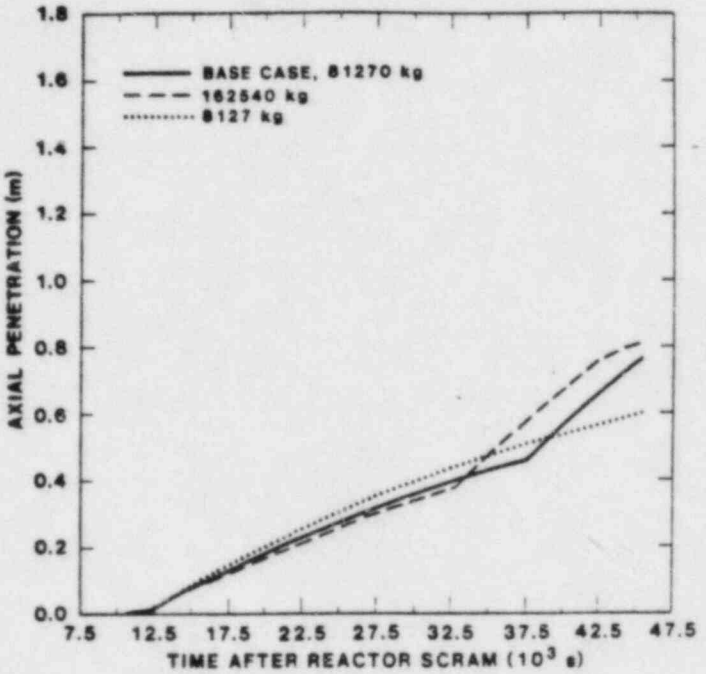

Figure C-3c Effect on axial penetration.

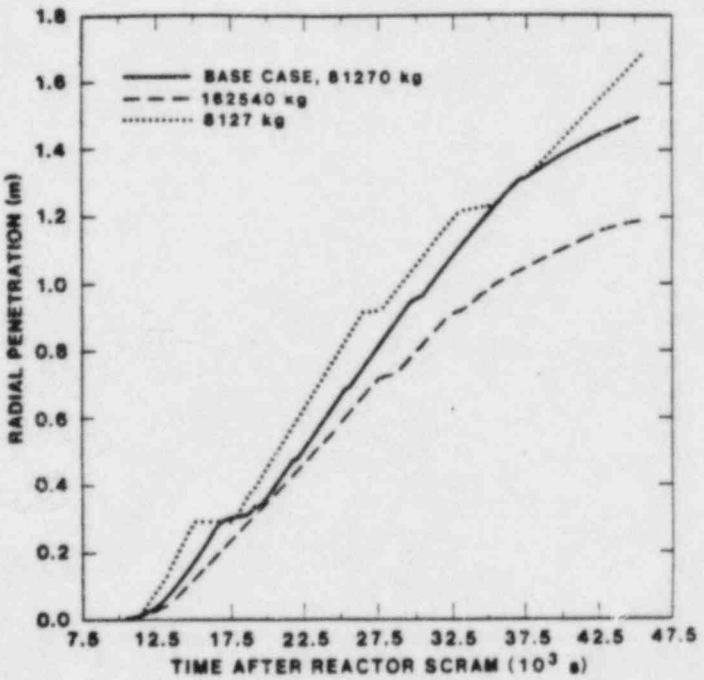

Figure C-3d Effect on radial penetration.

Figure C-3 Effect of variation in mass of steel in melt. (Continued).

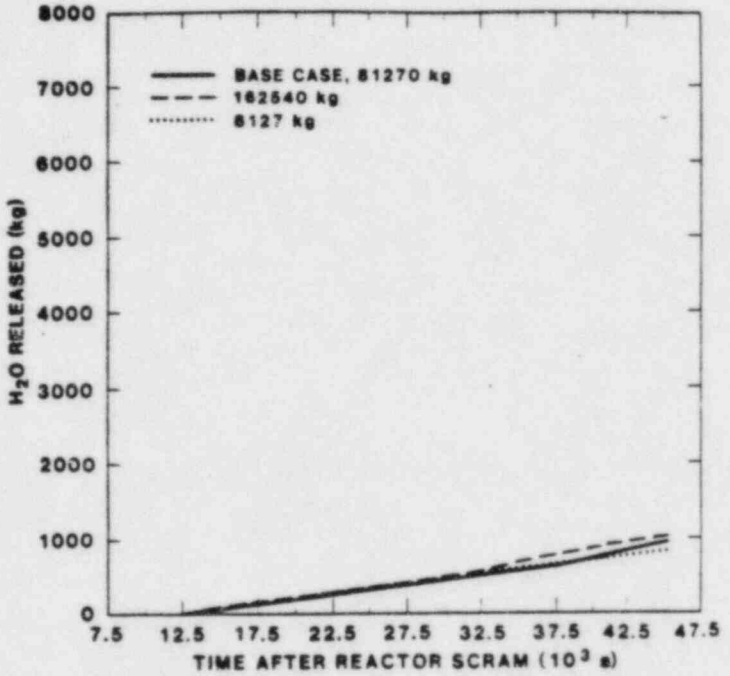

Figure C-3e Effect on H_2O released.

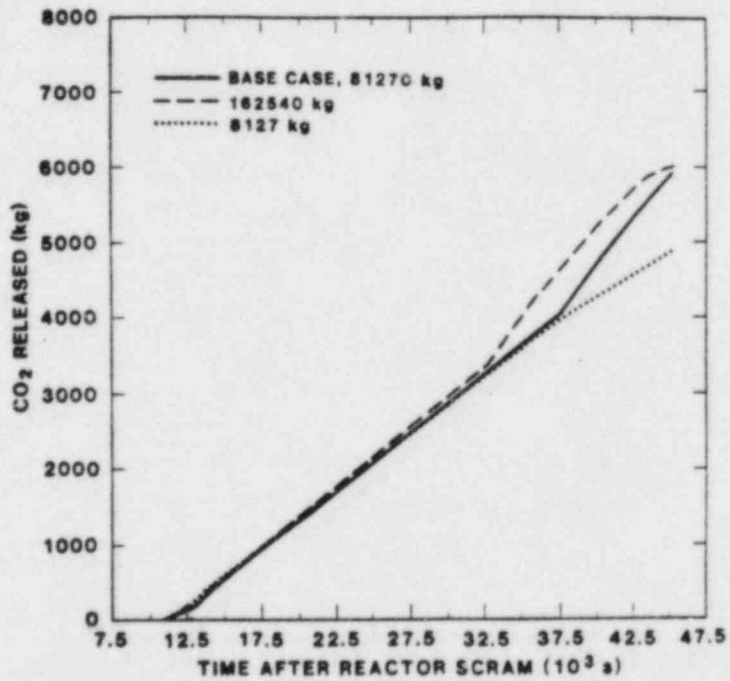

Figure C-3f Effect on CO_2 released.

Figure C-3 Effect of variation in mass of steel in melt. (Continued).

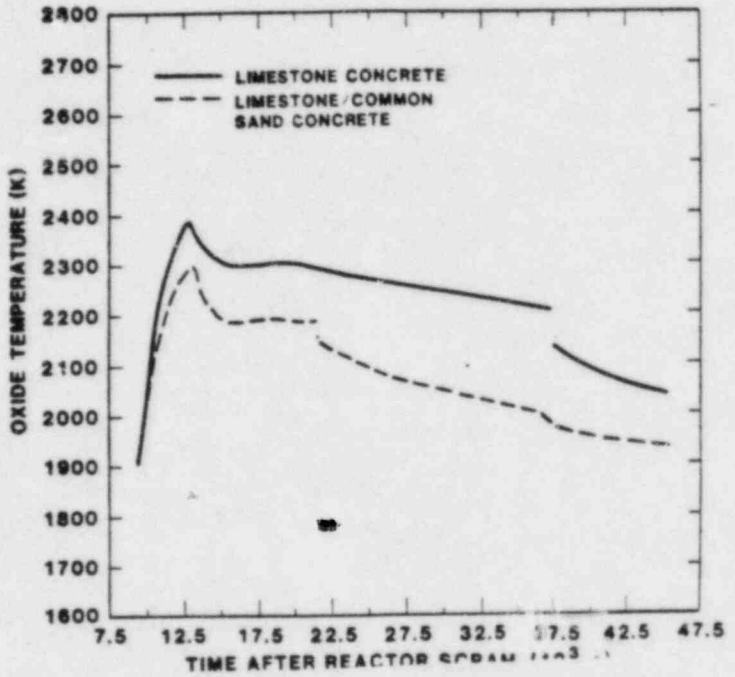

Figure C-4a Effect on oxide temperature.

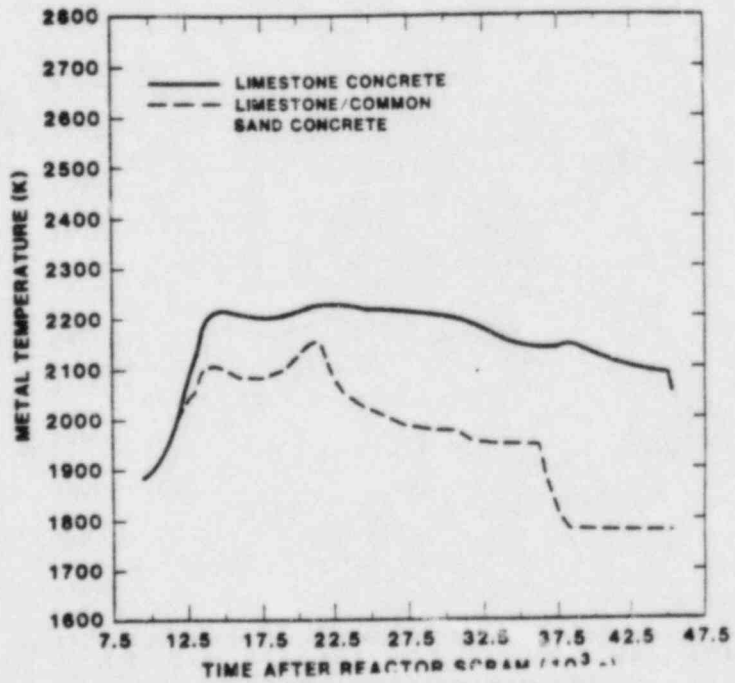

Figure C-4b Effect on metal temperature.

Figure C-4 Effect of variation in type of concrete.

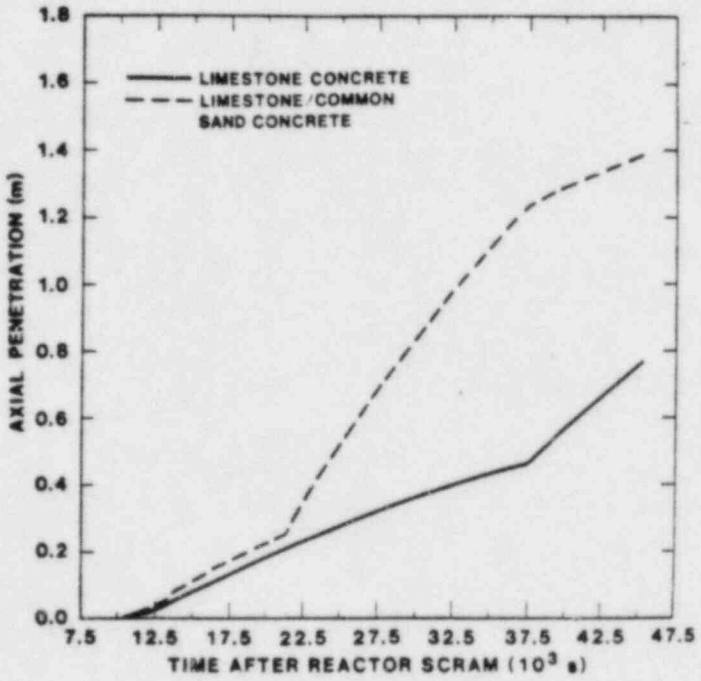

Figure C-4c Effect on axial penetration.

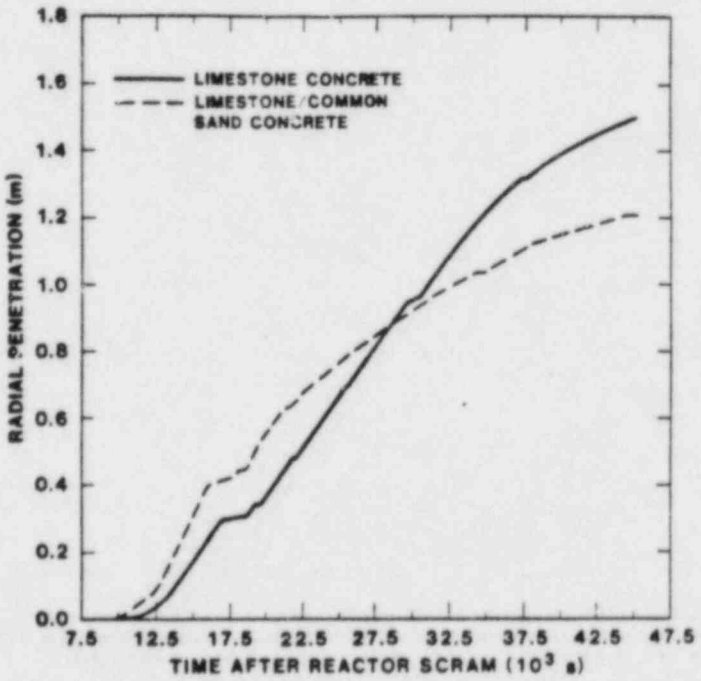

Figure C-4d Effect on radial penetration.

Figure C-4 Effect of variation in type of concrete. (Continued).

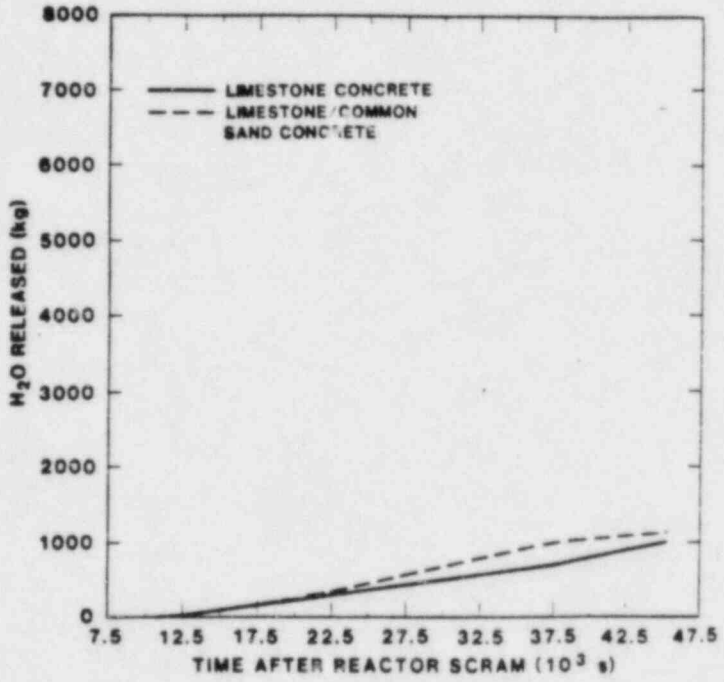

Figure C-4e Effect on H_2O released.

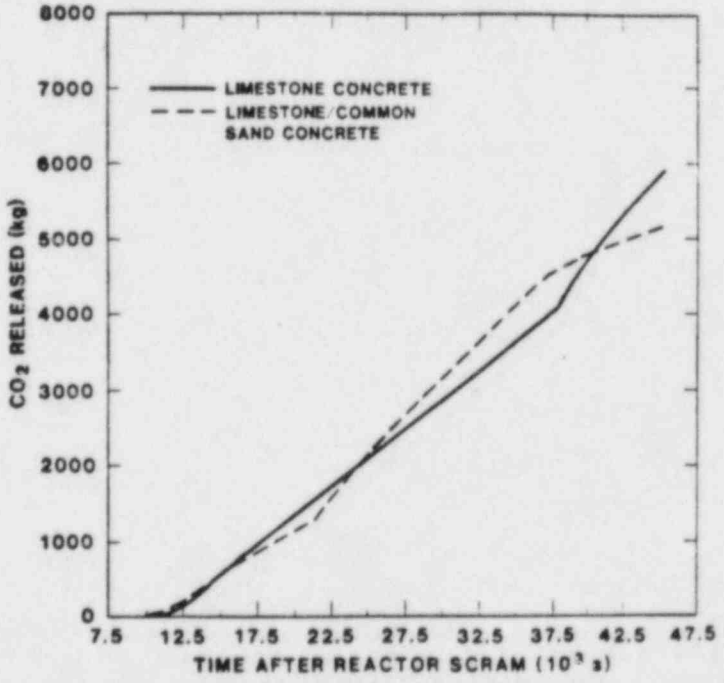

Figure C-4f Effect on CO_2 released.

Figure C-4 Effect of variation in type of concrete. (Continued).

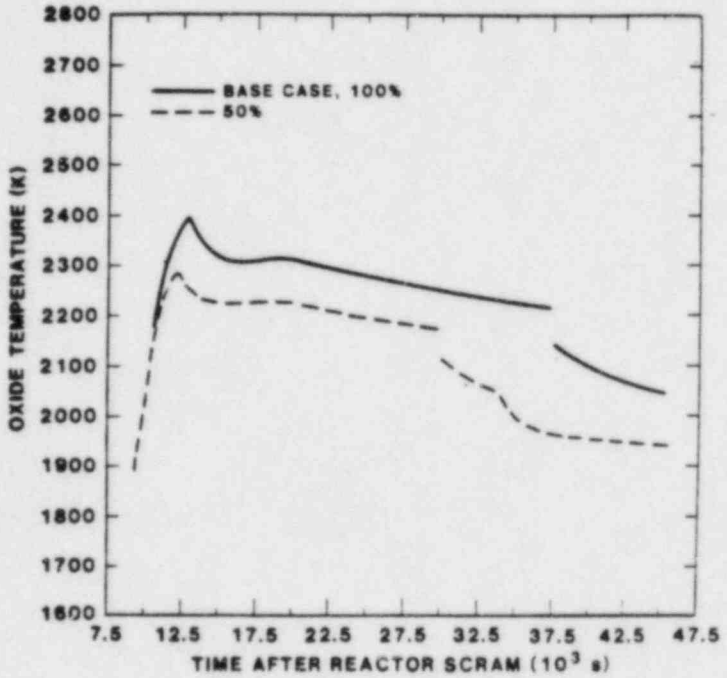

Figure C-5a Effect on oxide temperature.

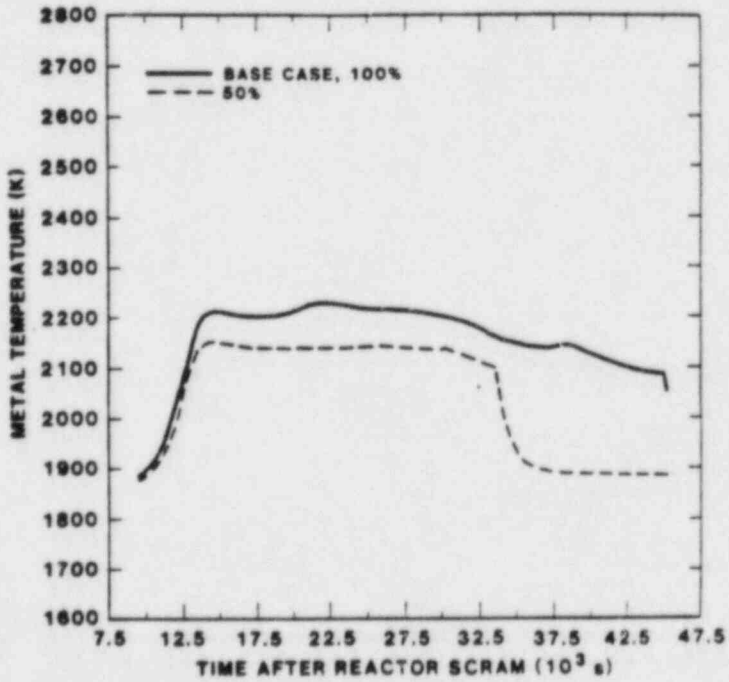

Figure C-5b Effect on metal temperature.

Figure C-5 Effect of variation in fraction of core in the melt.

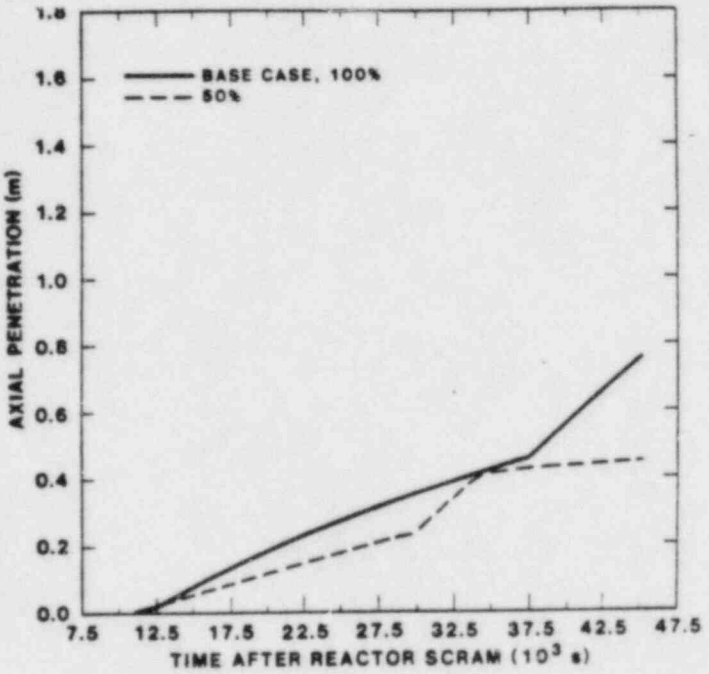

Figure C-5c Effect on axial penetration.

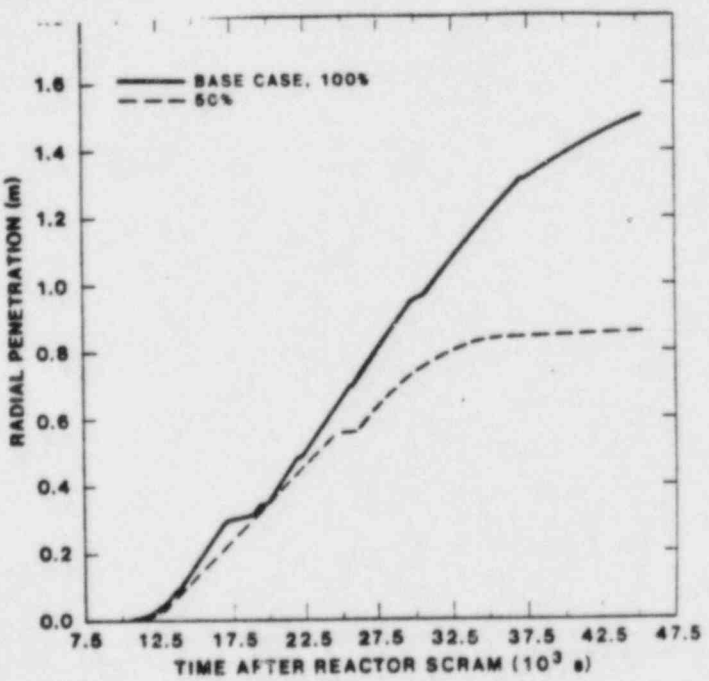

Figure C-5d Effect on radial penetration.

Figure C-5 Effect of variation in fraction of core in the melt. (Continued).

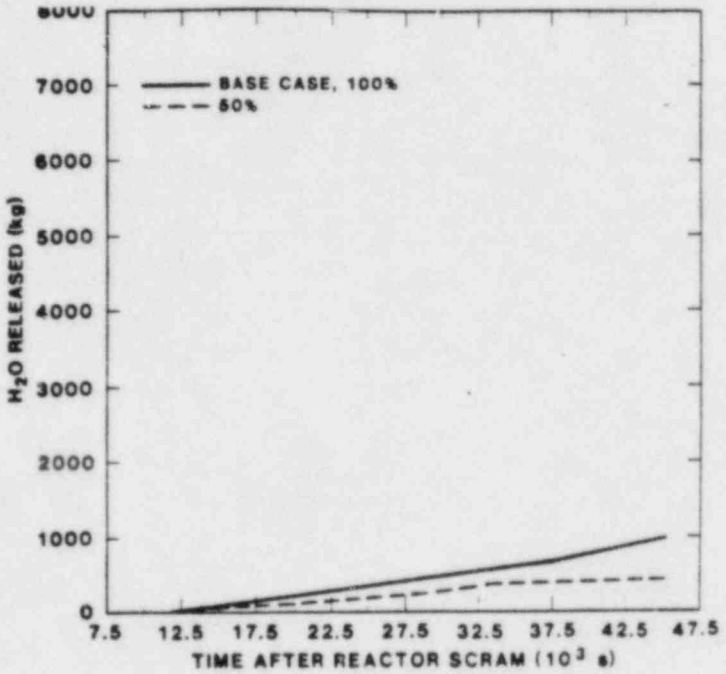

Figure C-5e Effect on H_2O released.

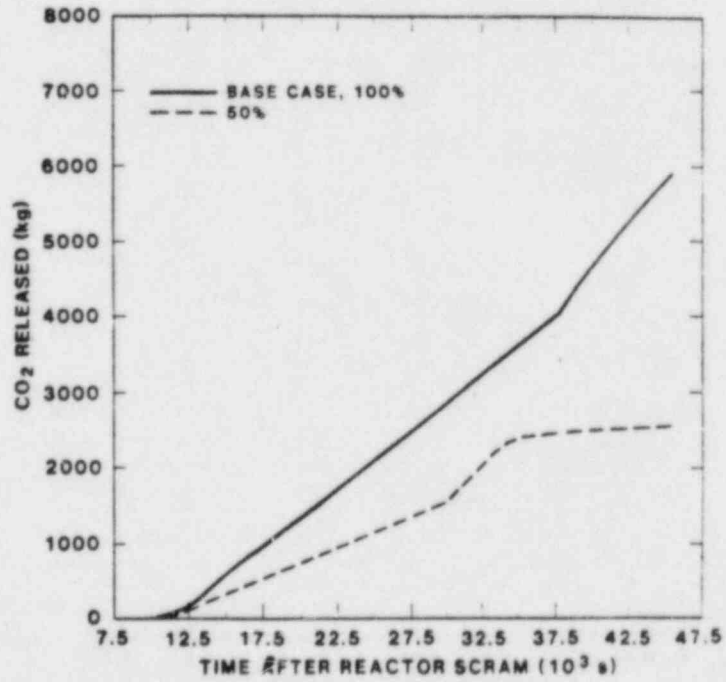

Figure C-5f Effect on CO_2 released.

Figure C-5 Effect of variation in fraction of core in the melt. (Continued).

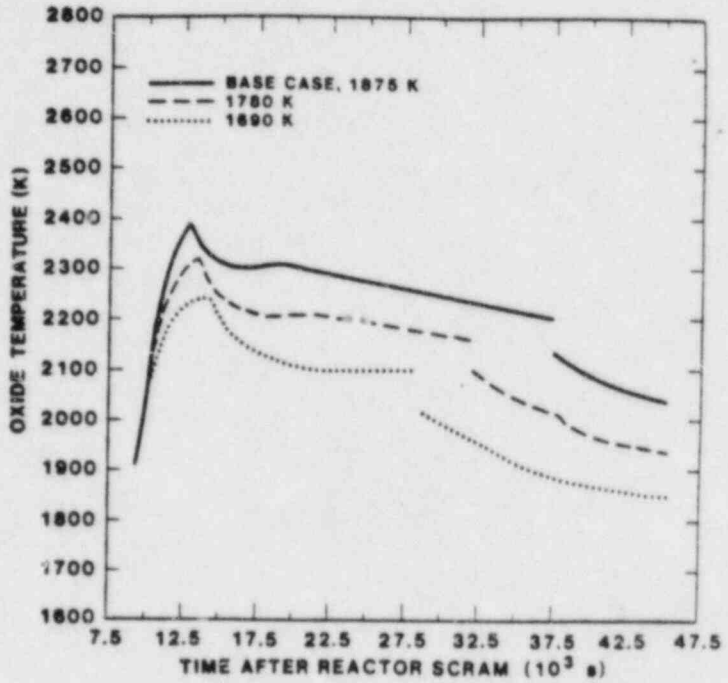

Figure C-6a Effect on oxide temperature.

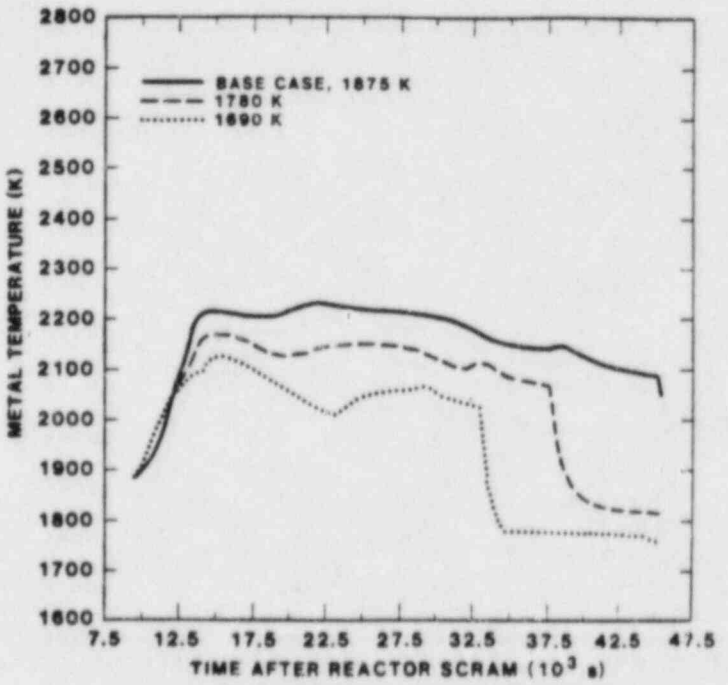

Figure C-6b Effect on metal temperature.

Figure C-6 Effect of variation in the concrete ablation temperature.

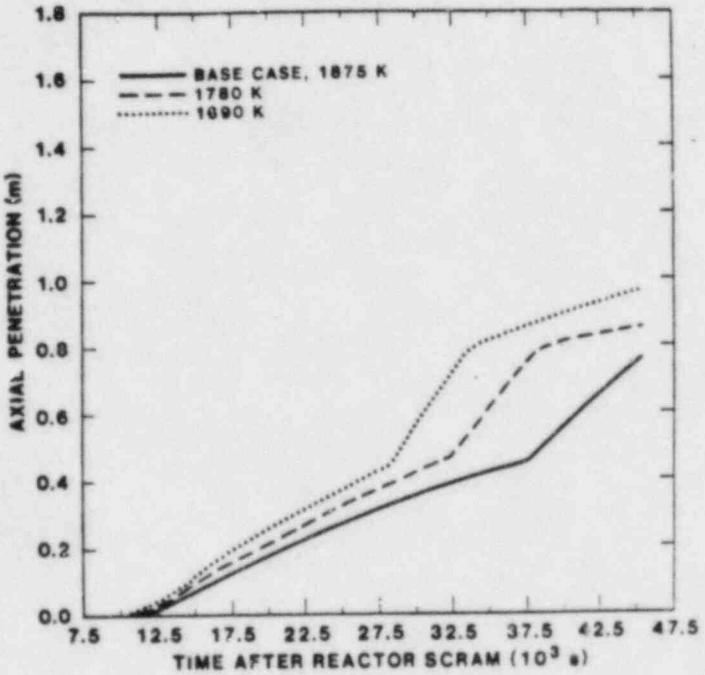

Figure C-6c Effect on axial penetration.

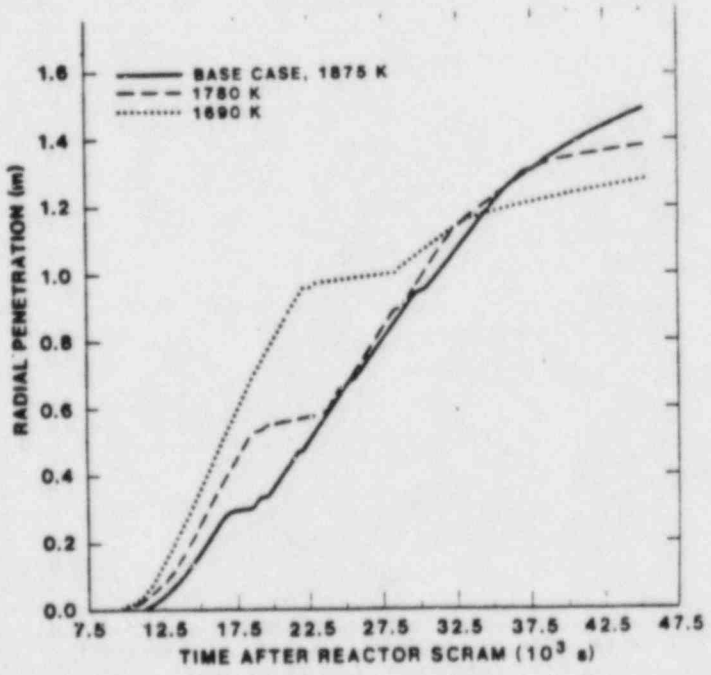

Figure C-6d Effect on radial penetration.

Figure C-6 Effect of variation in the concrete ablation temperature. (Continued).

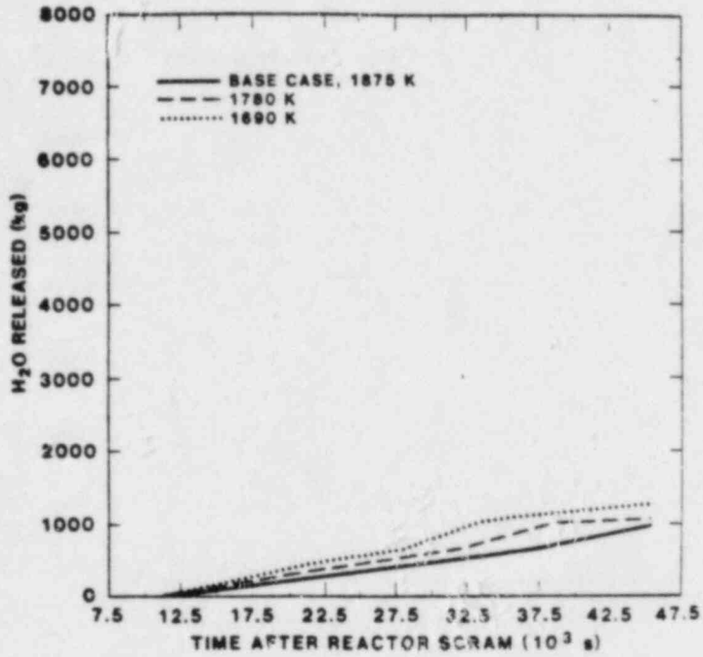

Figure C-6e Effect on H_2O released.

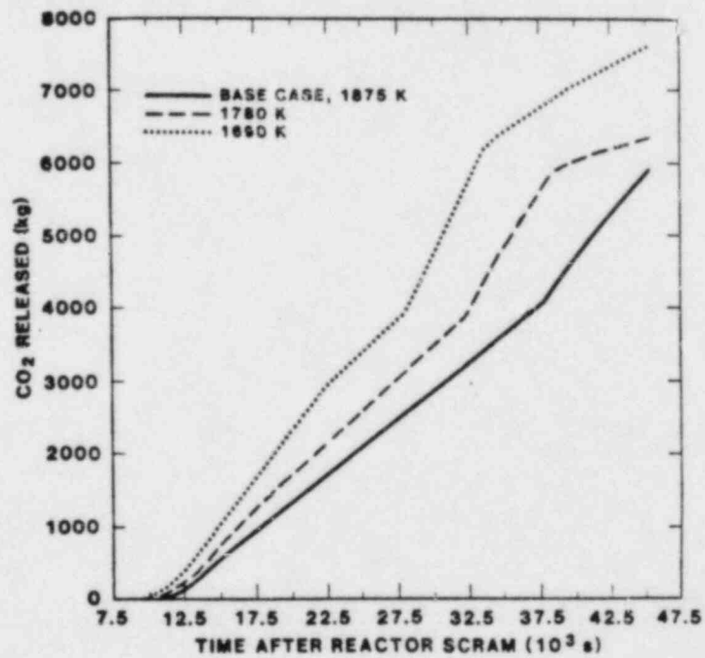

Figure C-6f Effect on CO_2 released.

Figure C-6 Effect of variation in the concrete ablation temperature. (Continued).

These plots present the temporal dependence of the oxidic and metallic layer temperatures, the axial and radial penetration distances, and the total water vapor and carbon dioxide released from the concrete. The layer temperature and gas release rates are included because they control aerosol and fission product release as calculated by the VANESA computer code (see Appendix D). Gases released from the concrete also contribute to the pressure in the containment which may fail if sufficient pressure builds up. Containment failure can also result from either axial or radial penetration of the cavity walls by the melt pool.

C.4 Results of the Zirconium Fraction in the Melt

C.4.1 Variation in the Zirconium Fraction in the Melt

The amount of in-vessel oxidation of zirconium has been the subject of considerable speculation in the reactor safety community. Scenarios have been postulated which result in either complete oxidation of the zirconium in-vessel or very little in-vessel oxidation. In this study, the Zr fraction was varied from a base value of 60% of the total core inventory to limits of 10% and 90%. These results are shown in Figures C.2a through C.2f.

As shown in the figures, the three low oxidation cases (90%, 70%, and 60% of the Zr remains) are almost identical except for a shift in the time of layer flip and the consequent change in the shapes of the various curves. The high oxidation case, on the other hand, differs significantly from the others. The reasons for this dramatic difference provide an illustration of the coupling between many of the phenomena considered in CORCON.

In the low Zr case, the melt temperature increases more slowly at the start than in the other cases because there is less Zr oxidation and hence a smaller chemical reaction energy source. Also, because of the higher ZrO_2 component in the oxide phase and thus lower oxide density, layer flip occurs much earlier. When the layers flip and the metallic phase moves to the bottom of the melt, there is a brief but rapid increase in the axial erosion rate. This results in a concomitant increase in the rate of H_2O and CO_2 released from the concrete and a boost in the rate of zirconium oxidation. In fact, for several minutes the chemical reaction energy exceeds the fission product decay energy. Because this energy is deposited in the metallic layer, there is a rapid increase in the metal phase temperature. However, very quickly the supply of Zr is exhausted and the metal temperature begins to decrease. This temperature drop is further enhanced by the occurrence of an endothermic reaction which provides a significant energy sink.

During the oxidation of the zirconium, much of the CO_2 released from the concrete is reduced to C rather than CO. When the zirconium supply is exhausted, the chemical equilibrium shifts rapidly in the direction of CO with the resulting reaction being very endothermic. As shown in Figures C.2a-2b, the combination of rapid heat transfer from the metallic layer to the concrete and an endothermic reaction cause the metal temperature and subsequently the oxide temperature to drop by hundreds of degrees in less than one hour. Once the layer temperature reaches an equilibrium, the axial penetration rate remains constant throughout the remainder of the calculation. Coincidentally, this rate is approximately the same as the erosion rate caused by the higher temperature oxide melts in the other three cases. Once layer flip occurs in the high Zr cases, however, the axial erosion rates take off as expected.

Note that the calculated radial erosion in the low Zr case is a factor of four less than that in the other three cases. This is due to the early layer flip and subsequent rapid decrease in the melt temperature for the low Zr case, while the sidewalls are exposed to the high temperature metallic phase for several hours in the other three cases. Total gas release, which is a measure of the total volume of concrete eroded, is also much smaller in the low Zr case.

C.4.2 Variation in the Mass of Steel in the Melt

The amount of steel contained in the melt can vary over a wide range depending on the progression of the in-vessel phase of the accident and the failure mode of the reactor pressure vessel. If the core melts and collects at the bottom of the pressure vessel, and subsequently melts a large portion of the steel vessel, the metallic phase of the melt will contain a large mass of steel. If, on the other hand, only the instrument guide tubes fail and little of the pressure vessel melts, there will be very little steel in the melt pool. As shown in Figures C.3a-3f, varying the mass of steel by a factor of twenty had only a small effect on the calculated results.

The major effect on the calculation of changing the mass of steel was observed in the metallic phase temperature. Here the smaller the mass of the metallic layer, the more quickly it responded to heating by the oxide layer and hence the smaller the ΔT between the two melt phases. This is shown in Figures C.3a-3b.

A secondary effect in the shift is the time of layer flip. When there is less steel in the melt relative to the zirconium component, the density of the metallic phase is smaller and more

dilution of the oxide phase is required before layer flip can occur. In fact, for the low steel case, no flip occurred during the 10 hours of calculation.

These effects can be clearly observed in the concrete erosion and gas release plots, Figures C.2c-2f. Both the axial and radial penetration curves demonstrate increased erosion for higher melt temperatures. Because the differences in the metal phase temperature are more pronounced, the increased penetration is more obvious in the radial penetration curves. Note also that when layer flip occurs in the base and high steel cases, there is a noticeable increase in the axial penetration rate and a somewhat less pronounced decrease in the radial penetration rates. The gas release curves show similar results.

C.4.3 Variation in the Type of Concrete Used

This test provides a measure of the effect on the calculation of uncertainties in the composition of the concrete. CORCON has three default concrete types that are representative of most reactor concrete used in the United States. Although specification of alternate concrete compositions is allowed in the code, unless a chemical analysis of the actual concrete used in the reactor plant is available, one of the default concretes would likely be chosen by a user.

The two default concretes chosen for this study are similar in that they both contain limestone aggregate, which has a high CO_2 content. However, the limestone/common sand concrete has significantly less CO_2 and a much higher silica content. Consequently, the limestone concrete has a much higher melting temperature range and heat of ablation (defined here as the total energy required to ablate a unit mass of concrete starting at its initial temperature).

The higher ablation temperature of the limestone concrete causes both the metallic and oxidic layer temperatures to be higher since the &DT between the melt and the concrete surface drives the heat transfer. Also, because of the higher heat of ablation for the limestone concrete, it ablates much more slowly than the limestone/common sand concrete. The slower ablation also leads to slower dilution of the heavy oxide phase by the less dense concrete oxides, and a longer time to layer flip. Because layer flip is delayed, the period of rapid radial erosion of the concrete by the metallic layer is extended. As shown in Figure C.4d, radial erosion of the limestone concrete eventually exceeds that of the limestone/common sand concrete for this reason. Gas release in the two cases is approximately the same as the higher gas content of the limestone concrete compensates for the slower ablation rate.

C.4.4 Variation in the Fraction of the Core in the Melt

In a reactor accident, the fraction of the core which melts and subsequently drops into the cavity below the pressure vessel can vary from essentially zero to 100%. Generally, in order to be conservative, the upper bound is chosen for accident analysis. This test examined the effect on the overall melt-concrete interaction if only half of the core is deposited into the cavity.

As expected, because of the controlling influence of the overall energy balance on the CORCON calculation, this parameter was found to be extremely important. Predictably, in the 50% case, the melt temperatures were lower and as a result, so were the ablation and gas release rates. Because the energy available for ablation of the concrete was one half of that in the full core case, the overall ablation and gas release were roughly half of the base case values. A similar proportionality would be expected if other core melt fractions were used.

C.4.5 Variation in the Concrete Ablation Temperature

Because of the constituents of the concrete melt over a wide range of temperatures, the determination of the ablation temperature is not straightforward. When some fraction of the components melt, it is conceivable that subsurface gas pressure may cause the interfacial concrete to break off and enter the melt. Unfortunately, it is not clear what fraction of the concrete must be molten for this phenomenon to occur. For this reason, it was necessary to investigate the sensitivity of the CORCON calculation to a variation in the ablation temperature. The base case value was chosen to be the concrete liquidus temperature (1875 K for limestone concrete), with the lower limit being the concrete solidus (1690 K). An intermediate value half way between these extremes (1780 K) was also included.

As was alluded to in Section C.4.3, the ablation temperature strongly influences the melt temperatures. It also affects the heat of ablation since more energy is required to heat the concrete to higher ablation temperatures. As shown in Figures C.6c-6f, the greater the heat of ablation, the lower the concrete ablation rates and the smaller the overall gas release. In these figures, the only perturbations in the expected proportional behavior occurs when the metallic and oxidic layers reverse positions.

C.5 Summary of the Results and Conclusions

Table C-2 presents a summary of the results in terms of several important variables: maximum oxide and metal phase temperatures, cumulative H_2O and CO_2 released, and maximum axial and radial concrete penetration. The peak layer temperatures were identified because they control the aerosol and fission product release rates as calculated by VANESA. (See Appendix D.) Peaks in the melt temperature lead to peaks in aerosol and fission product release. Total gas release was chosen because there is a linear relationship between gas flow and aerosol generation; the higher the flow rate the greater the release. Also, gases released from the concrete contribute to the pressure in the containment. This is especially true since for the melt temperatures calculated by CORCON, most of the steam and carbon dioxide would be reduced to H_2 and CO. Because these gases are flammable, they can lead to rapid over pressurization of the containment if ignited. Finally, containment failure can also result from either radial or axial penetration of the cavity concrete by the melt.

In the cases summarized in the table, there was not a wide variation in either metallic or oxidic layer temperatures. (For the oxide phase the temperatures ranged from 2240 K to 2420 K, while for the metal phase the range was 2120 K to 2330 K.) Hence, a large variation in aerosol and fission product release would not be expected, and in fact is not calculated by the VANESA computer code.

Table C-2 Summary of CORCON sensitivity study results

	Max. Temperature (K)		Total Gas (kg)		Max Penetration (m)	
Case	T_{ox}	T_{met}	H_2O	CO_2	Axial	Radial
Base	2390	2210	980	5900	0.76	1.51
Low Zr	2420	2295	500	3000	0.52	0.43
High Zr	2380	2240	850	5100	0.58	1.68
Low steel	2400	2230	825	4950	0.60	1.68
High steel	2390	2160	1000	6000	0.81	1.19
Limestone/ Common Sand	2300	2155	1150	5200	1.39	1.21
50% of core	2280	2150	450	2700	0.45	0.85
T_{abl} = 1690 K	2240	2120	1250	7600	0.85	1.28
T_{abl} = 1780 K	2315	2165	1050	6300	0.96	1.39

APPENDIX D

Uncertainties in Aerosol Removal By Suppression Pool Scrubbing

J. E. Brockmann

Introduction

In a boiling water reactor accident, radioactive release to the environment is mitigated when soluble gases and aerosol-laden gases vent through the suppression pool prior to escape to the outer containment building. In the process of bubbling the gases through the suppression pool water, soluble gases are dissolved in the water and aerosol particles are removed from the gas by scrubbing. The degree of removal is strongly dedpendent on aerosol particle size and bubble dynamics. This appendix deals with uncertainties in the removal of particulate material by scrubbing.

In the following sections, the current models and codes describing particulate scrubbing will be discussed. The mechanisms of particle removal and their sensitivity to model parameters will be described. The SPARC code (2) will be used to illustrate the variation in scrubbing decontamination factor over a range of input parameters selected to reflect the current uncertainty in their values. Finally, the applicability of extending models based on single bubble scrubbing to real world cases involving multiple bubbles will be discussed.

SCRUBBING MODELS

Fuchs[1] (1964) presented a simple model of particle removal from single spherical bubbles. The Fuchs model is the basis of all particle scrubbing models and codes currently in use for reactor analysis. This model identified three mechanisms of particle removal. They are:

1. Brownian diffusion of particles to the bubble wall (dominant for smaller particles)

2. Gravitational settling of particles to the lower bubble wall (dominant for larger particles)

3. Inertial deposition of particles on the bubble wall driven by the centrifugal acceleration produced in the internal circulation of the gas in the bubble (dominant for larger particles).

Because the first mechanism increases the decontamination factor, DF,* with decreasing particle size and the second and third mechanisms increase decontamination factor with increasing particle size, there is a minimum in the DF curve when plotted as a function of particle size (Figure 1). This "U"-shaped decontamination factor curve is also produced by more sophisticated models than the Fuchs model. Figure 1 shows two decontamination factor curves calculated by the Fuchs model. The figure illustrates the high sensitivity of decontamination to particle size and the sensitivity to bubble size and pool depth.

There are three more sophisticated models now in use. They are:

1. SPARC[2] written by Battelle Northwest Laboratory;
2. SUPRA [3] written by SAIC for EPRI;
3. A model written by General Electric[4].

---

* DF is defined as the intial concentration divided by the final concentration, (DF = 1 means no removal has occurred).

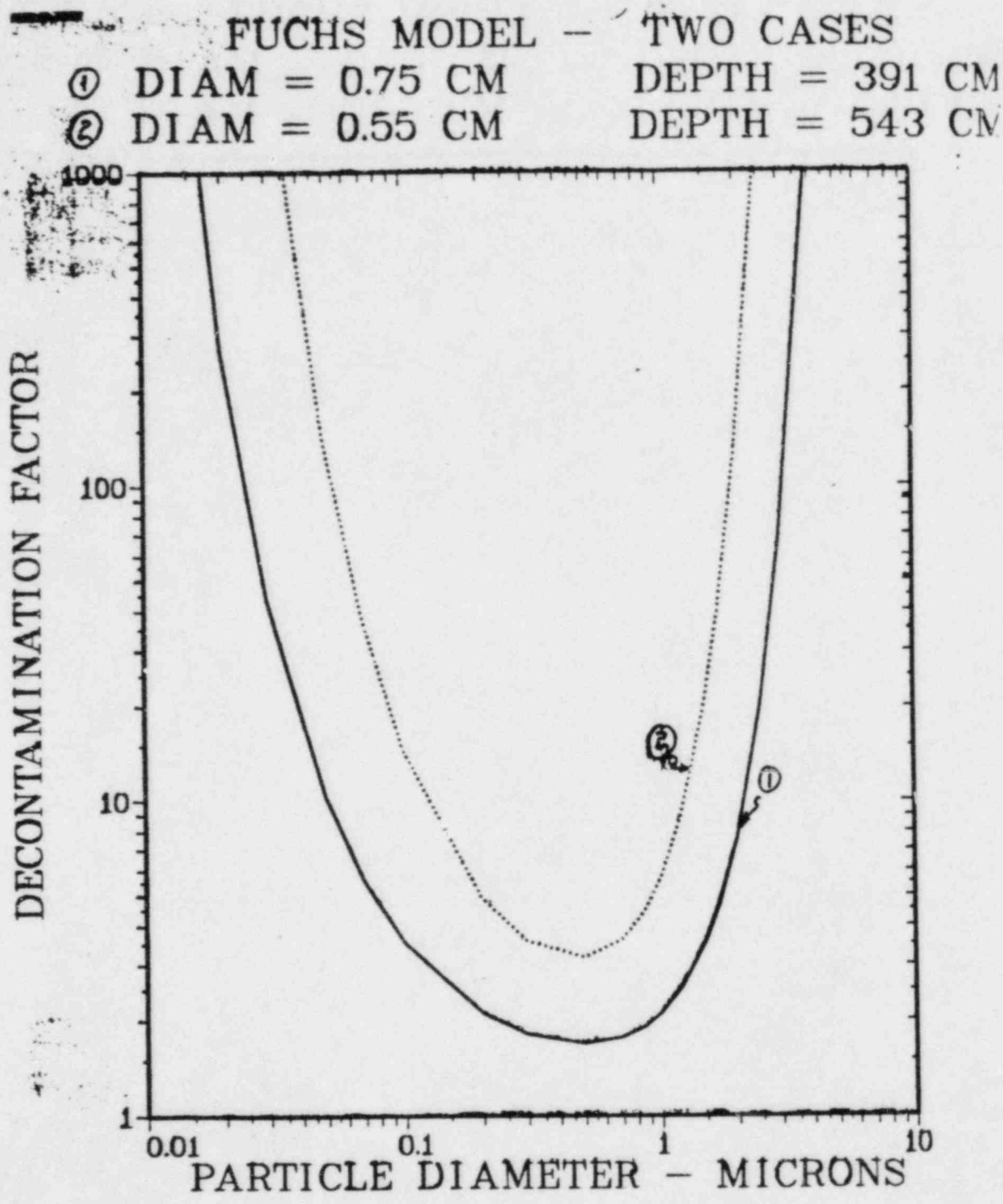

Figure 1 Variation in Decontamination Factor Within Particle Size

Each of these models incorporates the three particle removal mechanisms identified by Fuchs. In addition, they also have the capability to model elliptically shaped bubbles, an effect that becomes increasingly important for bubbles larger than two to three millimeters in diameter. The treatment of scrubbing for elliptical bubbles is based on the work of Moody[4].

In addition to the three removal mechamisms modeled by Fuchs, additional particle removal mechanisms are considered in these more sophisticated codes. These mechanisms are listed below with emphasis given to describing the level of treatment in the SPARC code (which is the basis for much of the calculational work in this appendix).

4. Diffusiophoresis: The transport of particles by diffusion of water vapor to or from the bubble walls (generally assumed to act uniformly over all particle sizes considered).

5. Steam condensation: May be considered a special case of diffusiophoresis (no particle size dependence assumed).

6. Convection: Caused by vapor flux to or from the bubble wall. The convection velocity is added algebraically to the deposition velocities calculated for other deposition mechanisms. SPARC uses convection and condensation in lieu of an explicit diffusiophoresis calculation (no particle size dependence).

7. Thermophoresis: The transport of particles driven by a thermal gradient at the bubble wall. SPARC does not include this mechanism, because calculations indicate (Moody) that the bubble rapidly comes to the pool temperature and thus thermophoresis would not be expected to be important. (Particle size dependence is not large and depends upon the treatment(_____)).

8. Impaction during gas injection into the pool: SPARC includes an optional injection impaction model (dominant for larger particles).

9. Particle growth in the bubble by water acquisition by deliquescing material in the particles: This is not specifically a removal mechanism, but it will enhance removal of larger particles by large particle dominant mechanisms and degrade removal of smaller particles by small particle dominant mechanisms. SPARC includes a particle growth model for water aquisition.

10. Particle growth by agglomeration: Similar behavior to particle growth by water acquisition.

The SPARC code is a single bubble scrubbing model employing an eliptical geometry which includes the following mechanisms:

Brownian Diffusion	(1)
Inertial Deposition	(2)
Gravitational Sedimentation	(3)
Steam Condensation	(5)
Convection	(6)
Inlet Impaction	(8)
Particle Growth	(9)

The SPARC code also includes bubble growth by humidification and expansion as the bubble rises through the pool.

SPARC

A detailed description of the SPARC code is available (Owczarski et. al.[2]) in the literature and will not be given here. The following is a list of the important input parameters to SPARC[5].

Most Important:

Particle size and density
Bubble size and shape
Volume fraction of steam in inlet gas

Intermediate Importance:

Pool temperature
Pool depth
Percent of soluble material in particles

Least Important:

Non-condensible gas composition
Pressure above pool.

The reference for the above list includes a sensitivity study of the SPARC code.

In this appendix decontamination factor curves calculated by SPARC will be presented to illustrate the importance of particle size distribution, particle material density, percent soluble material (used in the particle growth calculation), and bubble size, shape, and rise velocity. Retardation of the internal circulation velocity is a potentially important effect because

internal circulation drives the dominant mechanism for removal of super-micron sized particles. This effect will also be discussed.

Two base cases are presented for these discussions: one for venting from the reactor pressure vessel, and the other for venting from the drywell. The important parameters for these base cases are presented in Table I. Some of these parameters are taken from the BMI MARCH calculations for the Grand Gulf TC sequence. The conditions quoted for base case #1 correspond to time in the accident of 130.5 minutes and the conditions for case #2 correspond to 257.9 minutes. Parameter variations are applied to both base cases with the range of variation chosen to reflect a reasonable range of uncertainty.

Steam condensation is not included in this exercise for the sake of simplicity. The inlet gas volume fraction of steam is an input to SPARC that is calculated by preceeding codes in the code train. Owczarski and Postma[5] have shown that steam condensation can increase decontamination by an order of magnitude.

TABLE 1

PARAMETER VALUES FOR TWO BASE CASES

	1 In-Vessel	2 Ex-Vessel
Pool Depth (cm)	543	391
Pool Temp (^{o}C) (Saturated)	112	100
Pressure Above Pool (ATM)	1.56	1.04
Inlet Gas Flow and Composition:		
$^{+}H_2O$ (g/sec)	4794	900.6
H_2 (g/sec)	13.98	6.28
CO_2 (g/sec)	2.37	1647
CO (g/sec)	0	120.9
Air (g/sec)	4660	4.08
Inlet Gas Temp (^{o}C)	224	223
*Bubble Diameter (equivalent sphere) (cm)	.95	.95
*Bubble Aspect Ratio (-)	1.50	1.50
*Bubble Swarm Rise Velocity (cm/sec)	116	116
*Recirculation Velocity Multiplier (-)	1	1
*Particle Material Density (g/sec)**	3.0	3.0
*Percent Soluble Material (%)	0	0
Injection Impaction Used	No	No

+ Not sufficient quantity to be condensed in pool.

* Quantities to be varied.

** Particles treated as spheres of material density.

There are three types of parameters, each with an associated uncertainty:

1. Plant-dependent fixed quantities such as pool depth: The only uncertainty associated with this type of parameter is which plant is to be considered. Once the plant has been identified, the uncertainty is removed.

2. Scenario-dependent calculated quantities such as gas flow and composition: Once the scenario is selected, the uncertainty in these parameters is the propagated uncertainty from previous codes in the code suite.

3. Model specific quantities such as bubble size and shape: These parameters introduce the uncertainty in the model either by uncertainty in their values or by the extent to which modeled phenomena describe actual phenomena.

Table II is a list of the varied parameters, their type, and their range.

PARAMETER RANGES

The parameter ranges for the selected variables were chosen to reflect reasonable ranges of uncertainty.

Bubble diameter and aspect ratio are related, the larger bubble being more elliptical (Clift, Grace, and Weber).[6] The relationship also depends upon the purity of the water. It is difficult to achieve pure conditions in the experimental work described and impurity levels on the parts per million range are

sufficient to produce contaminated system bubble behavior. It is assumed that suppression pools are contaminated and that bubbles will behave according to the contaminated system correlations found in Clift, Grace, and Weber[6].

Figure 2 shows the aspect ratio (major to minor axis) of bubbles as a function of their equivalent spherical diameter. Two correlations from Clift, et. al.,[6] are given. One is for pure water and the other for contaminated water. As can be seen, water contamination results in a significant decrease in bubble aspect ratio. Another effect that could decrease bubble aspect ratio is bubble swarms (as opposed to single bubbles). This is demonstrated by the third curve in Figure 2, which shows results of some experiments in bubble hydrodynamics performed at Battelle Columbus Labs[5]. The data (observation) from these experiments show bubbles to be less elliptical than is predicted by the contaminated system correlation (which is based on single bubble data).

TABLE II

VARIED PARAMETERS IN MODEL

PARAMETER	TYPE	BASE CASE	VARIATIONS
Bubble Diameter and Aspect Ratio	3)	.95 cm/1.50	.95 cm/2.2 .55 cm/1.5 .55 cm/1.33 .35 cm/1.25
Bubble Swarm Rise Velocity	3)	116 cm/sec	50 cm/sec
Recirculation Velocity Multiplier	3)	1	0.1 0.5
Particle Material Density	2)	3 g/cc	2.5 g/cc 5.0 g/cc
Percent Soluble Particle Material	2)	0%	10% 70%

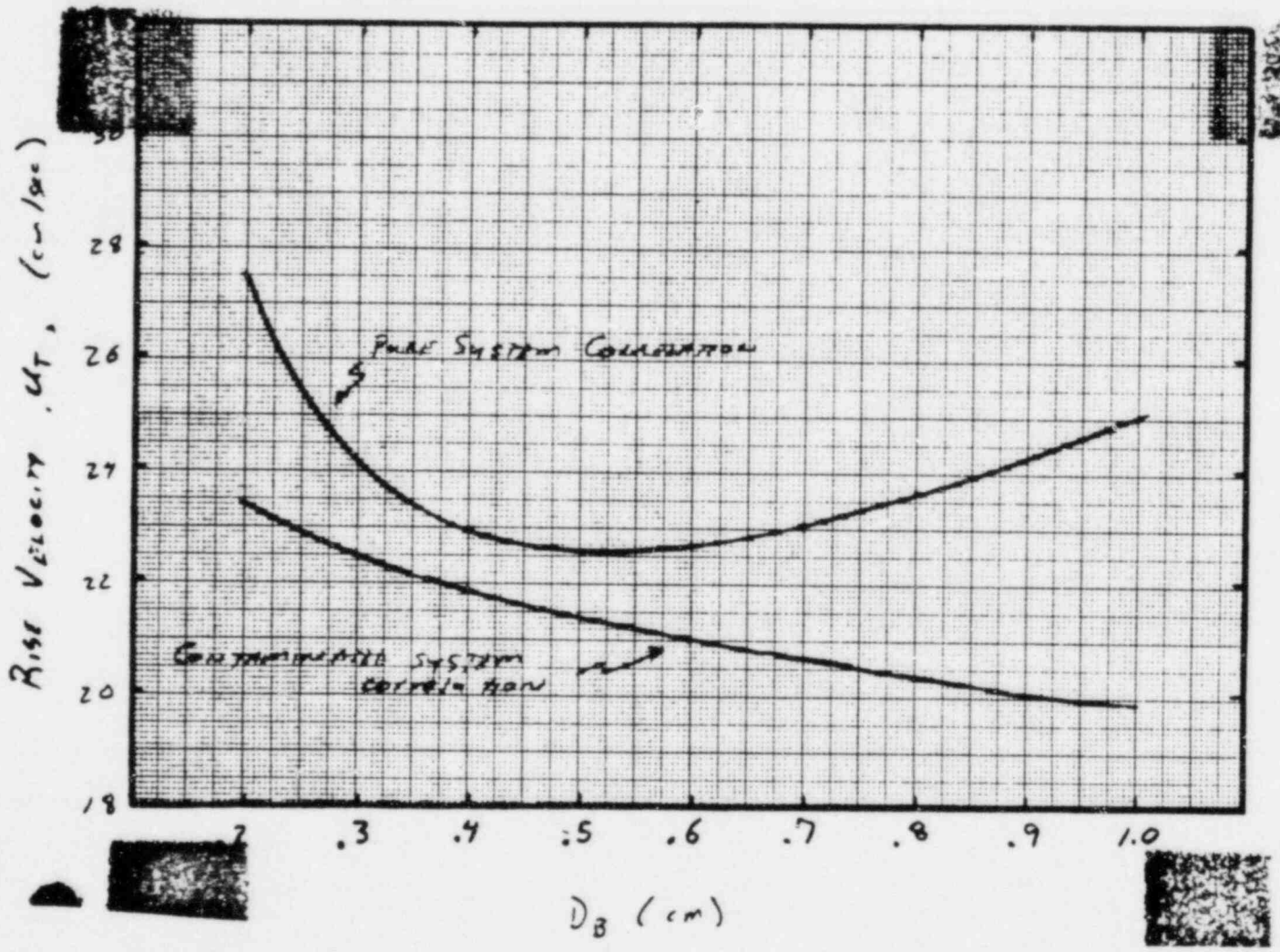

FIGURE 2 Single Bubble Rise Velocity for Water at 100°C

In actual accident cases, swarms of bubbles rather than single bubbles will be encountered. The bubble size in these swarms is a distribution. Bubbles continually fragment and coallesce in the swarm but maintain a constant size distribution during the rise. That is to say that a specific bundle of gas is not associated with the same bubble during the entire transit of the pool[8].

The bubble size distribution has been found to be independent of injection flow rate, injection angle, and number of injection points. There is, however, a dependence on condensible steam fraction. In each case, the distribution is well described by a log normal distribution[8].

Low or no condensation:

Geometric number mean diameter	= 0.55 cm
Geometric volume mean diameter	= 0.95 cm
Geometric standard deviation	= 1.53

High condensation:

Geometric number mean diameter	= 0.35 cm
Geometric volume mean diameter	= 0.60 cm
Geometric standard deviation	= 1.53

The decrease in mean size for high condensation may be caused by increased bubble separation and reduced collision rate.

The appropriate diameter to chose would be the volume weighted mean because scrubbing is a process acting on the volume of gas. The bubble diameters selected for the sensitivity study

are 0.95 cm, 0.55 cm, and 0.35 cm, to reflect the range from large volume mean diameter to small number mean diameter. The 0.55 cm diameter value does double duty as the large number mean diameter and small volume mean diameter.

The aspect ratio is selected from the lowest two curves in Figure 2. The resulting cases are given in Table II. The experimental work at Battelle [7] has reduced uncertainty in bubble size and shape.

The bubble swarm rise velocity determines the length of time during which scrubbing will take place. The two values chosen reflect some uncertainty which may actually overestimate the uncertainty. The higher value of 116 cm/sec is chosen because it is the value used in the SPARC code. The lower value of 50 cm/sec comes from experimental work conducted at Battelle [9].

A major uncertainty is the internal circulation velocity. It is this internal circulation which drives the inertial removal mechanism that is responsible for most of the super micron particle deposition. This internal circulation velocity is calculated for an elliptical bubble based on the bubble-liquid relative velocity for a single bubble. This calculated velocity would have a recirculation velocity multiplier of 1.0. Implicit in this value is the assumption that the internal circulation velocity is in no way retarded.

There are three possible causes for retardation of this velocity. The first is contamination. Clift, et. al., [6] reference experimental evidence of decreased internal circulation velocities in contaminated pools. We have reasonably assumed the suppression pool to be contaminated (if not at the start then thirty seconds after the beginning of blowdown). This argues for a multiplier less than 1.

The second cause of recirculation velocity retardation is the suggestion that wobble and oscillation of the bubble disrupts the internal circulation (Clift, et. al.,[6]. The bubbles in a swarm wobble and oscillate.

The third cause is the continuing fragmentation and coalescence of bubbles in the swarm. If the bubble lifetime is less than the time scale of flow development in the bubble, then internal circulation may not become established.

It should be pointed out that the last two mechanisms which reduce or eliminate internal circulation introduce an as yet unmodeled mechanism of turbulent inertial deposition. It is quite possible that the internal circulation-driven and turbulence-driven inertial deposition mechanisms behave so similarly that modeling of one adequately predicts the other. This could explain the success of these models in predicting pool scrubbing. There may be conditions, however, under which this success will not be realized. It is important to model the mechanism that is acting, not the one that isn't.

The values of recirculation velocity multiplier which have been selected to reflect this modeling uncertainty are 1., 0.5, and 0.1.

These three parameters are inputs to the SPARC model which have not been calculted by other codes or models. They are exogenous to the code and must be determined by the user. The next two parameters are propagated from previous codes and their ranges have been selected from the output ranges of these codes.

Particle material density has been selected as 2.5 g/cc, 3.0 g/cc and 5.0 g/cc. This is a sufficient variation to demonstrate the effect density has on decontamination factors. The effect of particle shape factors, which is certainly comparable to that of

material density, has not been examined. There is no provision in SPARC for shape factors.

Percent soluble material in the particles is calculated by TRAPMELT for in-vessel aerosols and by VANESA for ex-vessel aerosols. The values selected are 0%, 10%, and 70%.

The effect of size distribution has also been investigated. In addition to showing decontamination factor as a function of size for single particles, it is also shown as a function of geometric mass mean diameter for log-normal particle size distributions of various geometric standard deviations.

The figures which will be discussed below are graphs of decontamination factor versus particle size. They are of the type which varies one parameter or one set of correlated parameters about some base case, to demonstrate the effect of that parameter or parameter set. The two base cases are described in Table I and the parameter variations in Table II.

Figures 3a and 3b show the effect of bubble diameter aspect ratio variation on base case 1 and 2 respectively. The largest effect is the shifting of the steep portion of the curve between 1 and 2 microns. This is within the uncertainty with which the particle diameters are known.

Figures 4a and 4b show the effect of recirculation velocity multiplier variations on base cases 1 and 2, respectively. The effect is greater than that of bubble size and shape. This and particle size distribution are the two principal uncertainties.

FIGURE 3 Effect of bubble diameter aspect ratio variation on base case 1 and 2

VARIATION OF DIAM AND RATIO

BASE CASE : DIAM=.95, RATIO=1.5

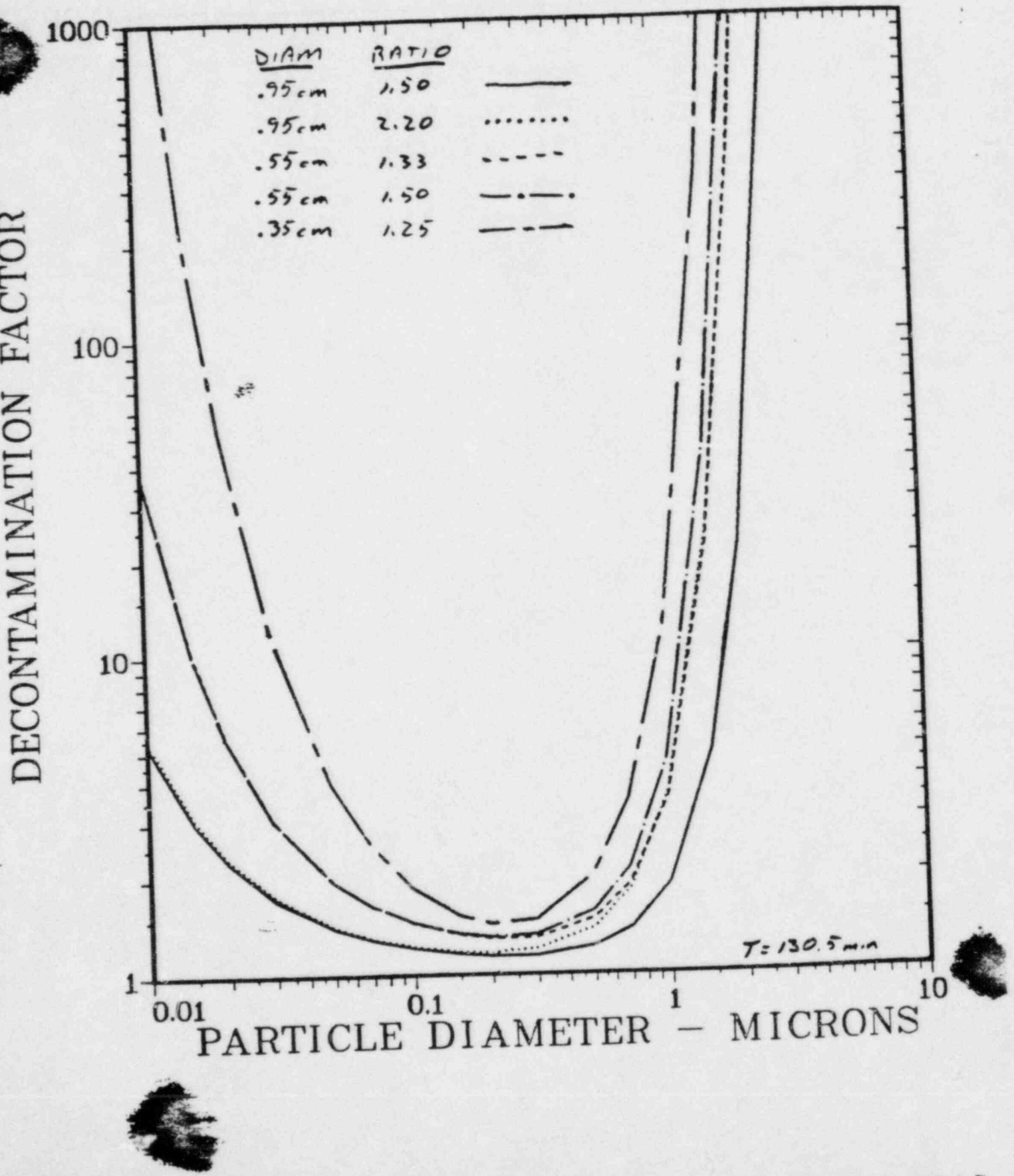

SPRACS20.PLT

VARIATION OF DIAM AND RATIO.

BASE CASE: DIAM=.95, RATIO=1.5

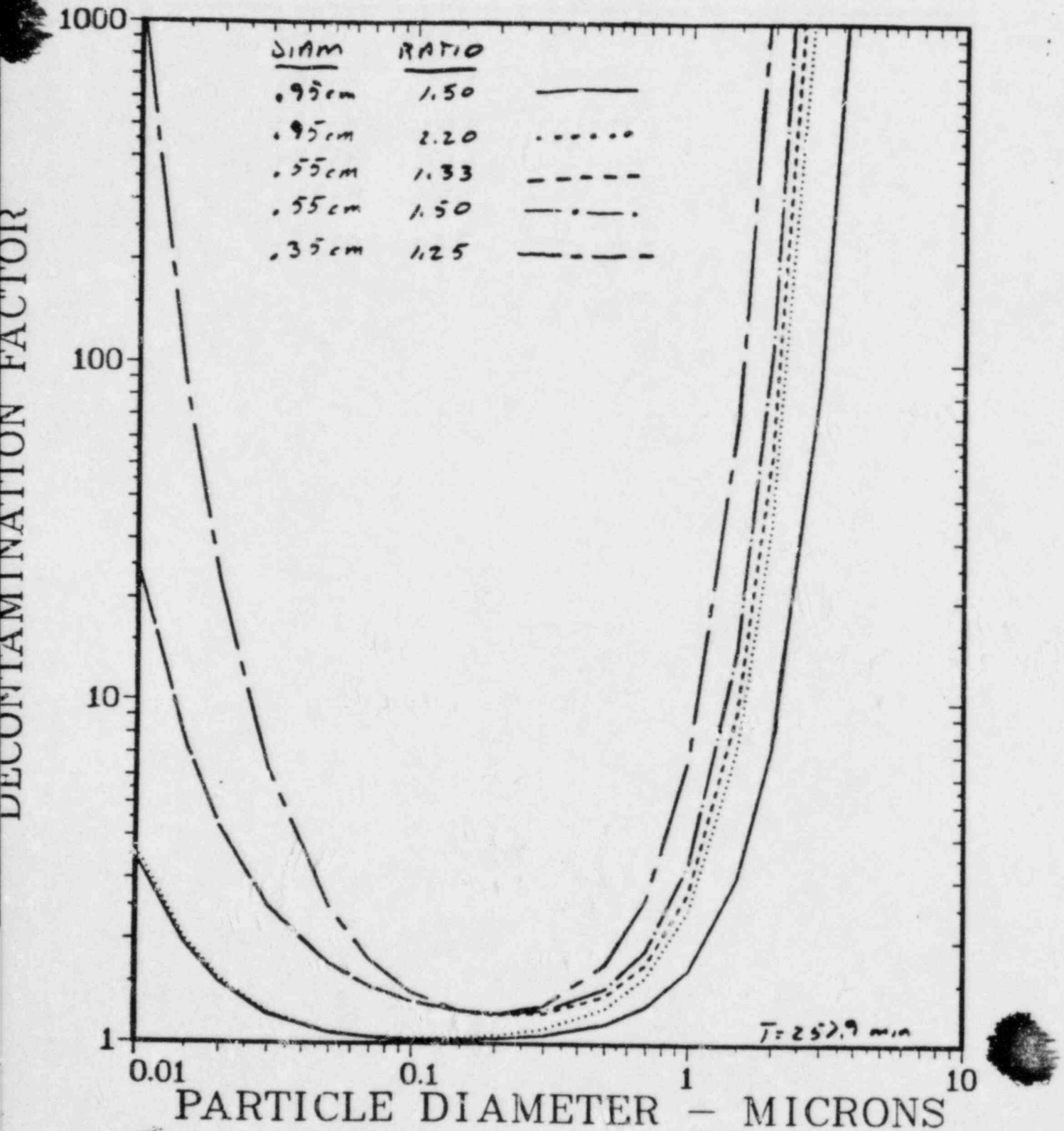

FIGURE 4 Effect of recirculation velocity multiplier variations on base cases 1 and 2

VARIATION OF VTMULT.

BASE CASE : VTMULT=1.

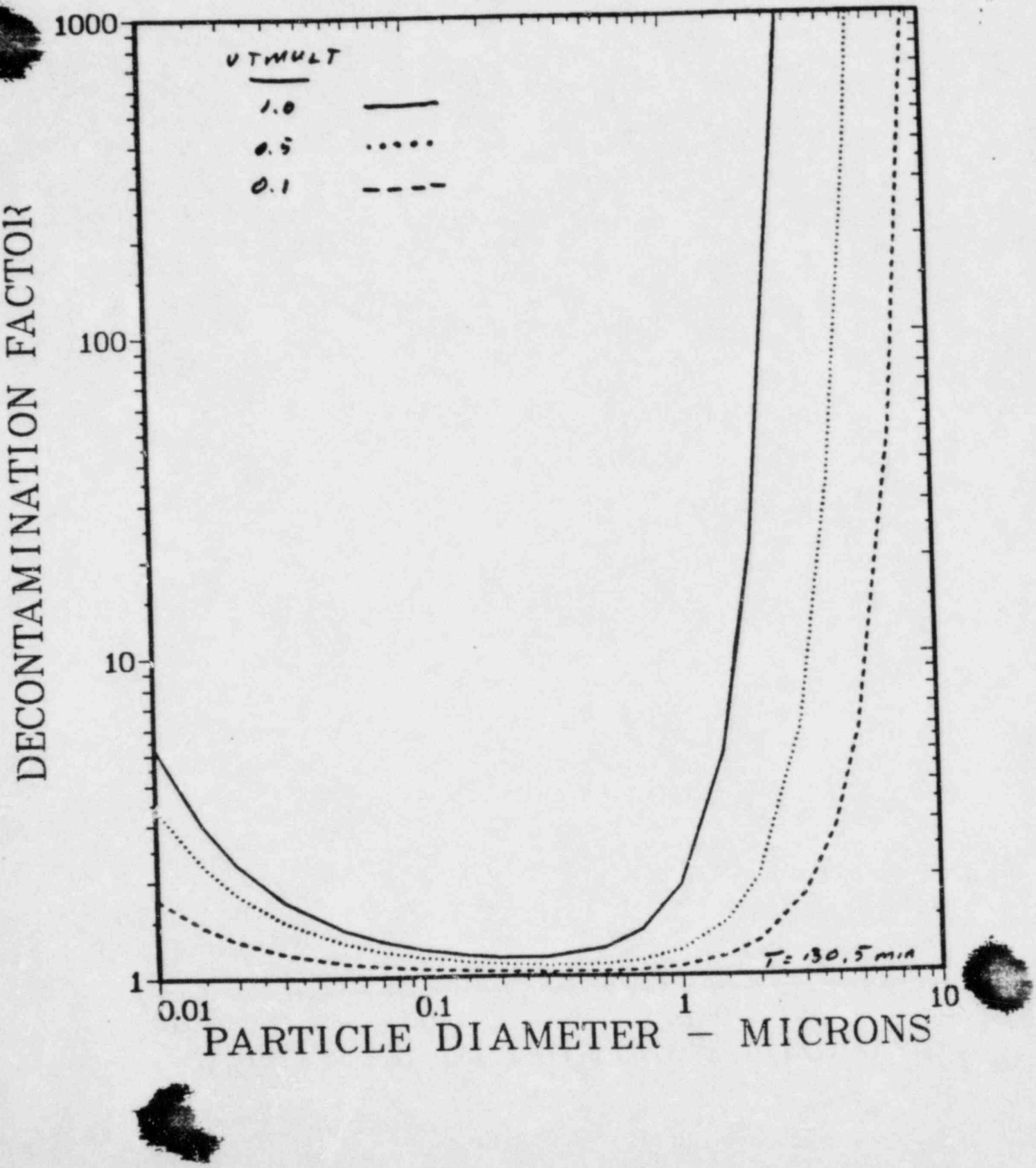

VARIATION OF VTMULT.

BASE CASE: VTMULT=1.

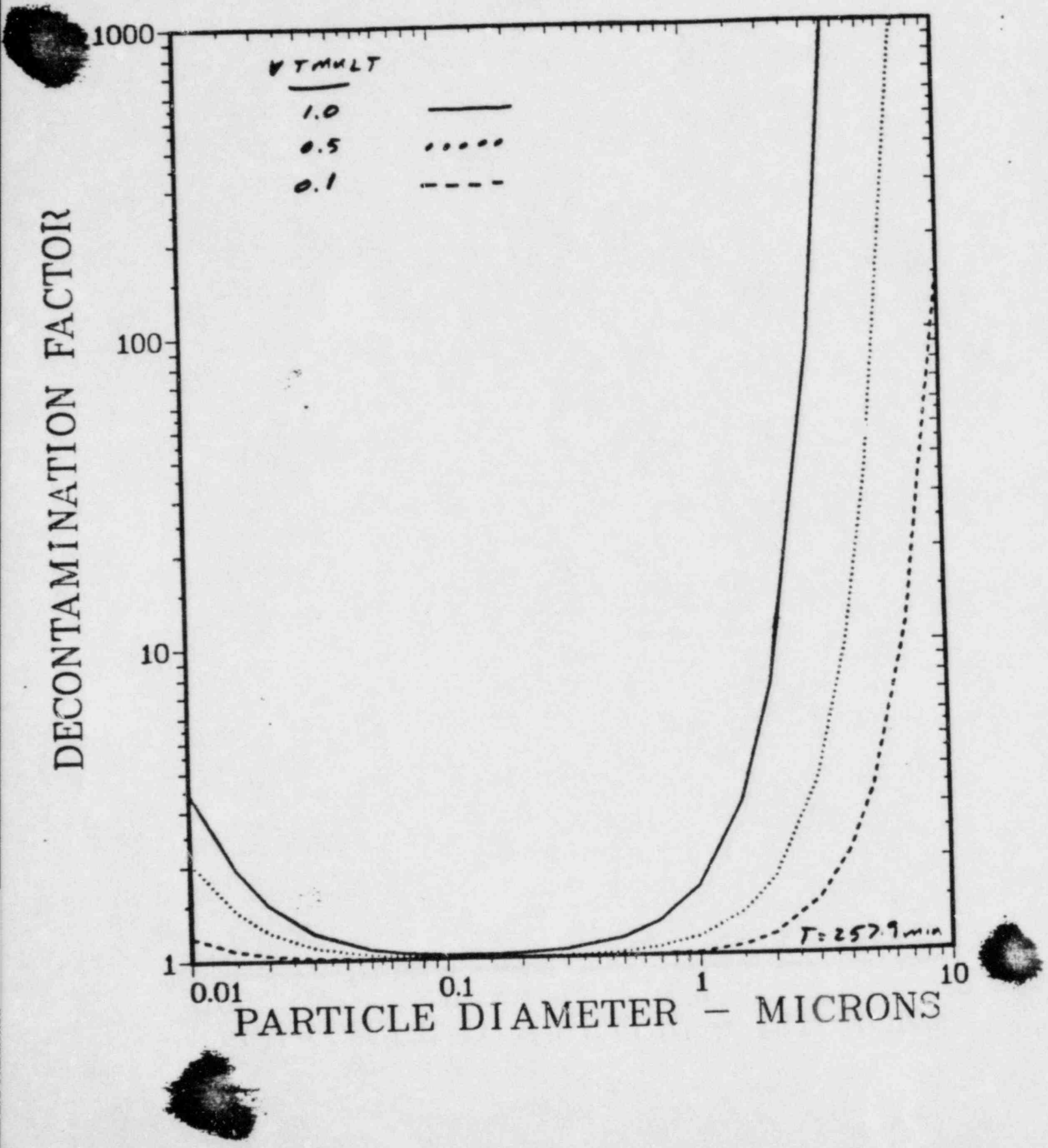

Figures 5a and 5b show the effect of particle material density variations on base cases 1 and 2, respectively. This uncertainty does not introduce great variation in DF until the particle sizes are larger than a micron. The uncertainty in the particle size distribution introduces more uncertainty in DF than this variation in particle material density.

Figures 6a and 6b show the effect of uncertainties in soluble material on the particle on base cases 1 and 2, respectively. It is interesting to note that, for smaller particles, particle growth decreases decontamination while, for larger particles, growth increases decontaminatin. Particle growth generally acts to shift the decontamination factor curve to the right.

Figures 7a and 7b show the effect of bubble swarm rise velocity variations on base cases 1 and 2, respectively. This is not a dominating uncertainty. As bubble swarm experiments are completed and correlations formulated, the bubble dynamics aspects of pool scrubbing will become better understood further reducing the importance of these uncertainties.

It has been mentioned that the uncertainty in particle size distribution accounts for much of the uncertainty in pool scrubbing calculations. As a particle size distribution increases in spread, the tails of the distribution are characterized by significantly different decontamination factors than the mean size. Thus, the integral decontaminatin factor for a distribution is also different than that for a single-sized particle of the distribution mean size. To illustrate this effect, a log-normal particle size distribution is taken and the integral decontamination factor is calculated. The DF is plotted against the geometric mass mean particle diameter for

FIGURE 5 Effect of particle material density variations on base cases 1 and 2

VARIATION OF RHO.

BASE CASE : RHO=3.0

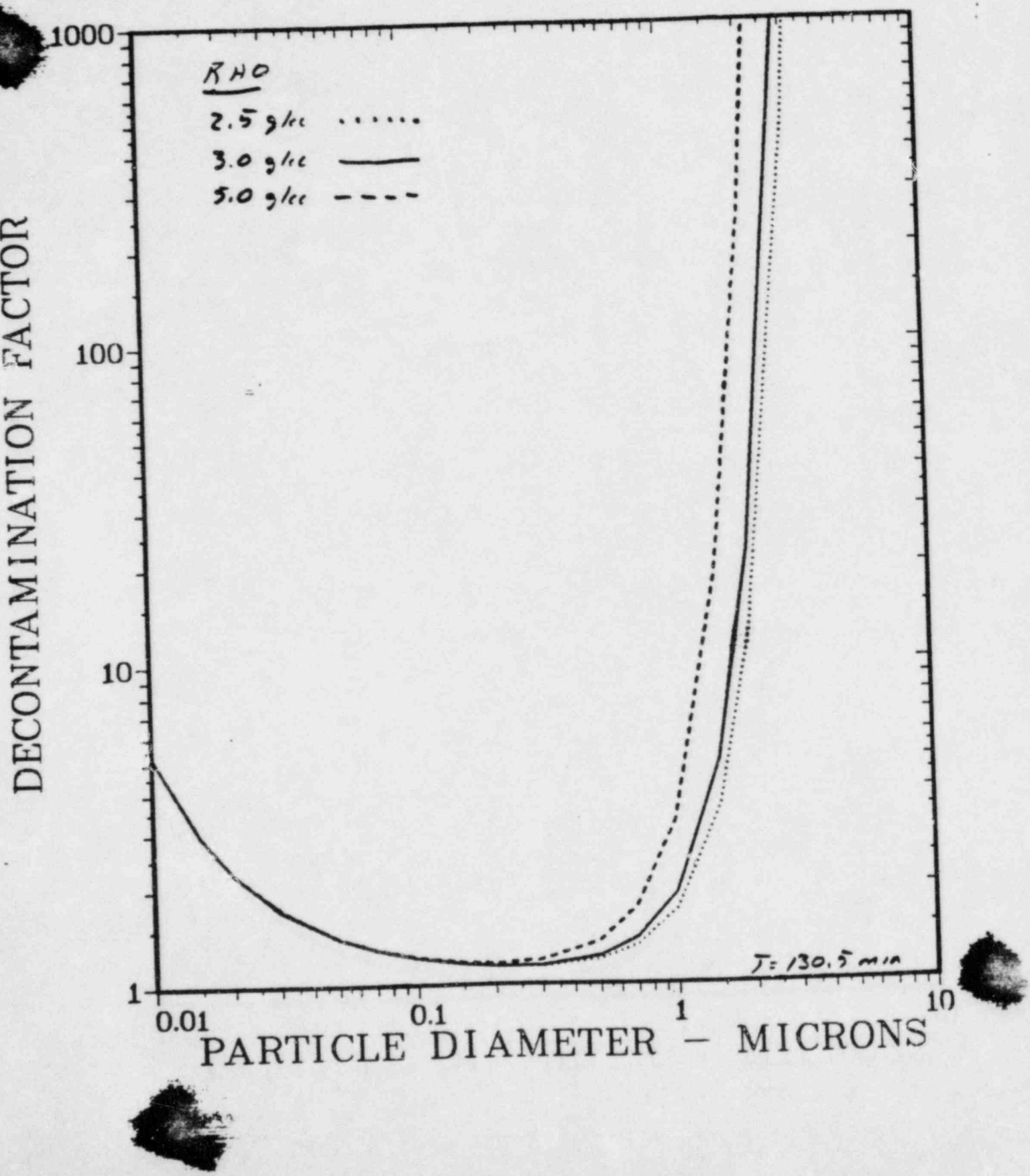

VARIATION OF RHO.

BASE CASE: RHO=3.0

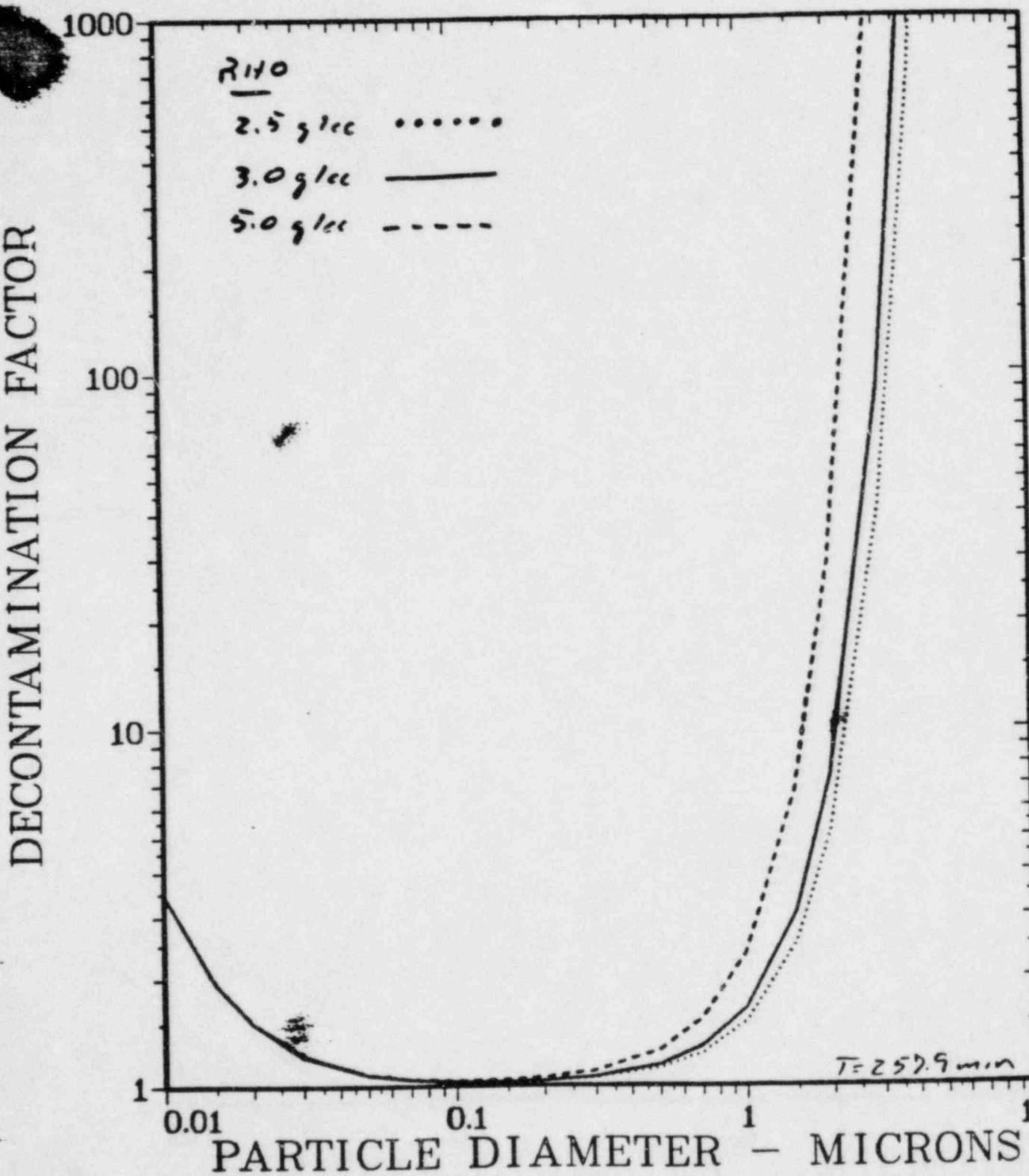

FIGURE 6 Effect of uncertainties in soluble material on the particle on base cases 1 and 2

VARIATION OF SOLF.

BASE CASE : SOLF=0.

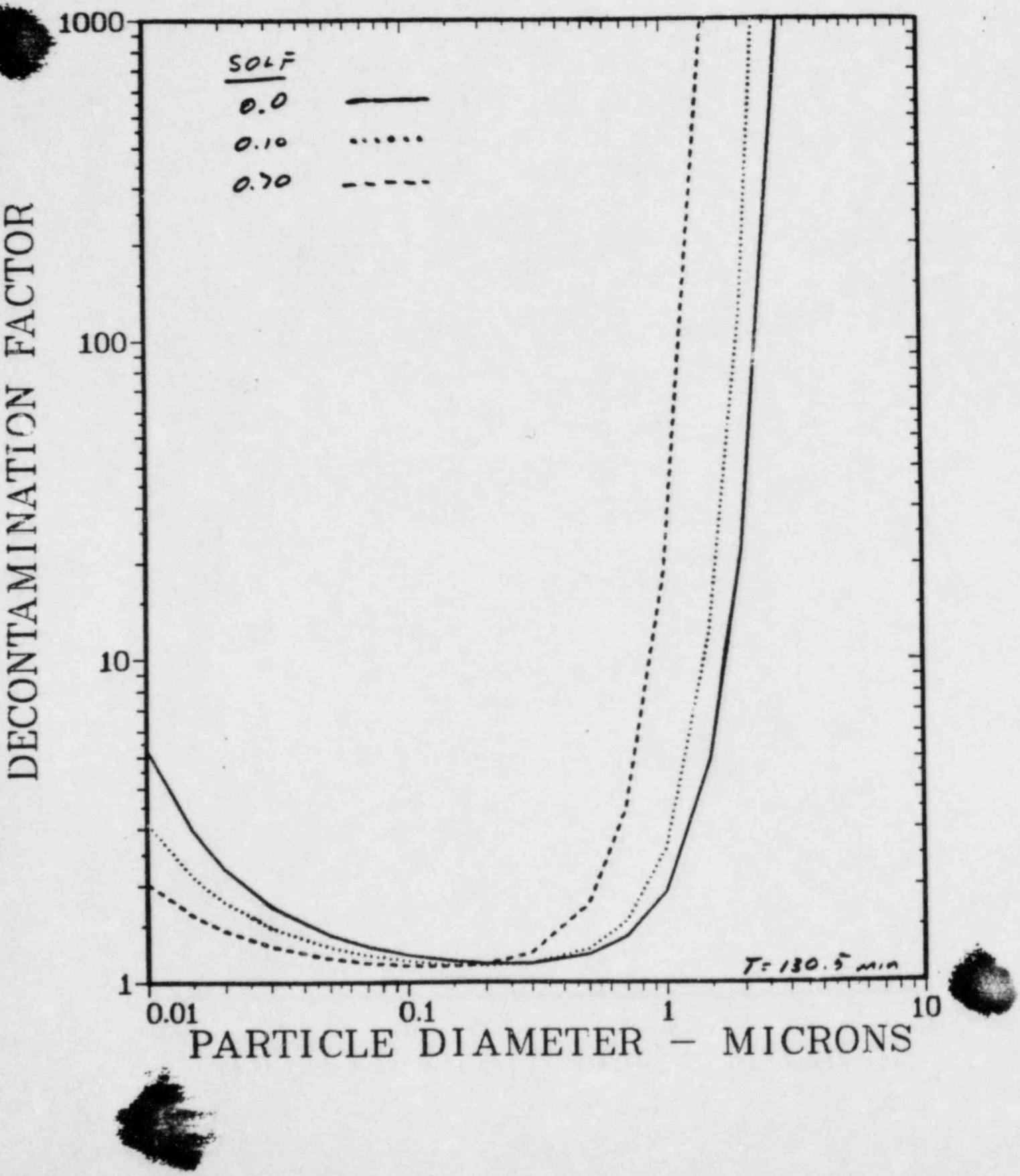

VARIATION OF SOLF.

BASE CASE: SOLF=0.

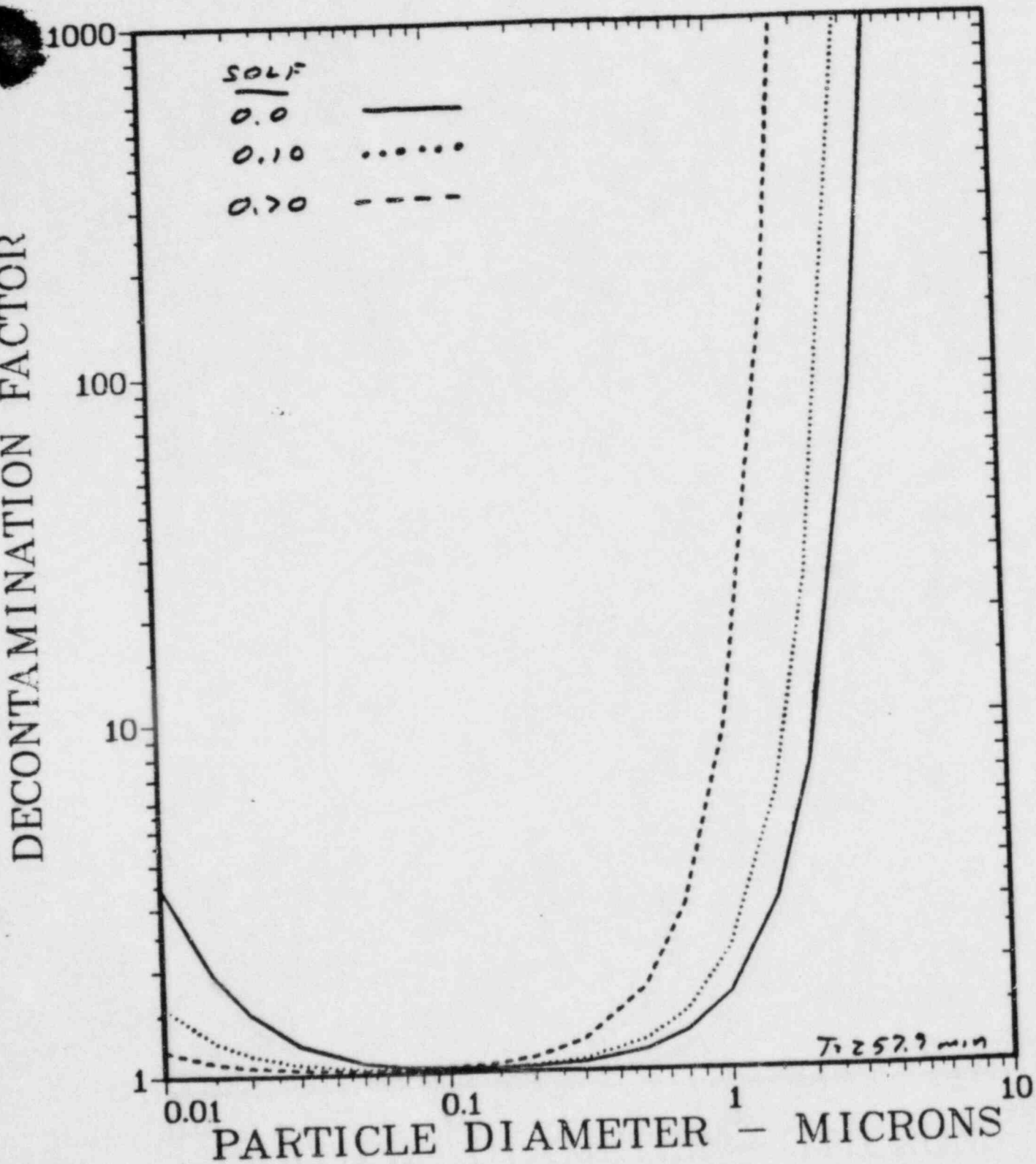

FIGURE 7 Effect of bubble swarm rise velocity variations on base cases 1 and 2

VARIATION OF VSWARM.

BASE CASE : VSWARM=116. CM/SEC.

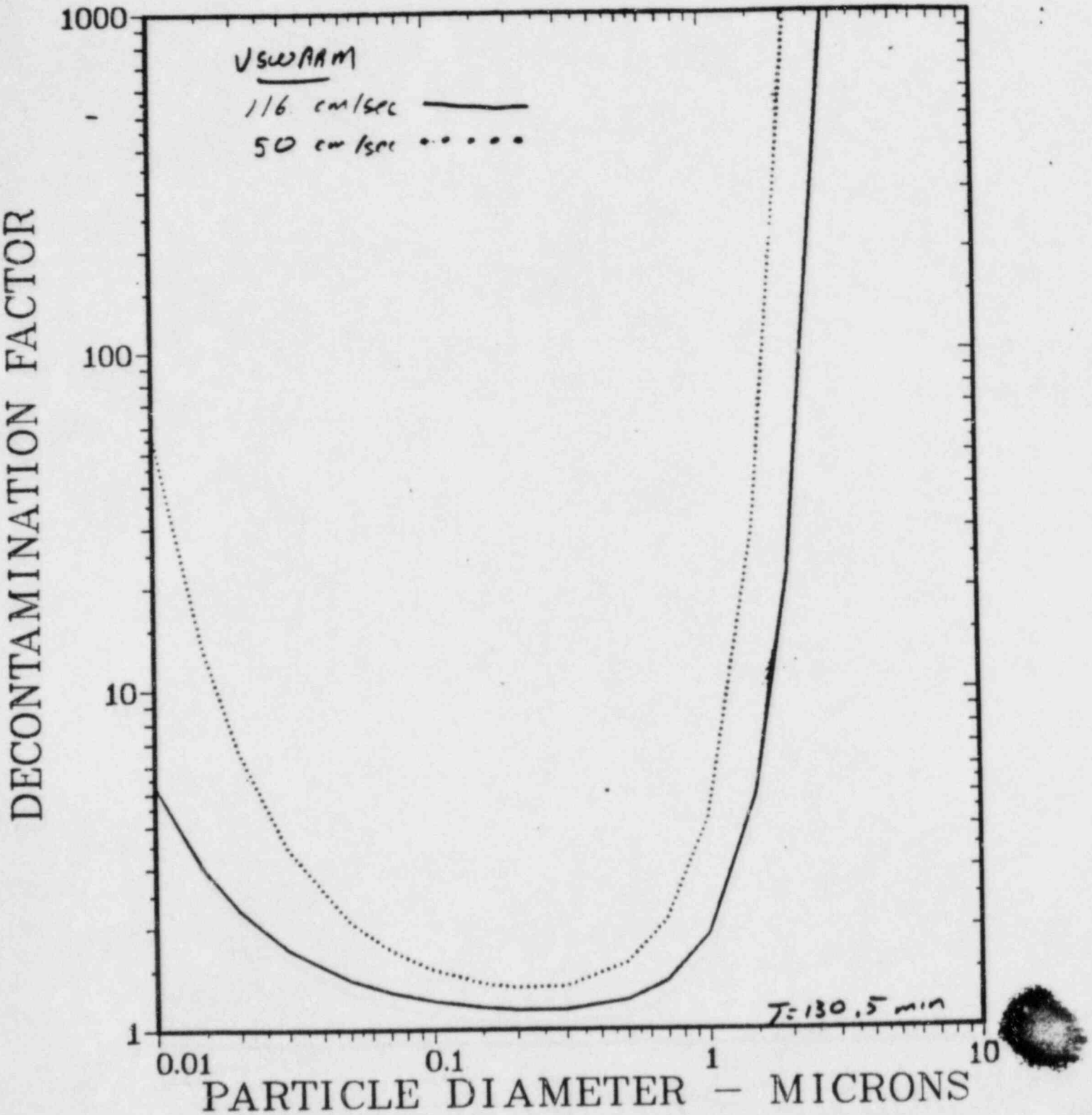

VARIATION OF VSWARM.

BASE CASE: VSWARM=116CM/SEC.

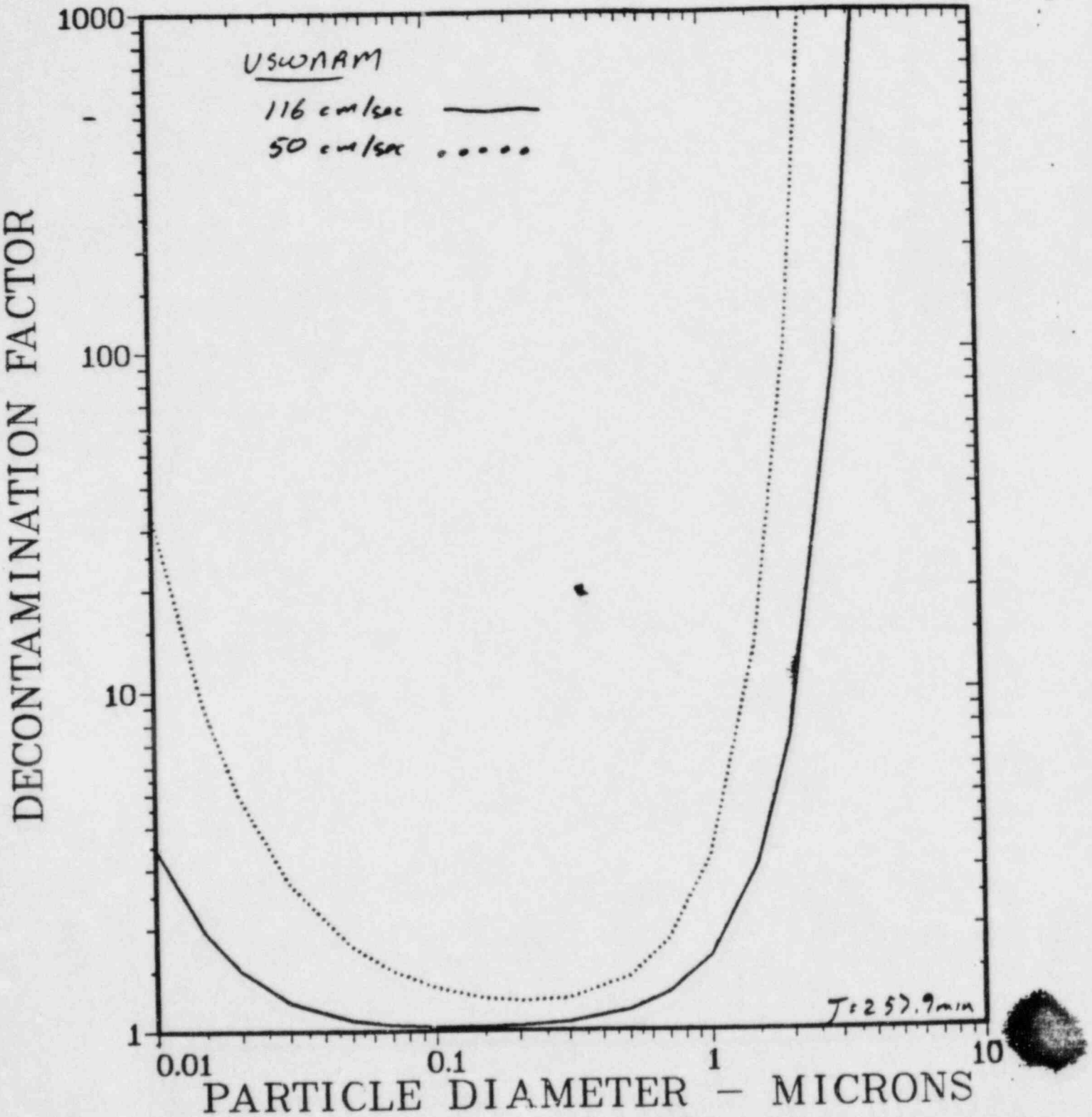

DL

SPARCS34.PLT

distributions with the same geometric standard deviation or spread. The mathematical form of the log-normal distribution is:

$$\frac{dM}{d\ln Dp} = \frac{MT}{\sqrt{2\pi}\ln\sigma_g} \exp\left[\frac{-(\ln DGM/Dp)^2}{2(\ln\sigma_g)^2}\right]$$

where dM/dlnp is the incremental aerosol mass in the
-> incremental range ln(DP) to ln(Dp+dDp)
MT is the total aerosol mass
Dp is the particle diameter
DGM is the geometric mass mean diameter
σ_g is the geometric standard deviation.

Figures 8a and 8b are plots of integral decontamination factor versus geometric mass mean diameter for various values of geometric standard deviation. Figures 8a and 8b are for base cases 1 and 2, respectively.

The curve for $\sigma_g = 1$ is for a monodisperse aerosol and is identical to the base case curves in Figures 3 through 7. As σ_g increases, the distribution spreads out. The most likely values for σ_g are between 1.4 and 2.5. A σ_g of 5 is simply a crude way to show the effect of a multimodal, broadly spread distribution, which may be encountered in the dry well.

It is important to note that spread in a particle size distribution acts to flatten the DF curve. Sensitivity to the mean of a polydisperse aerosol is less than the sensitivity to the same mean of a monodispersion. This tends to mitigate the effects of the parameter uncertainties illustrated in Figures 3 through 7. Uncertainty in particle size distribution is at least as important as uncertainty in other parameters.

FIGURE 8 Integral Decontamination Factors for Various Particle Size Distributions

DECONTAMINATION FACTORS FOR DISTRIBUTIONS.

SIGMA= 1.0, 1.4, 2.5, 5.0

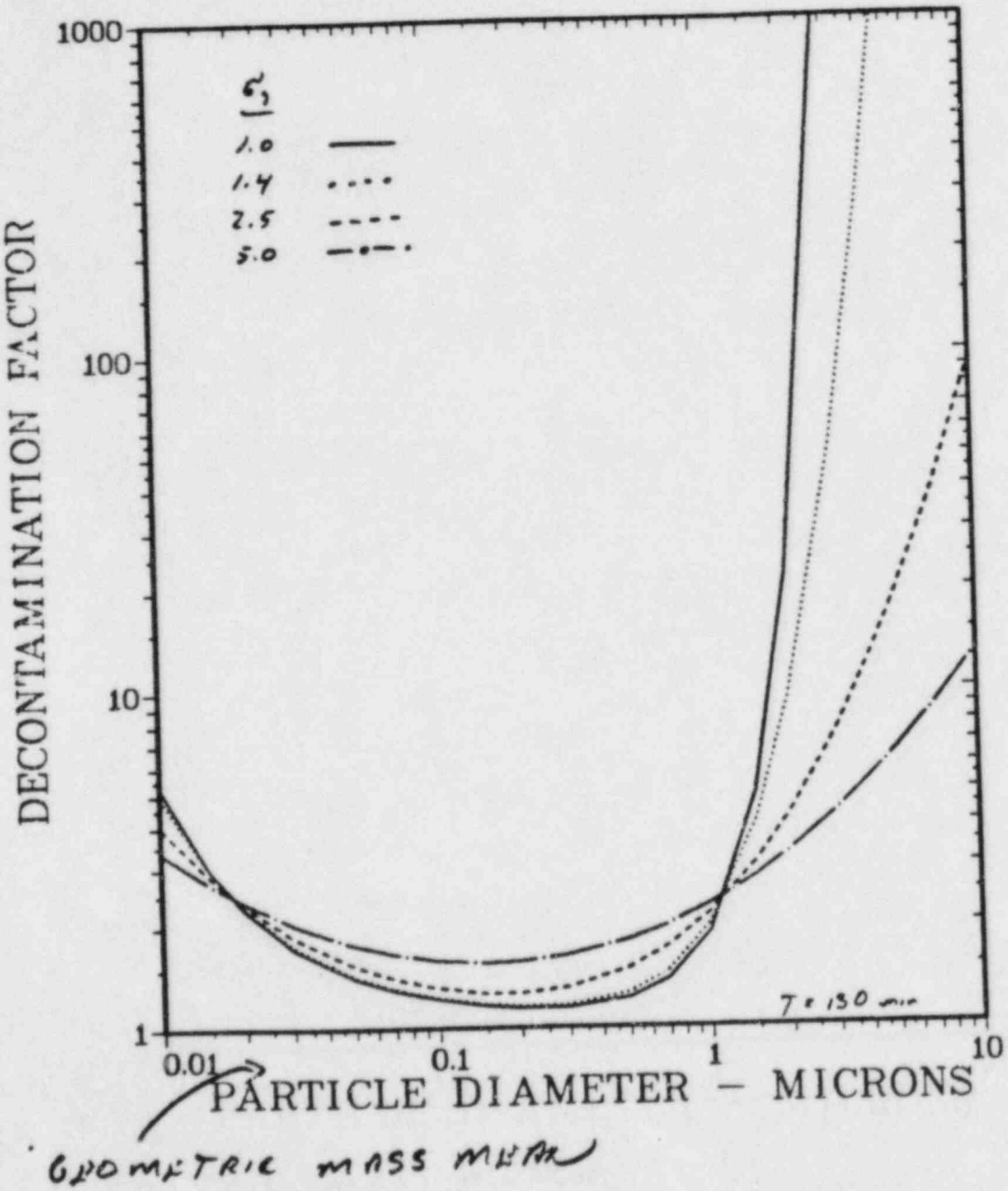

DECONTAMINATION FACTORS FOR DISTRIBUTIONS.

SIGMA= 1.0, 1.4, 2.5, 5.0

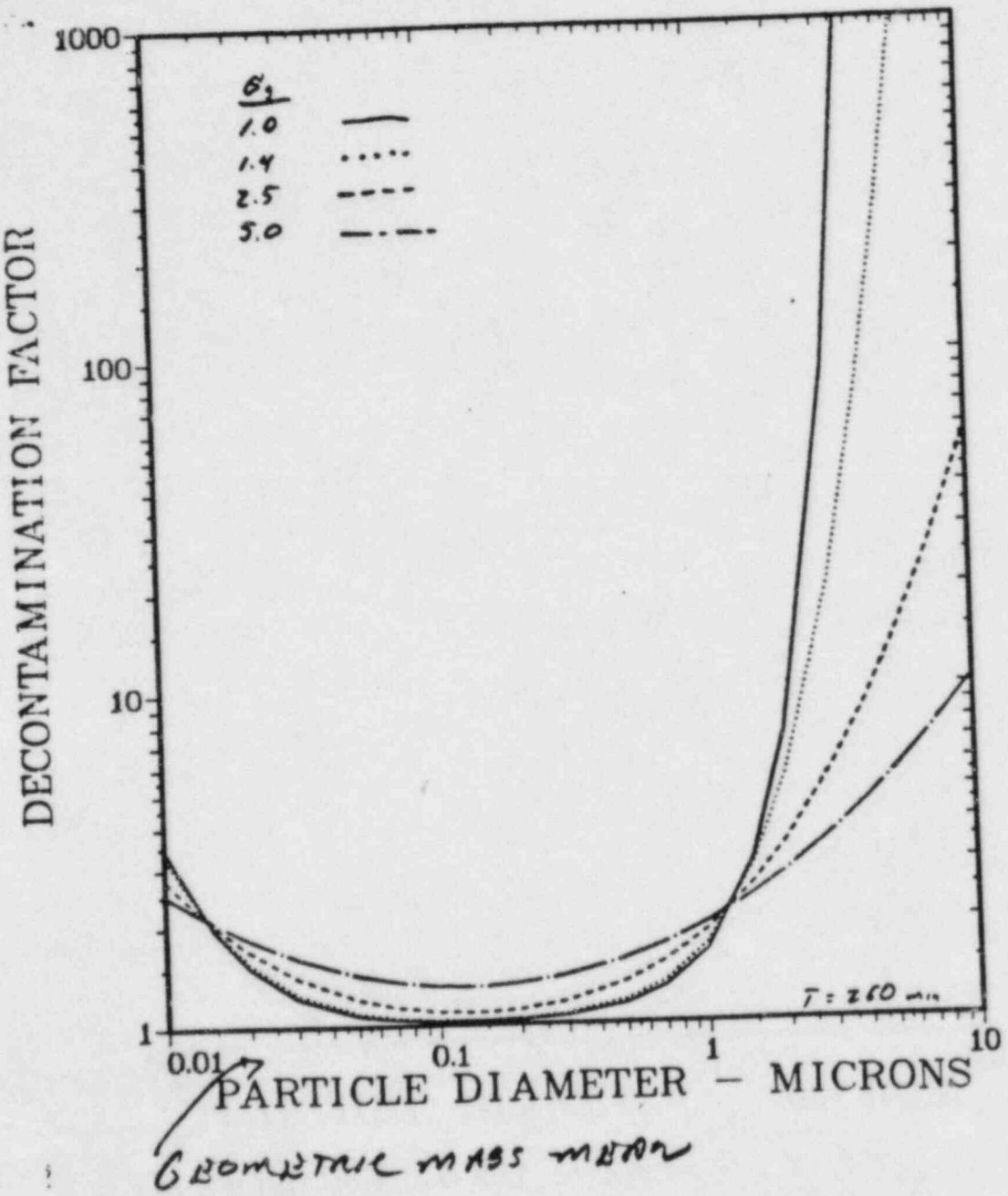

In general, the uncertainty for decontamination factors is thought to be on the order of a factor of 10 either way. Condensing steam has not been considered in this treatment but uncertainty in particle size distribution has.

The effects of unmodeled phenomena are not considered but will be discussed in the following section on the applicability of extending single bubble models to multiple bubble cases.

APLICABILITY OF SINGLE BUBBLE MODELING TO MULTIPLE BUBBLE CASES

An area of uncertainty that is in the class of phenomenological uncertainty is in extending single bubble modeling to cases involving multiple bubbles. The single bubble models have been reasonably accurate in describing multiple bubble scrubbing[10,11,12], but this may have been fortuitous.

Contaminated pools, bubble wobbling and oscillation, and bubble fragmentation and coalescence in multiple bubble systems may act to retard or eliminate bubble internal circulation. The last two phenomena may introduce turbulence, which acts to deposit particles by inertial effects. In both internal circulation-driven inertial deposition and turbulence-driven inertial deposition, the important particle property is the same: particle relaxation time. For multiple bubble systems undergoing fragmentation and coalescence, a more macroscopic modeling of the system would be appropriate. This would include turbulent inertial disposition and turbulent diffusion but exclude internal circulation effects if bubble lifetimes are too short for them to be established. Modeling of phoretic mechanisms would also need to be reconsidered if bubble lifetimes were too short to establish the driving gradients.

The developers of SPARC intend to include swarm effects and

turbulent deposition in their model. At the current level, the use of a slightly modified Fuchs model may well be adequate to predict aerosol scrubbing to within the identified uncertainty. The author has been unable to find a comparison of the Fuchs model to data. In light of the multiple bubble nature of the problem and the uncertainty in aerosol size distribution, improvements to single bubble modeling may be past the point of diminishing returns.

CONCLUSIONS

The model uncertainty arises from two sources: propagated parameter values and user supplied parameter values. Of the important quantities which are propagated, particle size distribution is the most important. Steam condensation can increase DF by a factor of 10, and particle material properties shift the steep right sides of the curve producing great sensitivity to particle size. Spread in particle size reduces the steepness and consequently the sensitivity to particle size. DF is strongly influenced by variation in size distribution.

The other source of model uncertainty, user supplied parameter values, is dominated by the bubble dynamics. Experimental investigation has reduced uncertainty in bubble size and shape but has not reduced uncertainty in the internal circulation behavior.

Internal circulation behavior in swarms is instrumental in examining phenomenological uncertainty. Phenomena of turbulent inertial deposition and turbulent diffusive deposition have not been modeled. It may be hypothesized that they replace internal

circulation driven mechanisms when bubbles are undergoing fragmentation and coallescence in swarms. That the single bubble models can describe experimental scrubbing data may be fortuitous or the result of parameter adjustment.

Model uncertainty may introduce a factor of 10 uncertainty in DF. Phenomenological uncertainty can't be quantified at this time.

REFERENCES

1. Fuchs (1964), Aerosol Mechnics.

2. P. C. Owczarski, A. K. Postma, R. L. Schrek, "Technical Bases and User's Manual for SPARC -- A Suppression Pool Aerosol Removal Code." NUREG/CR-3317, PNL-4742, 1983.

3. R. N. Oehlberg, "Source Term Technology: Radionuclide Removal By Pool Scrubbing," EPRI Journal, June 1984, p. 61 62.

4. F. J. Moody, "Derivation of an Elliptical Suppression Pool Scrubbing Model," F. J. Moody, General Electric Company, 1983.

4. GE Model Reference

5. P. C. Owczarski and A. K. Postma, October 1983, "Suppression Pool Modeling," Presentation at Eleventh Water Reactor Safety Research Information Meeting, Gaithersburg, MD, October 26, 1983.

6. Clift, Grace & Weber

7. Battelle Reference -- Ratio vs. _____

8. Battelle reference -- Swarm & Bubble Site Dist.

9. Battelle reference -- Swarm Rise Velocity

10. SPARC Reference -- Prediction versus Measured

11. SUPRA reference -- Prediction versus measured.

12. GE reference -- Prediction versus measured.